A “LABEL-FREE” METHOD FOR THE DETERMINATION OF POLYETHYLENE-GLYCOL FUNCTIONALIZATION EFFICIENCY ON GOLD MONOLAYER PROTECTED CLUSTERS

By

Charleson Sherard Bell

Thesis

Submitted to the Faculty of the

Graduate School of Vanderbilt University

in partial fulfillment of the requirements

for the degree of

MASTER OF SCIENCE

in

Biomedical Engineering

December 2009

Nashville, Tennessee

Approved

Dr. Todd Donald Giorgio, PhD

Dr. Hak-Joon Sung, PhD

ACKNOWLEDGEMENTS

First, I give all thanks and glory to GOD, my father in heaven, his Son, Jesus Christ my Lord and Savior, the Holy Spirit, a gift from God himself – without them I am nothing and would never have made it this far. . .

This research project was successfully completed thanks to the help of many individuals who assisted along the way. I gratefully acknowledge my research advisor and first nanotechnology professor, Dr. Todd D. Giorgio, for the patience and guidance he gave me towards the completion this research. The road was long and obstacle-ridden and I am grateful for his persistence in guiding me through my early struggles. I would also like to acknowledge Rossane Delapp for her assistance with ICP-AES measurements. In addition, I would like to acknowledge Dr. Donald Stec and Margaret Allaman for their assistance with NMR acquisition and analysis. I would also like to thank, Dr. Sarah Sewell Pierce, Dr. Amanda Lowery, and Dr. Chinmay Soman for their guidance and assistance in my early graduate school endeavors. Without their hands-on approach to training, I would have not quickly obtained the laboratory experience and dexterity that I have today.

Furthermore, I would like to thank Shann Yu, Joshua Trantum, Ryan Ortega, Joy Garnett and Michelle Lowe for their support during long days and nights in the laboratory.

Finally, I would like to thank my immediate and extended family for their undying support and encouragement through this process. Mom, Dad, Charreau, Maceo, Grandpa, my late Grandma, aunts, uncles, cousins and the like – I THANK you and LOVE you all!

Final thanks goes out to all who I have not specifically named in this acknowledgement. You know who you are and I sincerely and graciously thank you for your encouragement and support throughout my experiences here at Vanderbilt University.

TABLE OF CONTENTS

TABLE OF FIGURES

LIST OF TABLES

CHAPTER I

INTRODUCTION

Objective

The objective of this work was to characterize how variations in gold nanoparticle diameter affect the packing density, or functionalization efficiency, of surface functionalized thiolated poly(ethylene glycol) using a "label-free" conjugate quantification technique. Five gold particle diameters were selected and conjugated with poly(ethylene glycol) using a citrate-thiol place exchange reaction forming PEGylated gold monolayer protected clusters. The gold clusters were characterized using ultraviolet/visible spectroscopy and dynamic light scattering to evaluate gold solution concentration and conjugation confirmation, respectively. Gold clusters were decomposed using iodine and the conjugates were enumerated using nuclear magnetic resonance (NMR) spectroscopy and inductively coupled plasma mass spectroscopy (ICP-AES).

Specific Aims

1) Obtain colloidal gold particles of varying size and gain the ability to determine unknown concentrations.
2) Functionalize colloidal gold particles with thiolated poly(ethylene glycol) at constant reaction concentration.

3) Confirm conjugation of thiolated poly(ethylene glycol) to colloidal gold particles using a quantitative method.
4) Enumerate the number of conjugated ligands on the gold surface for each particle size using NMR spectroscopy and compare to predicted results.
5) Enumerate the number of conjugated ligands on the gold surface for each particle size using ICP-AES and compare to NMR and predicted results.

CHAPTER II

SIZE DEPENDENT FUNCTIONALIZATION EFFICIENCY OF POLYETHYLENE-GLYCOL CONJUGATED GOLD MONOLAYER PROTECTED CLUSTERS USING NUCLEAR MAGNETIC RESONANCE SPECTROSCOPY

Introduction

History. Gold monolayer protected clusters[1] (AuMPCs), also commonly referred to as gold nanoparticles[2], gold nanoclusters[3] or gold colloid[4], are among the oldest[5] and most studied metallic-core based particles used in biomedical applications. Colloidal gold is the generation of nanometer-sized gold particles in solution stabilized by salts or passivating compounds[6]. In the early 1600s, gold colloids were first described by Parcelsus as being formed by the reduction of auric chloride with an alcoholic extract of plants[7]. Since then, a multitude of methods for the synthesis of colloidal gold have been introduced in literature[8] including the two most popular methods: the Brust-Schiffrin Method[9] and the Turkevitch reaction[10]. The Turkevitch reaction is the most fundamental method of colloidal gold synthesis employing the citrate reduction of $HAuCl_4$ in water. This method allowed the generation of controlled gold nanoclusters – nanosized gold particles, stabilized by citrate ions, of pre-chosen size and medial stability. Further investigation into the reaction allowed controlled formation where adjusting the ratio between reducing/stabilizing agents would control the AuMPC size[11]. The Brust-Schiffrin method pioneered colloid technology by using Faraday's early two-phase system[4] with the use of thiol ligands that strongly bind gold due to the soft character of both gold and sulfur[9]. This method brought considerable impact to the colloid field because it proved a simplistic synthesis of thermally stable gold colloids of controlled size and dispersity with the ability to be functionalized like stable organic and molecular compounds. Like the Turkevitch reaction, adjusting the thiol to gold mole ratios adjust the average gold core sizes. Here, $AuCl_4^-$ is transferred to toluene using tetractylammonium bromide as the phase-transfer reagent and reduced by $NaBH_4$ in the presence of dodecanethiol. A paradigm shift, Brust et al. augmented their reaction protocols to include *p*-mercaptophenol stabilized gold colloids extending gold colloid synthesis to gold colloid *functionalization* allowing colloid stabilization by a plethora of functional thiolated ligands[12]. This breakthrough led to the eventual determination of the reactions which describe gold functionalization. Reported by the Murray group, the place exchange reaction describes the replacement of a controlled proportion of stabilizing salts or thiols with a variety of functional thiols[13]. With the ability to be protected and functionalized by a coat of functional molecules, gold colloids of this form were termed gold monolayer-protected clusters[14, 15].

As a therapeutic, colloidal gold was used in the middle ages to treat a plethora of diseases including: heart and venereal ailments, dysentery, epilepsy, tumors and as a diagnostic tool for syphilis[16]. Currently, colloidal gold is employed frequently in biological and biomedical applications. Lv et al. investigated trypsin loaded gold nanoparticle conjugates by mixing the particles with trypsin in an enzyme appropriate environment (pH=8.0)[17]. Following this blending procedure, bonds between the trypsin and gold colloid were detected via UV-vis spectroscopy. In addition, the group evaluated varying protease activity by initiating a comparative-causative study where trypsin protease activity was evaluated before and after mixing with the gold nanoparticle solution. Improved enzyme activity and stability was detected using a trypsin protease assay.

Current Implementation. Aside from novel uses of gold colloid to improve current experimental methods, a number of groups seek to employ gold colloid in the use of cancer diagnostics and therapeutics. Roa et al. examined the mechanism of glucose-capped nanoparticle enhanced radiation sensitivity in radiation-resistant human prostate cancer cells[18]. These particles enhanced growth inhibition (26.8% decrease in proliferation) and decreased cell survival rate (36% decrease at 14 days) in prostate cancer carcinoma cell line DU-145 cells. Even further, using MRC5 human diploid fibroblasts, it was found that these particles do not enhance the sensitivity of non-cancerous cells. In addition, it was also noted that such particles inhibit proliferation and survival by altering the cell cycle distribution through an increase in expression of cyclin B1 & cyclin E and a reduction of cyclin A. In addition to methods seeking to assist in the eradication of cancer cells via an endogenously delivered treatment, gold nanoparticles are also used as vectors to delivery drugs and other therapeutics. Prabaharan et al. investigated gold nanoparticles stabilized with a monolayer of folate-conjugated doxorubicin-poly(ethylene glycol) block copolymer for use as a tumor-targeted drug delivery carrier[19]. These particles formed stable unimolecular micelles in aqueous solution and were between 24-52 and 10-25 nm in diameter as measured by dynamic light scattering and transmission electron microscopy, respectively. The group found that the doxorubicin was released much more rapidly at pH lower (~ pH 5.3-6.6) than pH 7.4

from micelles that contained folate. Furthermore, it was observed that folate loaded micelle entered cells at a higher rate than unfolated micells due to facilitation by folate-receptor-mediated-endocytosis thus resulting in high cytotoxity in 4T1 mouse mammary carcinoma cell lines. Overall, it was concluded that such conjugated particles could be used for tumor targeted delivery as a vector with pH-triggered drug releasing properties.

Therapeutic Size Constraints. Such conjugated nanoparticles designed for tumor treatment via delivery of some agent must adhere to particular therapeutic size constraints – the size therapeutic window. Generally, the capillary permeability of the endothelial barrier in newly vascularized tumors is significantly greater than that of normal tissue[20]. Tumor vessels are less permeselective than normal vessels, thought to be due to large pores in the vessel wall. Such transport appears to be limited by diffusion through the pores. Conjugated nanoparticles must extravasate from the tumor vasculature while resisting leakage from normal vasculature. Pegaz et al. described that nanoparticles of larger sizes were taken up rapidly by both the mononuclear phagocyte system (MPS) and the reticuloendothelial system (RES) components[21]. Ishida et al. determined that surface protected liposomes with 120 nm average diameter, which exhibited the most prolonged vascular circulation when compared to other particles sizes, showed the highest accumulation into all the solid tumors employed in the experiment[22]. Accumulation of 63 nm liposomes into tumor tissue was comparably lower. Unezuki et al. examined liposomes 63, 133, 198 and 388 nm in average diameter surface protected by the ligand poly(ethylene glycol) (PEG)[23]. PEG effectively prolonged circulation and decreased liver uptake of liposomes with average diameter of 100 – 200 nm.

Diameters larger than 300 nm charted lower circulation times. PEGylated liposomes of the size which showed the most prolonged circulation were accumulated most effectively in the murine tumor – particles with average diameters of 137 +/- 38 nm exhibited an elevated tumor accumulation. Thus, nanoparticles of smaller size and longer circulation time will have more opportunity to transverse the tumor capillaries[22]. Due to this data, it can be concluded that the therapeutic window is between 80-180 nm. The lower threshold of 80 nm is selected to make sure that particles are: below the maximum size of tumor vasculature pore size[24], small enough to not be cleared by liver, spleen, RES or MPS, and to make sure the particle size is above a level allowing for nanoparticle uptake. The upper threshold of 180 nm is selected to ensure that the particle size is small enough to ensure tumor vasculature escape. Therefore particle sizes ranging from 80 – 180 nm were chosen with two particle sizes at a maximum and minimum outside the therapeutic window (5 nm and 250 nm, respectively). In order to ensure gold particle stability and delivery however, particles must resist the MPS and RES through surface passivation by some biological surface modifier.

Poly(ethylene glycol). One such biological surface modifier is thiolated poly(ethylene glycol) (SH-PEG)[25]. It has previously been determined that poly(ethylene glycol) ligands conjugate to gold surfaces in a particular conformation. Poly(ethylene glycol) forms two distinctly different molecular conformations when grafted onto lipid membranes: “brush” and “mushroom” conformations[26]. The mushroom conformation is formed when a low packing density is maintained and conjugate chains are oriented randomly whereas a ~10-fold greater packing density with more extended and weaker chain alignment forms the brush conformation.

More importantly, poly(ethylene glycol) is known for its ability to resist the activity of the reticuloendothelial system – a system composed of monocytes and macrophages that is located near reticular connective tissue such as the spleen[27]. The inherent purpose of these cells is for phagocytotic removal of cellular debris, pathogens and foreign substances, the intravascular nanoparticles for example, from the bloodstream[28]. For example, the attachment of polyethylene-glycol to anti-cancer pharmaceuticals, such as interferon-α, is currently used to lengthen the circulation time of these molecules in the bloodstream thus reducing the frequency of administration of these drugs thus increasing efficacy and patient tolerance[29]. The literature has suggested that photothermal cancer therapy based on gold nanoshells, metallodielectric nanoparticles consisting of a spherical dielectric core coated with a thin metallic shell, have instituted the use of thiolated poly(ethylene glycol) coatings to reduce unwanted protein adhesion under targeted local or systemic delivery [30, 31]. Thereafter, surface passivation of these nanoparticles using bound thiolated PEG, in concert with conjugated antibodies, assisted in maintaining antibody activity in targeted delivery[32, 33].

It can be hypothesized that the efficacy of surface passivation is dependent on the amount surface coverage by poly(ethylene glycol). Quantifying the number of poly(ethylene glycol) ligands on the surface – the functionalization efficiency - of gold nanoparticles will elucidate the passivation efficacy. Devising a method to determine the functionalization efficiency of SH-PEG on gold nanoparticles will facilitate future determinations for other thiolated functional groups.

Nuclear Magnetic Resonance. A number of chemical techniques have been instituted in order to enumerate the number of molecules on the surface of a nanoparticle. Nuclear magnetic resonance (NMR) spectroscopy is a common technique used in organic and medicinal chemistry in order to identify compounds, characterize unknown samples, or confirm chemical structures following synthesis[34-36]. NMR helps to identify the carbon-hydrogen framework of an organic compound. In the late 1940s, NMR spectroscopy was first developed by physical chemists to study nuclei with different spin states[37]. First developed as proton magnetic resonance (^{1}H NMR) in 1951, other spectrometers were later developed for ^{13}C NMR, ^{15}N NMR, ^{19}F NMR, ^{31}P NMR and other magnetic nuclei.

NMR operates by addressing the energy and number of nuclei in the lower energy α-spin state (nuclei aligned with an external magnetic field) and the higher energy β-spin state (nuclei aligned with an external magnetic field). If energetically suitable electromagnetic radiation is applied to nuclei that have been oriented by a magnetic field, a nucleus will in the α-spin state will absorb the energy, thus flipping its nuclear spin and therefore entering the β-spin state. This absorption of energy is detected and output as a signal in the NMR spectrum. The excited molecules return from their state of *resonance*, due to their alignment as a result of the impingement of electromagnetic radiation, and release their energy as heat.

In order to use NMR as quantitative technique, spectroscopists and chemists alike instituted the use of spectrum peak integration[38]. The extensive use of integration in ^{1}H NMR arises from the renowned doctrine that "the area of an NMR resonance is proportional to the relative number of nuclei giving rise to it." During data processing, a number of precautions must be taken to ensure the acquired data accurately reflects the relative ratios in the sample used to achieve precise integration. The signal to noise ratio must be optimized as well as the sensitivity and effective digitalization of the data. Careful phasing and removal of baseline distortions are essential for accurate integration. Although routine use of ^{1}H NMR integration yields only 10-20% accuracy[39], its use is paramount in the field of quantifying ligands conjugated to gold nanoparticles - following decomposition allowing desorption of the ligands[40].

Previous Ligand Enumeration Strategies. A number of previous endeavors at quantifying the number of ligands on the surface of gold nanoparticles with respect to particle size have been conducted. Hurst and Lytton-Jean et al. investigated the parameters that influence coverage on gold nanoparticles[41]. Evaluating the effects of salt concentration, spacer composition, nanoparticle size, and degree of sonication, maximum loading was obtained by salt aging the nanoparticles in the presence of DNA containing a PEG spacing in ~0.7 M NaCl. In order to quantify the surface loading of DNA on the gold nanoparticles, oligonucleotides were labeled with a fluorescent tag - 6'FAM3' – and quantified by comparing the ligand concentration (found by fluorescence) and the gold concentration (found by UV-Visible spectroscopy). Larger nanoparticles (250 nm) were

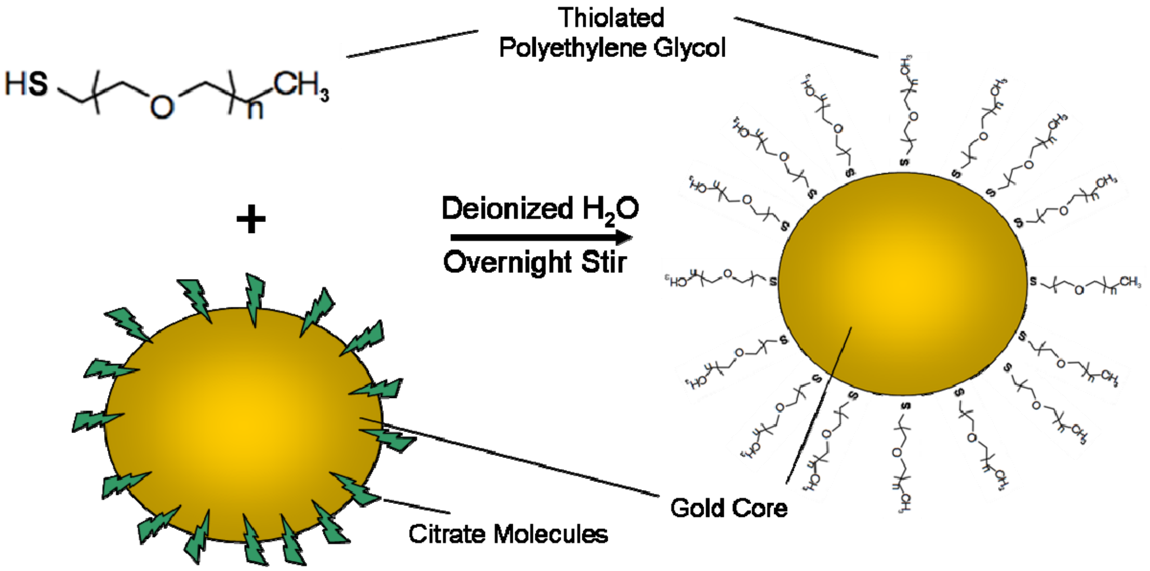

Figure 1. Functionalization strategy for PEGylation of gold monolayer protected clusters. Illustrated above are thiolated poly(ethylene glycol), stock unconjugated gold nanoparticles and PEGylated gold monolayer protected clusters.

found to have orders of magnitude higher DNA loading than smaller (13-30 nm) nanoparticles thought to be due to their larger surface area. Other groups have used fluorescence as the primary source of ligand quantification. Other groups used lactose molecules, labeled to the distal ends of the PEG ligands, and thermogravimetric analysis (TGA)[42]. Using the TGA, the weight decrease of PEG due to its thermal decomposition was determined. The number of PEG chains on each gold particle was calculated by using the concentration of gold particles provided by the manufacture and the weight loss measured by the TGA.

The use of NMR alone as a quantification tool following liberation of ligands from the particle does not require the use of surface-density altering ligands nor does it require the thermal or chemical decomposition of a large quantity of precious sample. Other methods of enumerating the number of ligands attached to AuMPCs use fluorescently tagged or labeled PEG agents which affect the packing of those ligands or involve protocols which require the destruction of high quantities of sample. Here, we both enumerate the number of PEG ligands on the surface using a “label-free,” NMR based method and characterize the loading capacity over a small range of particle sizes. We will also compare the findings from the NMR measurements against predicted considerations. From this, we will glean information regarding the functionalization efficiency of PEG to AuMPCs with respect to particle size and surface area. Thereafter, we will examine how PEG ligands are concentrated or packed onto the surface of varying sizes of AuMPCs. Such knowledge will enable a deeper insight into the efficacy of nanotechnology as it is related to and possibly governed by the functionalization efficiency of its individual technological apparatus.

Materials and Methods

Nanomaterials. Unconjugated AuMPCs 5, 80, 100, 150, and 250 nm in diameter were obtained from TedPella, Inc. (Redding, CA). Lyophilized SH-PEG (5,000 MW) was obtained from Laysan Bio, Inc. (Arab, AL). MilliQ® grade (Millipore Corporation, Billerica, MA) deionizied water (DI H_2O), obtained using a MilliQ® Academic System outfitted with a Quantum® EX Ultrapure Organex Cartridge, was used throughout all experimental phases.

Instrumentation and Assays. Absorbance measurements of AuMPCs were collected using a Varian Cary 5000 UV-VIS-NIR spectrophotometer (Varian, Inc., Palo Alto, CA). Particle diameter measurements were obtained using a Malvern Zetasizer Nano ZS dynamic light scattering based system (Malvern Instruments, Westborough, MA). NMR measurements were obtained using a 400 Hz instrument equipped with a 9.4 Tesla Oxford magnet which is controlled by a Bruker AV-400 console.

Predicted Loading Capacity. For analytical comparison with results from NMR, the predicted loading capacity was calculated. It was assumed that AuMPCs form spherical clusters and follow the fundamental surface area formulae, $SA=4\pi r^2$. In addition, it was assumed that SH-PEG adsorbs onto AuMPCs assuming the brush conformation as discussed by Wuelfing et al [1]. The brush conformation of SH-PEG occupies a molecular surface area footprint of 0.35 nm^2. The maximum number of SH-PEG ligands per AuMPC was calculated by dividing the total surface area of a spherical AuMPC by the SH-PEG molecular footprint. The maximum number of SH-PEG ligands per AuMPC was determined for each particle size.

Place Exchange Reaction. A clear 20 mM solution of SH-PEG was generated by adding lyophilized SH-PEG to DI H_2O at room temperature. Unconjugated AuMPCs at their stock concentration were vortexed, to ensure even suspension in solution, and added to the SH-PEG solution at a 1:1 volumetric ratio. Following a slow overnight stir, using a miniature magnetic stirring bar and stir plate thus allowing sufficient time for maximal functionalization, free citrate and unconjugated SH-PEG ligands were removed using Thermo Fisher Scientific Inc. Slide-A-Lyzer® osmotic dialysis cassettes with a membrane molecular weight cutoff of 10,000 MW. PEGylated AuMPCs (PEG-S-AuMPCs) were harvested from the cassettes and stored at 5°C. Three conjugation trials (n=3) were performed for each particle size to assess the variability of the conjugation protocol.

Determination of Unknown AuMPC Concentrations. Following conjugation and osmotic dialysis, the resultant AuMPC concentration is unknown. In order to determine unknown concentrations, absorbance vs. known concentration standard curves were generated for each particle size using stock AuMPC solutions and UV-VIS instrumentation. From the generation of the standard curves, both the molar extinction coefficient (ε) and the absorbance maximums (λ) were determined for each particle size. The absorbance values of conjugated AuMPC solutions of unknown concentration were then related to the standard curves using Beer's law ($A=\varepsilon lc$) to determine the subsequent concentration.

Conjugation Confirmation. Following the place exchange reaction, SH-PEG conjugation was confirmed by monitoring the diameter of the AuMPCs with dynamic light scattering. Stock solutions of the unconjugated AuMPCs were used as size controls for each particle diameter. Each conjugation trial for each particle diameter was evaluated to assess the variability of diameter increase due to the execution of the conjugation protocol. Following a strict protocol, particles were removed from the 5°C storage environment, allowed to warm to room temperature and vortexed for a minimum of five seconds to ensure colloidal resuspension. 1 ml of each conjugation trial was loaded into a low volume disposable cassette. Prior to measurement initialization, each cuvette was tilted back and forth three times to ensure colloidal resuspension. Typical count rates were between 100 and 350 kcps. Size-distribution profiles and average radii for each conjugation trial were obtained as the mean of triplicate measurements. Each conjugate trial average diameter was statistically compared against the unconjugated control diameter using the Paired t-test.

Quantification of Functionalized Conjugates. The number of poly(ethylene glycol) ligands conjugated to the surface of each AuMPC was quantified using nuclear magnetic resonance via a 400 MHz instrument equipped with a 9.4 Tesla Oxford magnet controlled by a Bruker AV-400 console. The main NMR probe for the instrument is a 5 mm Z-gradient broadband inverse (BBI) probe with automatic tuning and matching capability (ATM).

Samples of each conjugation trial for each particle size were obtained and equalized to a concentration of 49 μM at a volume of 500 μl. Each sample was placed into a Wilmad LabGlass (Vineland, NJ) 5MM Thin Wall, 7" Length, 500 MHz NMR tube. In order to quantify the number of ligands on the surface of the gold nanoparticles using NMR, the ligands must be removed from the surface of the nanoparticle. In order to achieve this removal, one to two large iodine (I_2) crystals were added to each tube. Chemically, the iodine has a higher affinity for the gold than the sulfur molecules [43]. Due to this difference in affinity, the iodine decomposes the AuMPCs where the SH-PEG molecules are released into solution. The place-exchange reaction of thiol for iodine to the gold clusters causes destabilization causing the iodinated gold to fall out of solution [44]. Typically, when thiolated ligands desorb from gold particles, they form disulfide bonds [14]. In addition, iodine decomposition was allowed to occur to completion for one hour as previously described [40] prior to spectrum measurement. In order for the NMR to "lock" onto each sample, each tube was spiked with 50 μl of D_2O.

In order to ensure a spectrum of the decomposed gold and emancipated ligands could be acquired, a pre-saturation technique was employed to suppress the enormous peak typically generated by H_2O. This allowed ample visualization of the more subtle peaks in the resulting spectrum. Each sample was measured following the same major parameters. The number of scans and receiver gain was held to 32. For the f1 channel, P0 and P1 were both held to 11.38 μs. One spectrum was collected per sample to ensure the occurrence of conjugate desorption.

In order to quantify the concentration of desorbed conjugates, the pre-saturation technique cannot be employed due to its inherent modulation of the spectrum baseline. Such modulation introduces error into any integral based quantification strategies. Therefore, a more common “zg30” program was used to acquire a spectrum without using a presaturation pulse. The number of scans was set to 16 whereas the receiver gain was held to 4. A delay (D1) of 10 seconds was added between scans thus ensuring a large enough relaxation time to minimize the effect of the H_2O peak on more subtle peaks. For the f1 channel, P1 was held to 11.38 μs. One spectrum was acquired per sample and integration was used enumerate the ratio between the PEG chain terminal group, CH_3-, peak and the disulfide, PEG-S-S-PEG, bond triplet peaks. Prior to any integration, all spectra were baseline corrected to zero using automatic and manual processes.

A serial dilution was also performed in order to generate a standard curve relating concentration to integral-ratio. In order to generate such integral-ratio values, the PEG terminal CH_3- peak for a concentration of 20 mM SH-PEG was directly compared to the CH_3- peaks of samples containing lower concentrations of SH-PEG. This comparison was achieved via spectral summation of the 20 mM SH-PEG and a ppm shifted spectra containing a lower conjugate concentration (APPENDIX C). Integration was used in order to determine the integral-ratio between the 20 mM sample peak and the lower concentration peak. A standard curve is then generated from integral-ratios of all samples in comparison to the 20 mM peak.

Desorbed-conjugate spectrums containing CH_3- peaks are then compared to the 20 mM SH-PEG CH_3- peak generating an integral-ratio. This integral ratio can be used to quantify the concentration of PEG ligands in the desorbed-conjugate sample. Using the integral-ratio between the CH_3- peaks and the triplet disulfide (PEG-S-S-PEG) peaks, the number of S-PEG ligands that desorbed from the gold colloid can be quantified. Figure 2 describes the entire NMR spectral analysis protocol in a flow chart format.

Statistical Analysis. Statistical Analysis was conducted using SigmaStat software. Paired t-tests for conjugation confirmation were conducted with a confidence interval of 99%. Paired t-tests for conjugate quantification were conducted with a confidence interval of 95%.

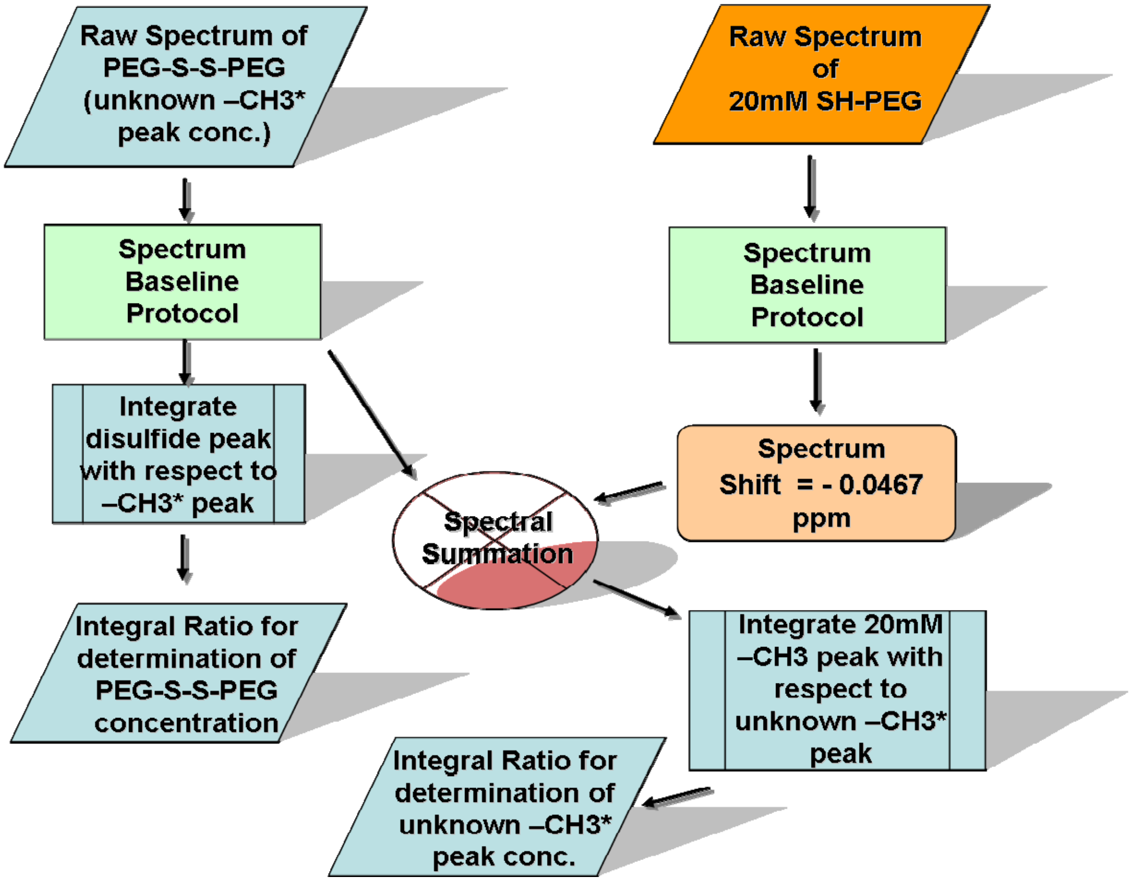

Figure 2. NMR spectral analysis protocol for the quantification of conjugated ligands depicted in flow chart format.

Results

Determination of Unknown AuMPC Concentration. In order to determine the AuMPC concentration following particle purification, the absorbance was obtained by monitoring the UV-Vis spectra of each unconjugated particle size (Figure 3). Standard absorbance-concentration curves were generated (Figure 4). The molar extinction coefficient was determined in accordance with Beer's law. The absorbance maxima (λ in mm) and molar extinction coefficients (ε in $Lmol^{-1}cm^{-1}$) are shown in Table 1. Following particle purification, the resultant concentrations were determined via Beer's law at the maximum absorbance wavelength for each particle size (Figure 5).

Conjugation Confirmation. Particle conjugation was assessed by monitoring the hydrodynamic radii of each conjugation trial. Used as a quantitative technique for qualitative assessment, significant diameter increases was used to infer successful conjugation. Dynamic light scattering (DLS) results are shown in Figure 6. DLS correctly sized unconjugated particle sizes. The size increase of the AuMPCs following PEGylation was also monitored using DLS. This size increase, presumably representing the radial thickness of the conjugated PEG coat, was significant for each particle diameter except 5 nm.

Quantification of Functionalized Conjugates. Conjugated PEG-S ligands were quantified using nuclear magnetic resonance spectroscopy. Integral ratios between peaks were acquired and analyzed in Bruker's TopSpin program. All non pre-saturated PEG-S-AuMPC spectra depicting integral ratios used in this work are shown in APPENDIX B.

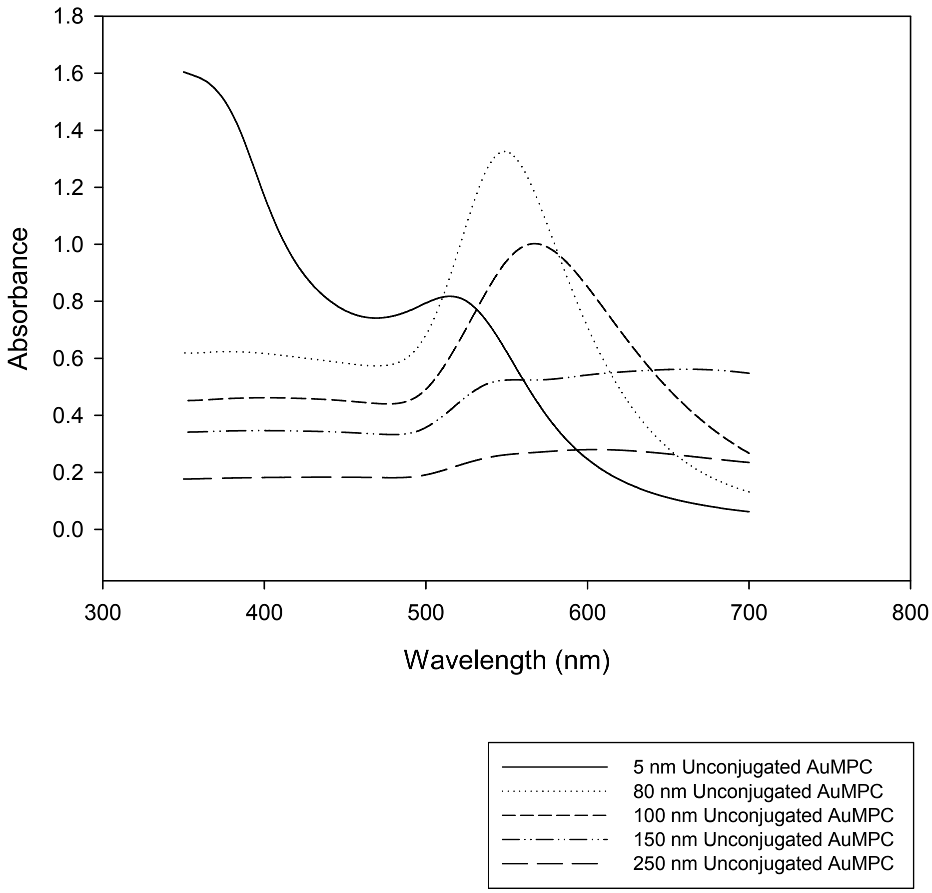

Figure 3. Absorbance as a function of wavelength for each stock nanoparticle solution over the UV-Vis range.

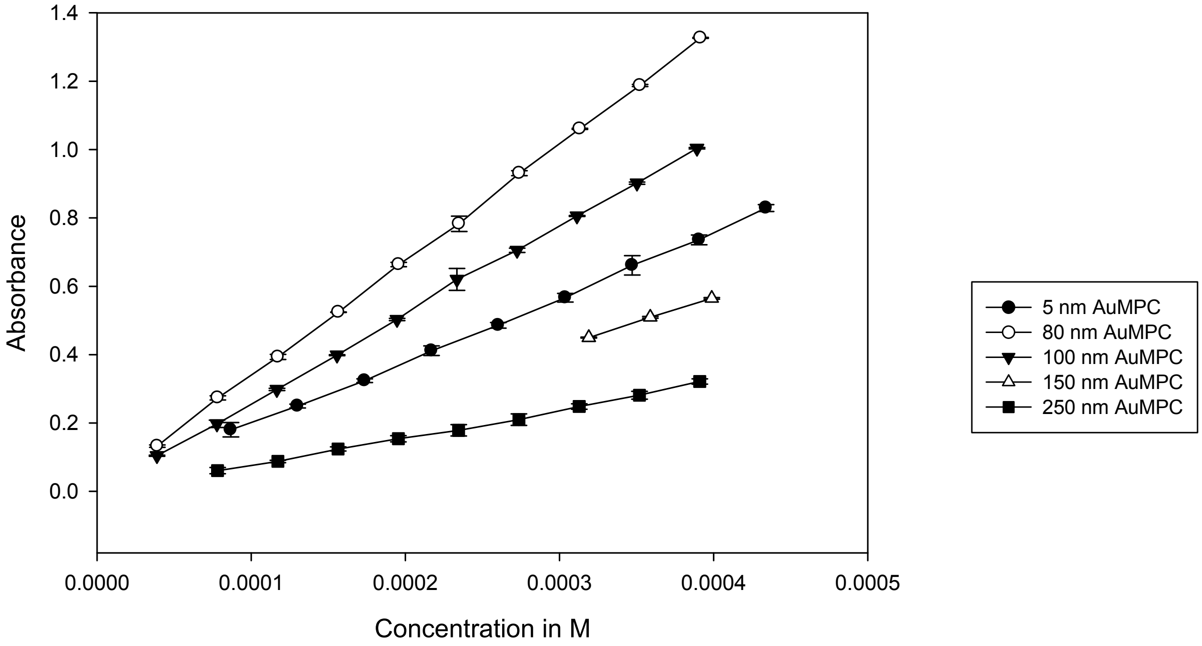

Figure 4. Standard absorbance-concentration curves generated from the absorbance spectroscopy of serial dilutions of unconjugated particles. These standard curves were used to determine the molar extinction coefficient following the linearity of Beer's Law (*A=εlc)*. This data is eventually used for the calculation of unknown particle concentrations.

PEG-S-AuMPC Particle Characteristics

Absorbance Spectroscopy

Diameter (nm)	Abs Max λ (nm)	Mol Ext. ε (L/(mol*cm))
5	515	1876.1
80	543	3379.2
100	568	2585.3
150	661	1441.7
250	605	822.48

Table 1. PEGylated gold monolayer protected cluster characteristics. This table includes the absorbance maxima and molar extinction coefficients used to calculate unknown particle concentrations following purification.

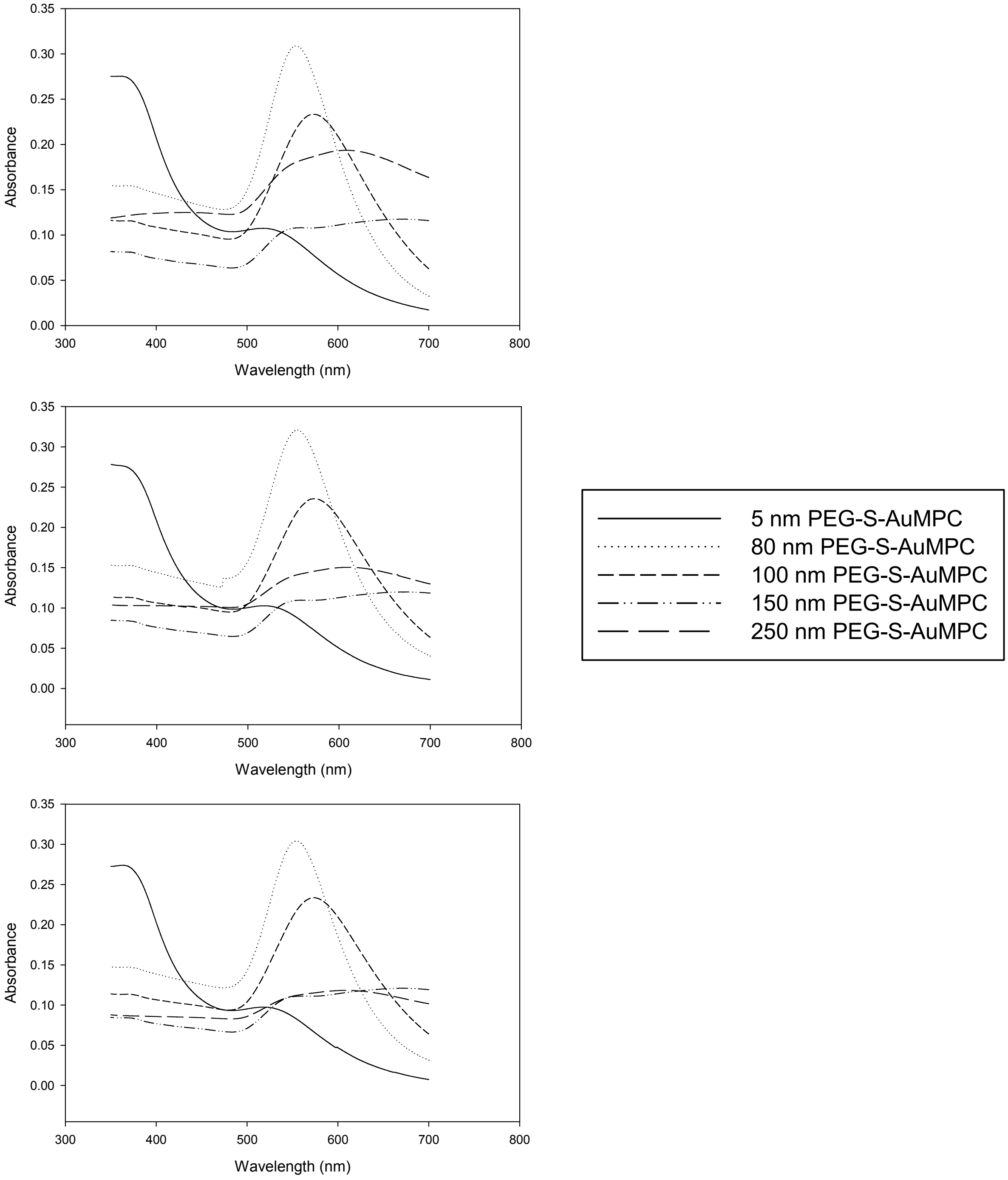

Figure 5. Absorbance of each PEGylated nanoparticle conjugation trial obtained by monitoring the UV-Vis spectra of each conjugated particle size. Trials 1, 2, and 3 top to bottom, respectively.

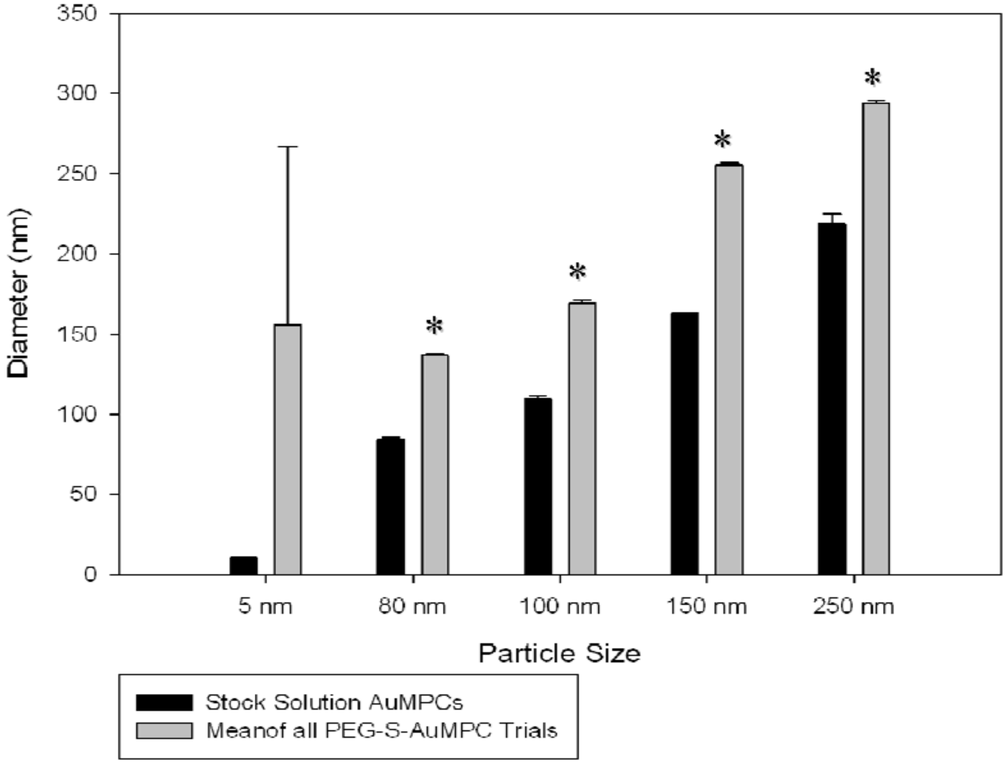

Figure 6. Particle conjugation was assessed by monitoring the difference between the hydrodynamic radii of conjugated and stock solutions of AuMPC using dynamic light scattering. Bar heights represent the mean of three experiments with error bars shown as the standard deviation *Significant size increase for $p<0.01$ using Paired T-Test.

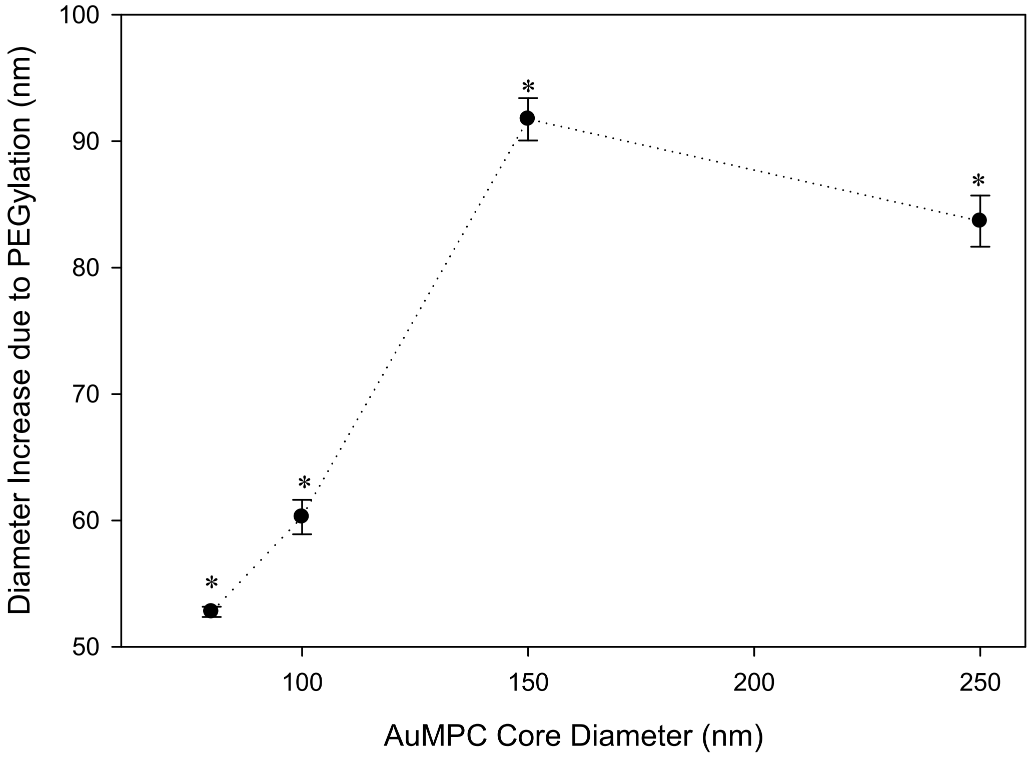

Figure 7. Diameter increase of AuMPCs following PEGylation determined by monitoring the hydrodynamic radii of each conjugation trial using dynamic light scattering. This size increase represents the radial thickness of the PEG coat. Data points represent the mean of triplicate experiments with error bars shown as the standard deviation. *Significant difference between size increase per data point for $p<0.01$ using Paired T-Test.

A serial dilution was used to create a standard curve relating integral ratio to concentration. A coefficient of determination (R^2) value larger than 0.9 was used as a cutoff value for acceptable linear congruency. The linear fit with R^2 value and resulting equation is shown in Figure 8. A R^2 value of 0.9172 confirms proof of concept for NMR as a quantitative technique to concentrations as low as 0.363 mM. All acquired and analyzed PEG-SH serial dilutions used in this work are shown in APPENDIX A.

As a further proof of concept, the difference in spectral response between PEG-SH and decomposed PEG-S-AuMPC samples was evaluated using pre-saturation to remove the background H_2O proton peak and reveal the ligand peaks. An example of the spectral distinctions between PEG-SH protons and liberated PEG-S-S-PEG protons is shown in Figure 9. The appearance of triplet peaks in the sulfide region suggests the expected formation of disulfide bonded liberated ligands.

In order to obtain quantifiable spectra, the pre-saturation technique can not be used due to its inherent modulation of the spectrum baseline. Non pre-saturated spectra were obtained and analyzed. A sample analyzed spectrum is shown in Figure 10 whereas other spectra are shown in APPENDIX B. The CH_3- proton peak occurring at ~3.3 ppm represents the distal moiety at the end of the PEG polymer chain thus depicting a single S-PEG ligand. The triplet peak occurring between 2.8-2.9 ppm represents the disulfide bond between two sulfur atoms of two S-PEG ligands. In a similar fashion, the CH_3-

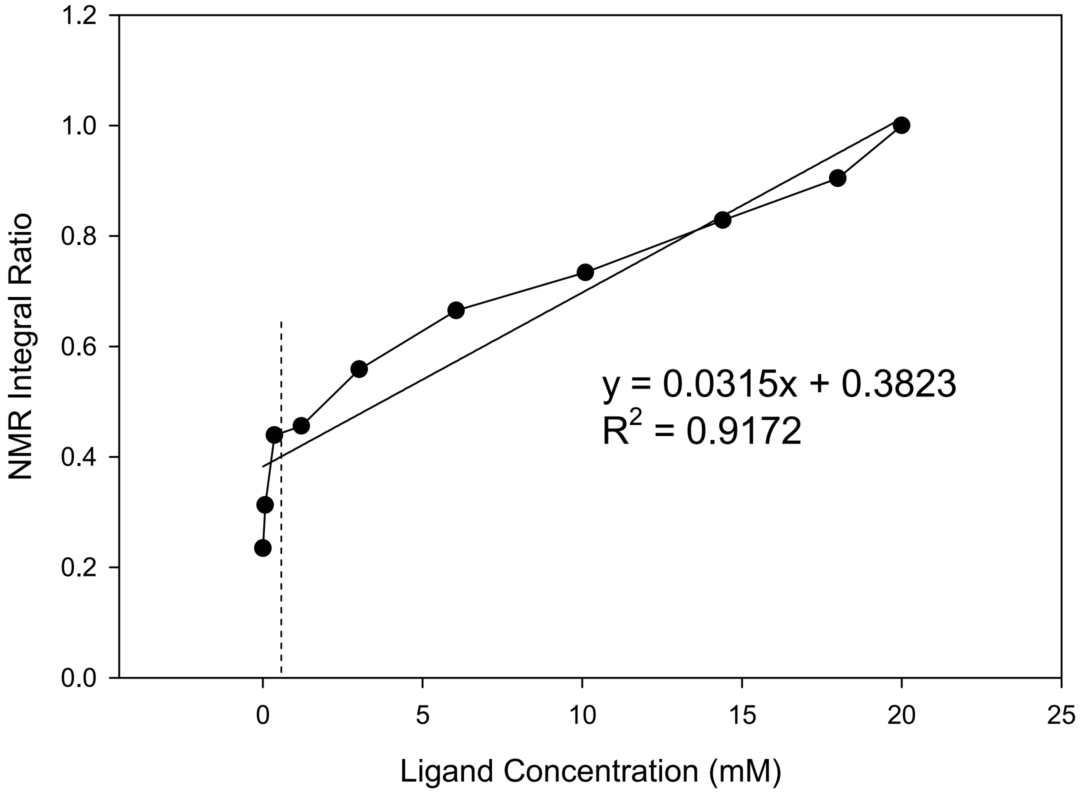

Figure 8. NMR integral ratio calibration as a function of poly(ethylene glycol) concentration as a proof of concept. A serial dilution was used to create a standard curve relating integral ratio to concentration. A R^2 value of 0.9172 demonstrates a proof of concept where NMR can be used as quantitative technique to measure poly(ethylene glycol) concentrations as low as 0.363 mM (vertical dotted line).

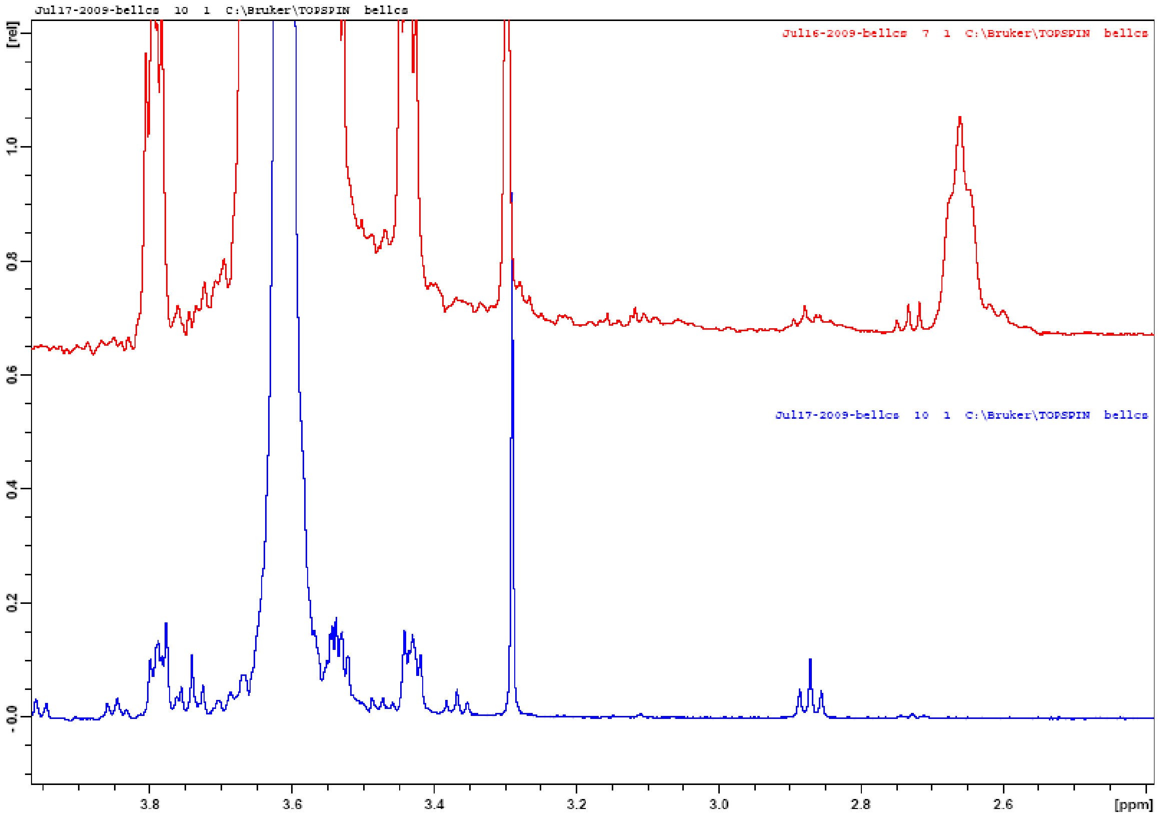

Figure 9. An example of the spectral distinctions between PEG-SH protons and liberated PEG-S-S-PEG protons. Top: 20 mM 5000 MW PEG. Bottom: Decomposed PEG-S-AuMPCs. The appearance of triplet peaks in the sulfide region (~2.8-2.9 ppm) following AuMPC decomposition suggests the expected formation of sulfide bonded PEG to gold from the disulfide bonded reagents.

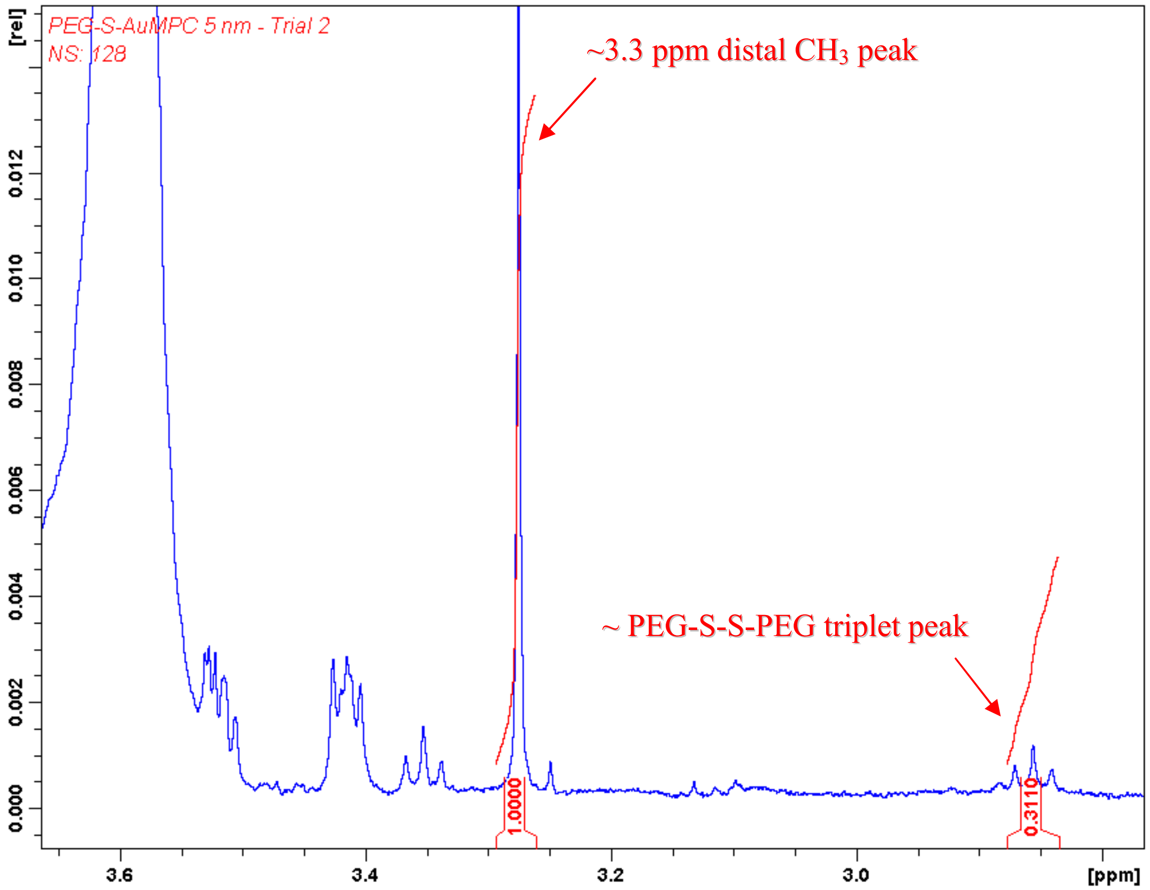

Figure 10. Sample NMR spectra of decomposed PEGylated gold monolayer protected clusters without using pre-saturation protocol. The CH_3- proton peak occurring at ~3.3 ppm represents the distal moiety at the end of the PEG polymer chain thus representing a single S-PEG ligand. The triplet peak occurring between 2.8-2.9 ppm represents the disulfide bond between two sulfur atoms of two S-PEG ligands.

peak to disulfide triplet peak integral-ratios were uploaded into Microsoft Excel. A 20 mM SH-PEG CH_3- peak was also compared to each liberated PEG-S-S-PEG CH_3- peak generating an integral-ratio in order to quantify the concentration of PEG in each sample. Comparing the concentration of PEG in each sample to the CH_3- peak to disulfide integral-ratio, the concentration of PEG-S-S-PEG in each sample can be calculated. The number of ligands per particle can be calculated by dividing the desorbed PEG-S-S-PEG concentration (ligands/volume of sample) by the AuMPC particle concentration (AuMPC particles/volume of sample) and multiplying by 2 - accounting for the dimeric nature of the desorbed PEG. The number of ligands per particle and the number of ligands per particle surface area are shown in Figure 11. Statistical significance between sample points is depicted in each figure. Predictive calculations of ligands per AuMPC and ligands with respect to total AuMPC surface area are shown superimposed in Figure 11 and shown in Figure 13.

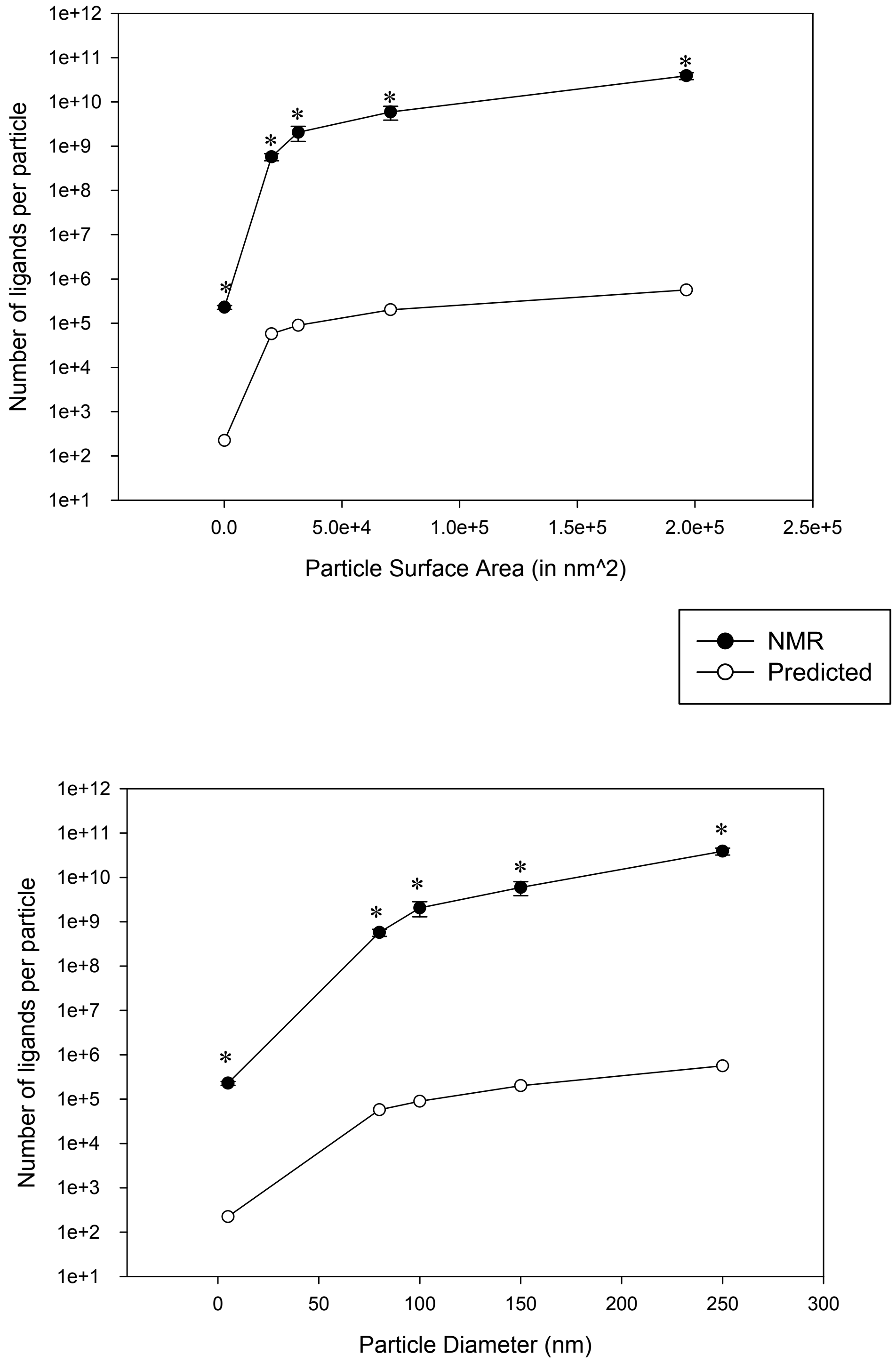

Figure 11. Conjugated ligand enumeration (NMR). Top: number of ligands per particle as a function of particle surface area. Bottom: number of ligands per particle areas a function of particle diameter. Significant size increase for $p<0.05$ using Paired T-Test was not observed.

Discussion

Studying the functionalization efficiency with respect to particle size was the overarching purpose of this work. In our initial assessment, we hypothesized that the molecular footprint of PEG on the surface of gold was constant, but unknown, especially as a function of substrate dimensions. Wuefling et al. estimated that the PEG-SH ligand footprint, the area occupied by the ligand on the surface of 2.8 nm gold particles, was 0.35 nm^2 [1]. Accordingly, we hypothesized that this ligand footprint was constant across a range of particle sizes in a defect-free packing arrangement. Predicted trends calculated based on Wueling et al. and extended to larger particle diameters are shown in Figure 13.

The number of ligands per particle and the number of ligands per particle surface area were calculated from experimental measurements, thus elucidating both ligand enumeration per particle and the surface packing of PEG on gold over a range of particle sizes. Ligand enumeration is shown in Figure 11. The number of ligands per particle via NMR increases with increasing particle size suggesting that the ligand loading of particles increases with available surface area. Comparison with the equivalent data predicted as an extrapolation from Wuefling et al. reveals similar trends with an absolute quantitative offset ranging from three to five orders of magnitude. This large deviation between predicted and actual data is consistent with the superposition of approximately 1 x 10^3 free (unconjugated) PEG ligands in the sample per particle and an increased relative ligand packing efficiency for particle diameters greater than the 2.8 nm used in the Wuefling et al. study.

Evidence for particle size-dependent ligand packing appears as Figure 12. Based on NMR data collected in this work, the number of ligands per particle surface area (ligand packing density) increases as the particle diameter increases. Ligand packing on large (from a molecular perspective), flat surfaces is unconstrained by curvature effects that may influence molecular interactions at the nanoscale. The PEG footprint reported by Wuefling et al. was estimated from association with AuMPC having a 2.8 nm diameter. Relief from nanoscale-induced packing constraints should be evident as the substrate dimensions become large relative to the molecular footprint of the ligand. The PEG ligand footprint of 0.35 nm^2 estimated by Wuefling et al. was obtained on particles with a surface area of 24.6 nm^2. Particle surface areas in this work range from 78.5 nm^2 to 2 x 10^5 nm^2 with the largest areas corresponding to the greatest difference in comparison with Wuefling et al.. This finding is consistent with the speculation of ligand packing constraint due to defects induced by nanoscale surface characteristics. Small molecular differences can have a profound effect on measured ligand packing density. Levin et al. report that that the molecular footprint of a PEG similar to the one used here, but modified to contain a fluorescein molecule, is 10.8 nm^2 on a 90 nm diameter AuMPC. While it is difficult to assess the relative contributions of substrate dimensions and molecular modifications of the ligand footprint, the value reported by Levin et al. is more than 30-fold greater than that by Wuefling et al. In any case, it is clear that the molecular packing density of ligand is reduced as substrate diameter decreases over the range from 250 nm to 5 nm diameter particles (Figure 12). The absolute value of ligand surface concentration should be assessed by an alternate technique to characterize potential contributions due to the presence of unconjugated free ligand, NMR calibration and/or quantitation deficiencies or other factors.

Monitoring of the absorbance of each particle size yielded five distinct SPR curves shown in Figure 3. In addition, each resonance curve had distinct absorbance maximums allowing for the computation of particle concentrations. The surface plasmon resonance curve profile of each particle size across each conjugation trial remained constant showing no SPR changes between conjugation trials following functionalization (Figure 5). Gold concentrations across replicate conjugation trials were found to be in the same order of magnitude suggesting success of the method at determining the unknown PEG-S-AuMPC concentration.

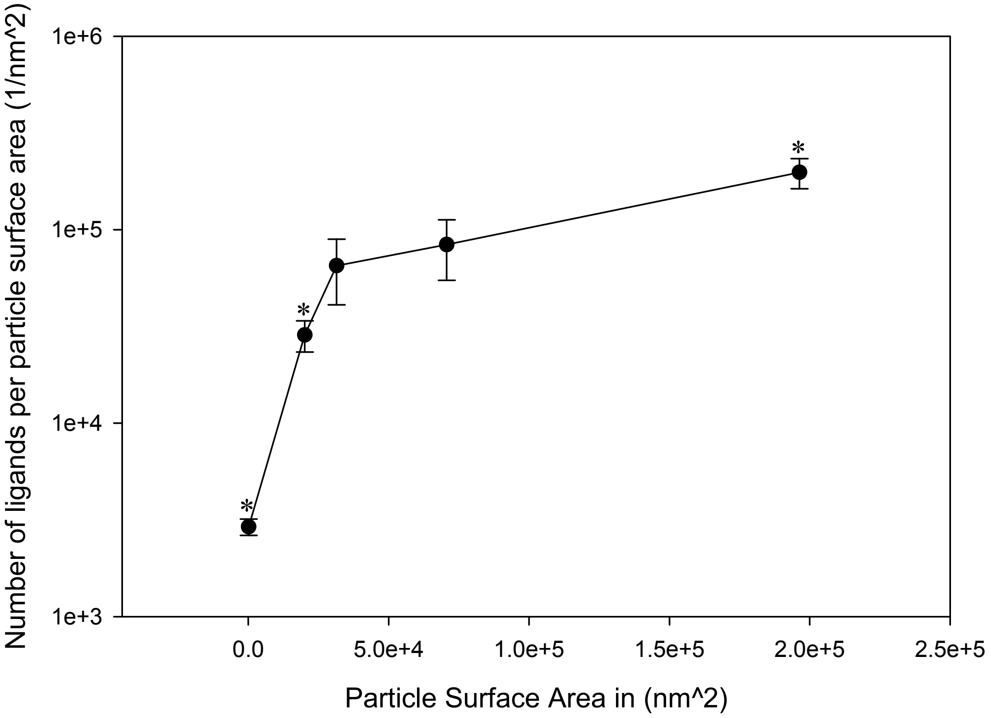

Figure 12. Surface packing of PEG on AuMPC as a function of particle surface area as quantified using NMR. Surface packing is defined as the number of PEG ligands per particle surface area. Data points represent the mean of three independent experiments with error bars as standard deviations. *Significant size increase for $p<0.05$ using Paired T-Test.

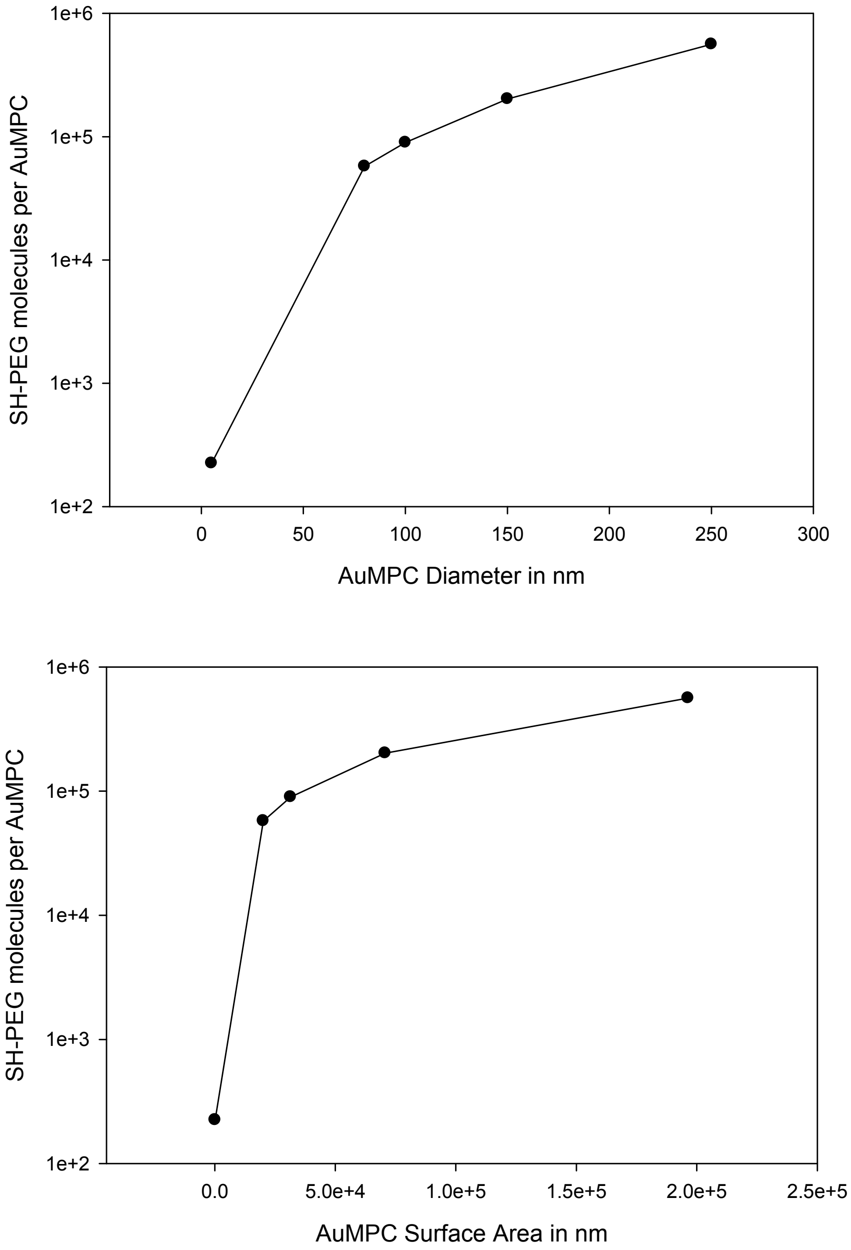

Figure 13. Predicted loading capacity of AuMPCs by SH-PEG. The Wuefling et al. estimation that the PEG-SH ligand footprint, the area occupied by the ligand on the surface of 2.8 nm gold particles, was 0.35 nm^2 was used to generate these estimates for AuMPC of greater diameter by extrapolation.

Particle conjugation was assessed using DLS. A significant increase in the hydrodynamic radii of the particles in solution was used to confirm conjugation. Unconjugated particle sizes 5, 80, 100, 150 and 250 nm in size were accurately measured by the DLS. Conjugated particles were measured and gold particles 80, 100, 150 and 250 nm in diameter were shown to significantly increase in size. The size increase was fully apparent in the 5 nm gold particles; however, the large standard deviation between conjugation trials lead to a statistical indifference. It can be ascertained that this large deviation could be due the agglomeration of unconjugated particles prior to functionalization[46] or the fact that the 5 nm particle size is near the detection limit of the instrument. A quantitative technique in this regard, DLS data was used to elucidate PEG layer thickness. Determination of the size increase of the AuMPCs following conjugation elucidates the radial thickness of the affixed PEG layer. This data, coupled with the approximate length of an individual PEG ligand, will provide some insight into the conformation of the PEG conjugates on the surface of AuMPCs. Such speculation will be confirmed in concert with the addition of the corroborative ligand enumerative strategy, ICP-AES.

References

1. Wuelfing, W.P.G., Stephen M.; Miles, Deon T.; Murray, Royce W. , *Nanometer Gold Clusters Protected by Surface-Bound Monolayers of Thiolated Poly(ethylene glycol) Polymer Electrolyte.* Journal of the American Chemical Society, 1998. **120**(48): p. 12696-12697.
2. Daniel, M.-C.A., Didier *Gold Nanoparticles: Assembly, Supramolecular Chemistry, Quantum-Size-Related Properties, and Applications toward Biology, Catalysis, and Nanotechnology* Chemical Reviews (Washington, DC, United States), 2004. **104**(1): p. 293-346.
3. White, C.W.Z., D. S.; Budai, J. D.; Zuhr, R. A.; Magruder, R. H., III; Osborne, D. H. , *Colloidal Au nanoclusters formed in fused silica by MeV ion implantation and annealing* Materials Research Society Symposium Proceedings, 1994 **316**(Materials Synthesis and Processing Using Ion Beams): p. 499-506.
4. Faraday, M., *Experimental relations of gold (and other metals) to light.* Philos. Trans. R. Soc. London., 1857. **147**: p. 145.
5. Weiser, H.B., Inorganic Colloid Chemistry, 1933. **1**: p. 21-57.
6. Hayat, M.A., *Colloidal Gold: Principles, Methods, and Applications*. Vol. 1. 1989, San Diego, Calif: Academic Press, Inc. 536.
7. Handley, D.A., *The Development and Application of Colloidal GTold as a Microscopic Probe*, in *Colloidal Gold: Principles, Methods, and Applications*, M.A. Hayat, Editor. 1989, Academic Press, Inc.: San Diego, Calif. p. 1-8.
8. Handley, D.A., *Methods for Synthesis of Collodial Gold*, in *Colloidal Gold: Priniciples, Methods, and Applications*, M.A. Hayat, Editor. 1989, Academic Press, Inc.: San Diego, Calif. p. 13-31.
9. Brust, M.W., Merryl; Bethell, Donald; Schiffrin, David J.; Whyman, Robin *Synthesis of thiol-derivatized gold nanoparticles in a two-phase liquid-liquid system* Journal of the Chemical Society, Chemical Communications, 1994(7): p. 801-802.
10. Turkevitch, J., Discuss. Faraday Soc., 1951. **11**: p. 55-59.
11. Yonezawa, T.K., T., *Practical Preparation of Anionic Mercapto Ligand-Stabilized Gold Nanoparticles and Their Immobilization.* Colloids Surf. A: Physicochem. Eng. Asp., 1999. **149**: p. Colloids Surf. A: Physicochem. Eng. Asp.
12. Brust, M.F., J.; Bethell, D.; Schiffrin, D. J.; Kiely, C. J., *Synthesis and Reactions of Functionalised Gold Nanoparticles.* J. Chem. Soc., Chem. Commun., 1995: p. 1655-1656.
13. Templeton, A.C.W., W. Peter; Murray, Royce W. , *Monolayer-Protected Cluster Molecules* Accounts of Chemical Research, 2000. **33**(1): p. 27-36.
14. Hostetler, M.J.G., Stephen J.; Stokes, Jennifer J.; Murray, Royce W. , *Monolayers in three dimensions: synthesis and electrochemistry of ω-functionalized alkanethiolate-stabilized gold cluster compounds.* Journal of the American Chemical Society, 1996. **118**(17): p. 4212-4213.

15. Chen, S.M., Royce W., *Arenethiolate Monolayer-Protected Gold Clusters* Langmuir, 1999. **15**(3): p. 682-689.
16. Antonii, F., *Panacea Aurea-Auro Potabile*, in *Bibliopolio Frobeniano*. 1618: Hamburg.
17. Lv M, Z.E., Su Y, Li Q, Li W, Zhao Y, Huang Q, *Trypsin-Gold Nanoparticle Conjugates: Binding, Enzymatic Activity, and Stability.* Preparative Biochemistry and Biotechnology, 2009. **39**(4): p. 429-438.
18. Roa W, Z.X., Guo L, Shaw A, Hu X, Xiong Y, Gulavita S, Patel S, Sun X, Chen J, Moore R, Xing JZ., *Gold nanoparticle sensitize radiotherapy of prostate cancer cells by regulation of the cell cycle. .* Nanotechnology 2009. **2**(37).
19. Prabaharan M, G.J., Pilla S, Steeber DA, Gong S., *Gold nanoparticles with a monolayer of doxorubicin-conjugated amphiphilic block copolymer for tumor-targeted drug delivery.* Biomaterials, 2009. **30**(30): p. 6065-75.
20. Jain RK, G.L., *Extravascular transport in normal and tumor tissues.* Crit Rev Oncol Hematol., 1986. **5**(2): p. 115-70.
21. Pegaz B, D.E., Ballini JP, Konan-Kouakou YN, van den Bergh H, *Effect of nanoparticle size on the extravasation and the photothrombic activity of meso(p-tetracarboxyphenyl)porphyrin.* J Photochem Photobiol B., 2006. **85**(3): p. 216-22.
22. Ishida O, M.K., Sasaki K, Iwatsuru M., *Size-dependent extravasation and interstitial localization of polyethyleneglycol liposomes in solid tumor-bearing mice.* Int J Pharm., 1999. **190**(1): p. 49-56.
23. Unezaki S, M.K., Hosoda J, et al., *Direct measurement of extravasation of polyethyleneglycol-coated liposomes into solid tumor tissue by in vivo fluorescence microscopy.* Int J Pharm 1996. **144**: p. 11-7.
24. Kong G, B.R., Dewhirst MW., *Hyperthermia enables tumor-specific nanoparticle delivery: effect of particle size.* Cancer Res., 2000 **60**(16): p. 4440-5.
25. Olivier JC, H.R., Lee HJ, Calon F, Pardridge WM., *Synthesis of PEGylated immunonanoparticles.* Pharm Res., 2002 **19**(8): p. 1137-43.
26. Marsh D, B.R., Sportelli L., *Lipid membranes with grafted polymers: physicochemical aspects.* Biochim Biophys Acta, 2003 **1615**(1-2): p. 33-59.
27. Klemperer, P., *The reticulo-endothelial system.* Hawaii Med J., 1948. **8**(2): p. 96.
28. Marshall AH, W.R., *Reactions of the reticular tissues to antigens.* Br J Exp Pathol., 1950 **31**(2): p. 157-74.
29. Crawford, J., Cancer treat. Rev., 2002. **A**: p. 7-11.
30. al., D.O.N.e., Cancer Lett., 2004. **209**: p. 171-176.
31. al., L.H.e., Proc. Natl. Acad. Sci. U.S.A., 2004. **100**: p. 13549-13554.
32. Loo C, L.A., Halas N, West J, Drezek R., *Immunotargeted nanoshells for integrated cancer imaging and therapy.* Nano Lett., 2005. **5**(4): p. 709-711.
33. Loo C, L.A., Hirsch L, Lee MH, Barton J, Halas N, West J, Drezek R., *Nanoshell-enabled photonics-based imaging and therapy of cancer.* Technol Cancer Res Treat., 2004 **3**(1): p. 33-40.
34. Gooden, J., *Nuclear resonance and magnetic field changes of 1 in 106.* Nature, 1950. **165**(4208): p. 1014-5.
35. Sheppard, N., *Appendix-Notes on the nuclear-magnetic-resonance spectrum of omega-fluorodecanoic acid and of a fluoro-octadecenoic acid of unknown structure.* Biochem J. , 1960. **77**(1): p. 22-3.

36. JH Ridd, R.W., *Nuclear magnetic resonance spectrum of beta-pyrazol-1-ylalanine.* Biochem J., 1960. **77**: p. 546-7.
37. F. Bloch, W.H.a.M.P., *Nuclear induction.* Phys. Rev., 1946. **69**: p. 127.
38. Swift TJ, F.O.J., *A proton spin-echo study of the state of water in frog nerves.* Biophys J., 1969 **9**(1): p. 54-9.
39. Claridge, T.D.W., *High Resolution NMR Techniques in Organic Chemistry*. Tetrahedron Organic Chemistry Series, ed. J.E.B. J.-E. Backvall, R.M. Williams. Vol. 27. 2009, Amsterdam: Elsevier.
40. Ailette Aguila, R.W.M., *Monolayer-Protected Clusters with Fluorescent Dansyl Ligands.* Langmuir, 2000. **16**(14): p. 5949–5954.
41. Hurst SJ, L.-J.A., Mirkin CA., *Maximizing DNA loading on a range of gold nanoparticle sizes.* Anal Chem., 2006. **78**(24): p. 8313-8.
42. S Takae, Y.A., H Otsuka, T Nakamura, Y Nagasaki, K Kataoka, *Ligand Density Effect on Biorecognition by PEGylated Gold Nanoparticles: Regulated Interaction of RCA120 Lectin with Lactose Installed to the Distal End of Tethered PEG Strands on Gold Surface.* Biomacromolecules, 2005. **6**: p. 818-824.
43. Verma A, U.O., Hu Y, Hu Y, Han HS, Watson N, Chen S, Irvine DJ, Stellacci F., *Surface-structure-regulated cell-membrane penetration by monolayer-protected nanoparticles.* Nat Mater., 2008. **7**(7): p. 588-95.
44. Templeton AC, H.M., Kraft CT, and Murray RC, *Reactivity of Monolayer-Protected Gold Cluster Molecules: Steric Effects.* J. Am. Chem. Soc., 1998. **120**(8): p. 1906-1911.
45. Eck W, C.G., Sigdel A, Ritter G, Old LJ, Tang L, Brennan MF, Allen PJ, Mason MD, *PEGylated gold nanoparticles conjugated to monoclonal F19 antibodies as targeted labeling agents for human pancreatic carcinoma tissue.* ACS Nano, 2008. **2**(11): p. 2263-72.
46. Robin, J.T., Christian *Stimulated emission of aluminum and titanium resonance lines at very low concentration in a HF [high frequency] argon plasma.* Sciences Physiques, 1975. **281**(16): p. 345-7.
47. Lichte, F.K., SR, *Induction coupled plasma emission from a different angle.* ICP. Inf. Newsl., 1976. **2**: p. 192.
48. Lichte, F.E.K., S. R., *A simplified torch design for inductively coupled plasma optical emission spectrometry.* ICP Information Newsletter, 1976. **1**(9): p. 200-2.
49. H Karami, O.R.-O., *Synthesis of Iron Nanoclusters by Pulsed Current Method.* . Journal of Cluster Science 2009. **20**(3): p. 587-600.
50. K. Zhu, J.H., and R. Richards., *Aerobic oxidation of cyclohexane by gold nanoparticles immobilized upon mesoporous silica.* Catalysis Letters, 2005. **100**(3-4): p. 195-199.
51. Fischer, H.F.-B., S; Pang, KS; Chan, WCW, *Quantitative detection of engineered nanoparticles in tissues and organs: an investigation of efficacy and linear dynamic ranges using ICP-AES.* NanoBiotechnology 2007. **3**(1): p. 46-54.
52. Hill, S., *Inductively Coupled Plasma Spectrometry and its Applications*. Analytical Chemistry, ed. A.J.H.a.J.M. Chalmers. 2007, Oxford: Blackwell Publishing Ltd.
53. Harris JM, M.N., Modi M., *Pegylation: a novel process for modifying pharmacokinetics.* Clinical Pharmacokinetics, 2001. **40**(7): p. 539-51.

54. Frisman I, S.D., Bianco-Peled H., *Nanostructuring of PEG-fibrinogen polyneric scaffolds.* Acta Biomaterialia, 2009. **Article in Press**.

CHAPTER III

Manuscript: INDUCTIVELY COUPLED PLASMA ATOMIC EMISSION SPECTROSCOPY AS A NEW TOOL FOR QUANTIFICATION OF THIOLATED CONJUGATES BOUND TO GOLD NANOPARTICLES

Introduction

History. Gold monolayer protected clusters[1] (AuMPCs), also commonly recognized as gold nanoparticles[2], gold nanoclusters[3] or gold colloid[4], are among the oldest[5] and most studied metallic-core based particles used in biomedical applications. Colloidal gold is the formation of nanometer-sized gold particles in solution stabilized by salts or passivating compounds[6]. A number of methods for the formation of colloidal gold have been introduced in literature[8] including the two most popular methods: the Brust-Schiffrin Method[9] and the Turkevitch reaction[10]. The Brust-Schiffrin method pioneered colloid technology by using Faraday's early two-phase system[4] with the use of thiol ligands that strongly bind gold due to the soft character of both gold and sulfur[9].

Recognizing their ability to actively change the surface properties of gold colloid, Brust et al. augmented their reaction protocols to include *p*-mercaptophenol stabilized gold colloids, thus extending gold colloid synthesis to gold colloid *functionalization* allowing colloid stabilization by a plethora of functional thiolated ligands[12]. This advancement in colloid technology led to the eventual determination of the reactions which describe gold functionalization. Described by the Murray group, the place exchange reaction describes the replacement of a controlled proportion of stabilizing salts or thiols with a variety of functional thiols[13]. With the ability to be protected and functionalized by a layer of functional molecules, gold colloids of this form were phrased gold monolayer-protected clusters[14, 15].

Poly(ethylene glycol). One such surface modifier used to functionalize colloidal gold is thiolated polyethylene glycol (SH-PEG)[25]. It can be assumed that polyethylene glycol ligands conjugate to gold surfaces in a particular conformation. Comparably, polyethylene glycol forms two distinctly different molecular conformations when grafted onto lipid membranes: “brush” and “mushroom” conformations[26]. The mushroom conformation is formed when a low packing density is maintained and ligand chains are oriented randomly. Contrarily, a ~10-fold greater packing density with a more extended and weaker chain alignment forms the brush conformation.

Moreover, polyethylene glycol is known for its ability to resist the activity of the reticuloendothelial system. This innate biological defense mechanism is a system composed of monocytes and macrophages that is located near reticular connective tissue such as the spleen[27]. The inherent purpose of these cells is for phagocytosing and removing cellular debris, pathogens and foreign substances, the intravascular nanoparticles for example, from the bloodstream[28]. A surface passivant, PEG is used throughout medical literature to thwart the activity of the RES. For instance, the attachment of PEG to oncological pharmaceuticals, such as interferon-α, is currently used to lengthen the circulation time of these molecules in the bloodstream [29]. This reduces the frequency of administration of these drugs thus increasing therapeutic efficacy and patient tolerance. In addition, PEG has been used with gold nanoshells - metallodielectric nanoparticles consisting of a spherical dielectric core coated with a thin metallic shell. Used in photothermal cancer therapy, gold nanoshells can be loaded with thiolated polyethylene glycol coatings to reduce unwanted protein adhesion under targeted local or systemic delivery [30, 31]. Thereafter, surface passivation of these nanoparticles using bound thiolated PEG, in concert with conjugated antibodies, assisted in maintaining antibody activity in targeted delivery[32, 33].

It can be hypothesized that the efficacy of surface passivation is dependent on the amount surface coverage by polyethylene glycol. Quantifying the number of polyethylene glycol ligands on the surface – the functionalization efficiency - of gold nanoparticles will elucidate the passivation efficacy. Devising a method to determine the functionalization efficiency of SH-PEG on gold nanoparticles will facilitate future quantification for other thiolated functional groups.

Nuclear Magnetic Resonance. A number of analytical techniques have been instituted in order to enumerate the number of conjugated molecules on the surface of a nanoparticle. Used in organic and medicinal chemistry, Nuclear magnetic resonance (NMR) spectroscopy is a common technique used in order to identify compounds, characterize unknown samples, or confirm chemical structures following synthesis[34-36]. NMR helps to identify the carbon-hydrogen framework of an organic compound.

Spectroscopists instituted the use of spectrum peak integration in order to use NMR as a quantitative technique [38]. The extensive use of integration in ^{1}H NMR arises from the renowned doctrine that "the area of an NMR resonance is proportional to the relative number of nuclei giving rise to it." Although routine use of ^{1}H NMR integration yields only 10-20% accuracy[39], its use is paramount in the field of quantifying ligands conjugated to gold nanoparticles - following decomposition allowing desorption of the ligands[40].

Previous Ligand Enumeration Strategies. A number of previous endeavors at quantifying the number of ligands on the surface of gold nanoparticles with respect to particle size have been conducted. Hurst and Lytton-Jean et al. investigated the parameters that influence coverage on gold nanoparticles[41]. Analytically evaluating the effects of salt concentration, spacer composition, nanoparticle size, and degree of sonication, maximum loading was obtained by salt aging the nanoparticles in the presence of DNA containing a PEG spacing in ~0.7 M NaCl. To quantify the surface loading of DNA on the gold colloid, oligonucleotides were labeled with a fluorescent tag - 6'FAM3' – and quantified by comparing the ligand concentration (measured by fluorescence) and the gold concentration (determined by UV-Visible spectroscopy). As a result, larger nanoparticles (250 nm) were found to have orders of magnitude higher DNA loading than smaller (13-30 nm) nanoparticles. This disparity was thought to be due to their larger surface area. Other groups have used fluorescence as the primary source of ligand quantification. Other groups used lactose molecules, labeled to the distal ends of the PEG ligands, and thermogravimetric analysis (TGA)[42]. Using the TGA, the weight decrease of PEG, due to its thermal decomposition, was measured. The number of PEG chains on each gold particle was calculated by using the concentration of gold particles and the weight loss measured by the TGA.

Although all studies seeking to quantify the loading of their gold particles were successful, here, we aim to quantify the number of PEG ligands on the surface of our AuMPCs using only "label-free" methods which will not affect surface loading or require decomposition of a significant amount of sample.

ICP-AES. Inductively coupled plasma atomic emission spectroscopy (ICP-AES), also referred to as inductively coupled plasma optical emission spectroscopy (ICP-OES), is an analytical technique normally used to assist in the detection of trace metals in collected or synthesized samples [47, 48]. Using a stream of inductively coupled plasma[49], a plasma source supplied energetically by electrical currents which are produced by time varying magnetic fields, excited atoms are generated that emit electromagnetic radiation at wavelengths characteristics of that element. The intensity of the emission of electromagnetic radiation is quantitatively correlated with the concentration of each element in the sample.

There are a number of applications of current use for ICP-AES in the field of biomedical engineering. Karami and Rostami-Ostadkalayeh used ICP-AES during their investigation into the synthesis of iron nanoclusters with more porous structure using a pulsed current electrochemical method[50]. In this study ICP-AES was used for bulk analysis of the optimum iron nanocluster samples. Revealing elemental composition with more precision than X-ray diffraction (XRD) and energy-dispersive X-ray spectroscopy (EDX) measurements, ICP-AES was used to confirm that the silver composition of each sample was lower than 0.01 %wt, thus negligible. XRD and EDX were also used, however, this silver impurity was not detected due to the fact that the silver was located at the center of each iron nanoparticle (silver is the starting agent for crystallization). Concordantly, Zhu et al. investigated aerobic oxidation by immobilized gold nanoparticles and used ICP-AES to measure the gold content of the gold immobilized silica mesostructure samples[51]. As a further example, Fischer et al. employed ICP-AES in order to determine *in vivo* nanoparticle kinetics and distribution using a non-isotopic quantification method [52]. The authors concluded that ICP-AES was an effective method for detecting CdSe/ZnS quantum dots and gold nanoparticles in biological tissue because the elemental detection sensitivity of the instrument, in moles of particles per gram, was at a suitable limit. One limitation discovered was that ICP-AES could not detect Fe_3O_4 nanoparticles effectively in these biological samples. The authors attributed this limitation to the presence of natural Fe^{2+} in tissues, thus illustrating the fact that the technique should not be utilized for measuring nanoparticles or biomaterials composed of endogenous elements.

More specifically, concerning the mechanism by which the ICP-AES measures the atomic concentration, when a sample in aerosol form enters the central channel of the inductively coupled plasma, a number of specific events occur[53]. The sample dissolves, the matrix breaks down and the resulting analyte and solvent vapor undergo excitation to produce atomic and ionic species in various energy states. Some of this energy is released as electromagnetic radiation at a wavelength which is characteristic of the emitting atom or molecule. Elemental concentrations determined by the intensity of the element's electromagnetic radiation, as compared to an elemental standard curve, are obtained from ICP-AES in mg/L. Using the elemental concentration of sulfur and gold and basic stoichiometry, one can calculate the number of sulfur atoms per gold nanoparticle, thus quantifying the number of PEG ligands on the AuMPC-PEG constructs studies in this work.

More advantageous than other forms used in literature as a quantification technique, ICP-AES does not require the use of surface-density altering ligands nor does it require the thermal or chemical decomposition of a large quantity of sample. Other methods of enumerating the number of ligands attached to AuMPCs use fluorescently tagged or labeled PEG agents which may affect the packing of those ligands or involve protocols which require the destruction of large quantities of material. Here, we both enumerate the number of PEG ligands on the surface using a "label-free," ICP-AES based method and characterize the loading capacity over a range of nanoparticle sizes. We will also compare the findings from the ICP-AES measurements against predicted considerations. As in the NMR study, here we will also obtain information regarding the functionalization efficiency of PEG on AuMPCs with respect to particle size and surface area. Thereafter, we will examine how PEG ligands are concentrated or packed onto the surface of varying sizes of AuMPCs. Such knowledge will enable a deeper insight into the efficacy of nanotechnology as it is related to and possibly governed by the functionalization efficiency of its individual technological apparatus.

Materials and Methods

Nanomaterials. Unconjugated AuMPCs 80, 100, 150 nm in diameter were acquired from TedPella, Inc. (Redding, CA). Lyophilized SH-PEG (5,000 MW) was purchased from Laysan Bio, Inc. (Arab, AL). 70% HNO_3 (Nitric Acid), and both 1000 mg/L Gold in 10% HCl and 1000 mg/L Sulfur in H_2O ICP-AES element calibration standards were purchased from Thermo Fisher Scientific, Inc. (Waltham, MA). MilliQ® grade (Millipore Corporation, Billerica, MA) deionizied water (DI H_2O), obtained using a MilliQ® Academic System outfitted with a Quantum® EX Ultrapure Organex Cartridge, was utilized throughout all experimental phases.

Instrumentation and Assays. Absorbance measurements of AuMPCs were gathered using a Varian Cary 5000 UV-VIS-NIR spectrophotometer (Varian, Inc., Palo Alto, CA). Particle diameter measurements were acquired using a Malvern Zetasizer Nano ZS dynamic light scattering based system (Malvern Instruments, Westborough, MA). Baseline SH-PEG concentrations following osmotic dialysis were obtained using the Measure-iT™ Thiol Assay Kit (Invitrogen Corporation, Carlsbad, CA) and the Perkin Elmer LS 50 B Luminescence Spectrometer. NMR measurements were acquired using a 400 Hz instrument equipped with a 9.4 Tesla Oxford magnet which is controlled by a Bruker AV-400 console. ICP-AES measurements were collected using a Varian 720-ES Inductively-coupled Plasma Atomic Emissions Spectrometer (ICP-AES).

Predicted Loading Capacity. For analytical comparison with results from ICP-AES measurements, the predicted loading capacity was calculated. It was assumed that

AuMPCs form spherical clusters and follow the fundamental surface area formulae, $SA=4\pi r^2$. In addition, it was assumed that SH-PEG ligands adsorb onto AuMPCs assuming the Brush conformation as discussed by Wuelfing et al [1]. The Brush conformation of SH-PEG occupies a molecular surface area footprint of 0.35 nm^2 on colloidal gold. The maximum number of SH-PEG ligands per AuMPC was calculated by dividing the total surface area of a spherical AuMPC by the SH-PEG molecular footprint. The maximum number of SH-PEG ligands per AuMPC was calculated for each particle size.

Place Exchange Reaction. A clear 20 mM solution of SH-PEG was generated by adding lyophilized SH-PEG to DI H_2O at room temperature (23°C). Unconjugated AuMPCs at their stock concentration were vortexed, to ensure even suspension in solution, and added to the SH-PEG solution at a 1:1 volumetric ratio. Following a slow overnight stir, using a miniature magnetic stirring bar and stir plate thus allowing sufficient time for maximal functionalization, free citrate and unconjugated SH-PEG ligands were removed using a Thermo Fisher Scientific Inc. Slide-A-Lyzer® osmotic dialysis cassette with a membrane molecular weight cutoff of 10,000 MW. PEGylated AuMPCs (PEG-S-AuMPCs) were harvested from the cassettes and stored at 5°C. Three conjugation trials (n=3) were performed for each particle size to assess the variability of the conjugation protocol.

Determination of Unknown AuMPC Concentrations. Following the conjugation and osmotic dialysis of PEGylated AuMPCs, the resultant AuMPC concentration is unknown. In order to determine unknown concentrations, absorbance vs. known concentration standard curves were generated for each particle size using unconjugated stock AuMPC solutions and UV-VIS analysis. From the creation of the standard curves, both the molar extinction coefficient (ε) and the absorbance maxima (λ) were determined for each particle size. The absorbance values of conjugated AuMPC solutions of unknown concentration were then correlated to the standard curves using Beer's law ($A=\varepsilon lc$) to determine the subsequent concentration.

Conjugation Confirmation. Following the overnight place exchange reaction, SH-PEG conjugation was confirmed by monitoring the diameter of the AuMPCs with dynamic light scattering. Stock solutions of the unconjugated AuMPCs were used as size controls for each particle diameter. Each conjugation trial was evaluated to assess the variability of diameter increase due to the execution of the conjugation protocol. PEG-S-AuMPCs were removed from the 5°C storage environment, allowed to warm to room temperature and vortexed for a minimum of five seconds to ensure colloidal resuspension. 1 ml of each conjugation trial was loaded into a low volume disposable cassette. Prior to measurement initialization, each cuvette was tilted back and forth three times to ensure colloidal resuspension. Typical count rates were between 100 and 350 kcps. Size-distribution profiles and average radii for each conjugation trial were obtained as the mean of triplicate measurements. Each conjugated trial average diameter was statistically compared against the unconjugated control diameter using the Paired t-test.

Determination of the Free Thiol Baseline. In order to determine both the effectiveness of the osmotic dialysis at removal of the free thiol and to determine a baseline concentration of the free SH-PEG ligands contained in the conjugated AuMPC solutions, a NMR-based free thiol measurement protocol was employed

The most reliable form of compound quantification, and therefore primary form, available to the authors was ^{1}H NMR. Here, we instituted a novel method of reliably determining the free thiol baseline in each sample. The free thiol baseline was measured via a 400 MHz instrument equipped with a 9.4 Tesla Oxford magnet controlled by a Bruker AV-400 console. The main NMR probe for the instrument was a 5 mm Z-gradient broadband inverse (BBI) probe with automatic tuning and matching capability (ATM). Samples of each conjugation trial for each particle size were obtained and equalized to a concentration of 49 μM at a volume of 500 μl. Each sample was placed into a Wilmad LabGlass (Vineland, NJ) 5MM Thin Wall, 7" Length, 500 MHz NMR tube.

In order to quantify the number of ligands on the surface of the AuMPCs using NMR, the ligands must be removed from the surface of the nanoparticle. In order to achieve this desorption, one to two large iodine (I_2) crystals were added to each tube. Chemically, the iodine has a higher affinity for the gold than the sulfur molecules [43]. Due to this disparity in affinity, the iodine decomposes the AuMPCs where the SH-PEG molecules are released into solution. This place-exchange reaction of thiol for iodine to the gold clusters causes destabilization causing the iodinated gold to fall out of solution [44] into a dark brown solid. Typically, when thiolated ligands desorb from gold particles, they form disulfide bonds [14]. In addition, iodine decomposition was allowed to occur to completion for one hour as previously described [40] prior to spectrum measurement. In order for the NMR to "lock" onto each sample, each tube was spiked with 50 µl of D_2O creating a H_2O+D_2O based solvent.

To ensure a spectrum of the decomposed gold and emancipated ligands could be acquired, a pre-saturation technique was employed to suppress the enormous peak typically generated by H_2O. This allowed ample visualization of the more subtle peaks in the resulting spectrum. Each sample was measured following the same major parameters. The number of scans and receiver gain was held to 32. For the f1 channel, P0 and P1 were both held to 11.38 µs. One spectrum was collected per sample to ensure conjugate desorption was occurring.

In order to quantify the concentration of desorbed conjugates, the pre-saturation technique cannot be employed due to its inherent modulation of the spectrum baseline. Such modulation introduces error into any integral based quantification strategies. Therefore, a more common "zg30" program was used to acquire a spectrum for quantification methods to be implemented. The number of scans was set to 16 whereas the receiver gain was held to 4. A delay (D1) of 10 seconds was added between scans thus ensuring a large enough relaxation time to minimize the effect of the H_2O peak on more subtle peaks. For the f1 channel, P1 was held to 11.38 µs. One spectrum was acquired per sample and integration was used enumerate the ratio between the PEG chain terminal group, CH_3-, peak and the disulfide, PEG-S-S-PEG, bond triplet peaks. Prior to any integration, all spectra were baseline corrected to zero using automatic and manual processes.

A serial dilution was also performed in order to generate a standard curve relating concentration to integral-ratio. In order to generate such integral-ratio values, the PEG terminal CH_3- peak for a concentration of a 20 mM SH-PEG was directly compared to the CH_3- peaks of samples containing lower concentrations of SH-PEG. This comparison was achieved via spectral summation of the 20 mM SH-PEG with a ppm shifted spectra containing a lower conjugate concentration (APPENDIX C). Integration was used in order to determine the integral-ratio between the 20 mM sample peak and the lesser concentration peak. A standard curve was then generated from integral-ratios of all samples in comparison to the 20 mM peak.

Desorbed-conjugate spectrums containing CH_3- peaks were then compared to the 20 mM SH-PEG CH_3- peak generating an integral-ratio. This integral ratio can be used to quantify the concentration of PEG ligands in the desorbed-conjugate sample. Using the difference in the integral-ratio between the CH_3- peaks and the triplet disulfide (PEG-S-S-PEG) peaks from unity (1-integral ratio), the number of S-PEG ligands that in no way came into contact with the gold colloid can be quantified.

Quantification of Functionalized Conjugates. The number of polyethylene glycol ligands conjugated to the surface of each AuMPC was quantified using a 720-ES Varian ICP-AES. Samples of each conjugation trial for each particle size were obtained and equalized to a concentration of 49 μM at 5 ml in volume. 50 μl of 1% nitric acid in DI H_2O was added to each sample to provide a viable matrix for the ICP-AES instrument. One emission wavelength per element was used to indicate the gold and the SH-PEG ligand concentration (267.54 and 181.972 nm for Au and S). Using the certified elemental calibration standards, a 5-point calibration, including a blanked sample, was performed. Samples and calibration standards, assayed at the same emission wavelengths, were compared for quantification in compliance with the following instrumental analysis conditions. Nebulizer flow, necessary in order to spray the sample into the plasma, was held to 0.75 L/min. The radio frequency power was adjusted to 1.2 kW. The plasma gas flow and auxiliary gas flow was held to 15 and 1.5 L/min. The internal standard used for all of measurements was yttrium. The replicate read time (read time per sample) was 5 sec and there were 3 replicates per reading. Results for each conjugation trial per each particle size were exported in elemental concentrations of gold and sulfur in mg/L.

The free thiol baseline from both the ^{1}H NMR and Thiol Assay Kit were compared for congruency. Following conversion of all units to molar concentrations, the relative free thiol concentration from the ^{1}H NMR was subtracted from the total sulfur concentration yielding the true molar concentration of thiol groups attached to the AuMPCs. These sulfur concentrations with their respective gold concentration were then expressed in sulfur molecules per AuMPC for each trial per each particle diameter.

Statistical Analysis. Statistical Analysis was conducted using SigmaStat software. Paired t-tests were conducted with a confidence interval of 99%.

Results

Determination of Unknown AuMPC Concentration. In order to determine the AuMPC concentration following particle purification, the surface plasmon resonance was obtained by monitoring the UV-Vis spectra of each unconjugated particle size (Figure 3). Standard absorbance-concentration curves were produced (Figure 4). The molar extinction coefficient was determined in accordance with Beer's law. The absorbance maxima (λ in mm) and molar extinction coefficients (ε in $Lmol^{-1}cm^{-1}$) are shown in Table 1. Following particle purification, the AuMPC concentrations were determined via Beer's law by monitoring the absorbance maxima of the surface plasmon resonance curves (Figure 5).

Conjugation Confirmation. Particle conjugation was assessed by monitoring the hydrodynamic radii of each conjugation trial. Used as a quantitative technique for qualitative assessment, significant increases in diameter increases were used to implicate conjugation. Dynamic light scattering results are shown in Figure 6. Dynamic light scattering correctly sized unconjugated particle sizes. The size increase of the AuMPCs following PEGylation was also monitored using DLS. This size increase represents the radial thickness of the conjugated PEG coat and was found to be significantly different for all particle diameters except 5 nm.

Determination of the Free Thiol Baseline. The free thiol baseline was quantified using NMR spectroscopy. Integral ratios between peaks were acquired and analyzed in

Bruker's TopSpin program. All non pre-saturated acquired and analyzed PEG-S-AuMPC spectrums depicting integral ratios used in this work are shown in APPENDIX B.

As a proof of concept a serial dilution was used to create a standard curve relating integral ratio to concentration. A coefficient of determination (R^2) value larger than 0.9 was used as a cutoff value to prove linear congruency. The linear fit with R^2 value and resulting equation is shown in Figure 8. A R^2 value of 0.9172 confirms the proof of concept of NMR assessment as a quantitative technique to determine ligand concentrations as low as 0.363 mM. All acquired and analyzed PEG-SH serial dilutions used in this work are shown in APPENDIX A.

As a further proof of concept, the differences in spectral response between PEG-SH and decomposed PEG-S-AuMPC samples were evaluated using pre-saturation method to remove the H_2O proton peak that masks the ligand peaks and confirm the existence of quantifiable peaks. An example of the spectral distinctions between PEG-SH protons and liberated PEG-S-S-PEG protons is shown in Figure 9. The appearance of triplet peaks in the sulfide region suggests the expected formation of disulfide bonded liberated ligands.

In order to obtain quantifiable spectra, the pre-saturation technique can not be used. Non pre-saturated spectra were obtained and analyzed. A sample analyzed spectrum is shown in Figure 10 whereas other spectra are shown in APPENDIX C. The CH_3- proton peak occurring at ~3.3 ppm represents the distal moiety at the end of the PEG polymer chain thus represents a single S-PEG ligand. The triplet peak occurring between 2.8-2.9 ppm represents the disulfide bond between two sulfur atoms of two S-PEG ligands. The CH_3- peak to disulfide triplet peak integral-ratios were uploaded into Microsoft Excel. A 20 mM SH-PEG CH_3- peak was also compared to each liberated PEG-S-S-PEG CH_3- peak generating an integral-ratio in order to quantify the concentration of PEG in each sample. Thus, unknown PEG-S-S-PEG concentrations were estimated by comparison of the –CH_3/disulfide peak integral ration with that generated by a 20 mM SH-EG standard.

The free thiol baseline is calculated by first determining the free thiol integral-ratio – unity minus the integral ratio between the CH_3- peak and PEG-S-S-PEG triplet peaks in the desorbed samples. The free thiol concentration is then calculated by computing the free thiol integration with concentration of PEG in each sample.

Quantification of Functionalized Conjugates. Conjugated PEG-S ligands were quantified using inductively coupled plasma mass spectroscopy (ICP-AES). Following the completion of the ICP-AES elemental concentration acquisition protocol, the concentrations of gold and sulfur elements were obtained in mg/L. Each elemental concentration was baselined against the threshold gold and sulfur concentrations determined by the ICP-AES acquisition protocol. The sulfur mass concentration was estimated from the ICP-AES measurement following subtraction of the corresponding free sulfur background as determined by NMR. Number concentration of the PEG ligand was computed from the measured mass concentration of sulfur, the relative molecular masses of sulfur and the PEG ligand and Avogadro’s number. The number concentration of AuMPCs was estimated from the measured gold mass using the density of bulk gold

(19.3 g/cm^3) and the gold particle volume based on diameter. As reported previously [41], the number of ligands per particle and the number of ligands per particle surface area were estimated. The results of these experiments, comparison with one set of predicted values are shown in Figure 14 superimposed with NMR data from the previous chapter. The qualitative trend in ligand association as a function of AuMPC size reported by ICP-AES is similar to those documented in the previous chapter for measurement by NMR and for a prediction based on a literature value. The absolute ligand association values obtained by ICP-AES, based either on particle size or surface area, are one to three orders of magnitude greater than the corresponding results from NMR data. Ligand packing density trends are shown in Figure 16. Statistical significance between sample points is noted in each figure.

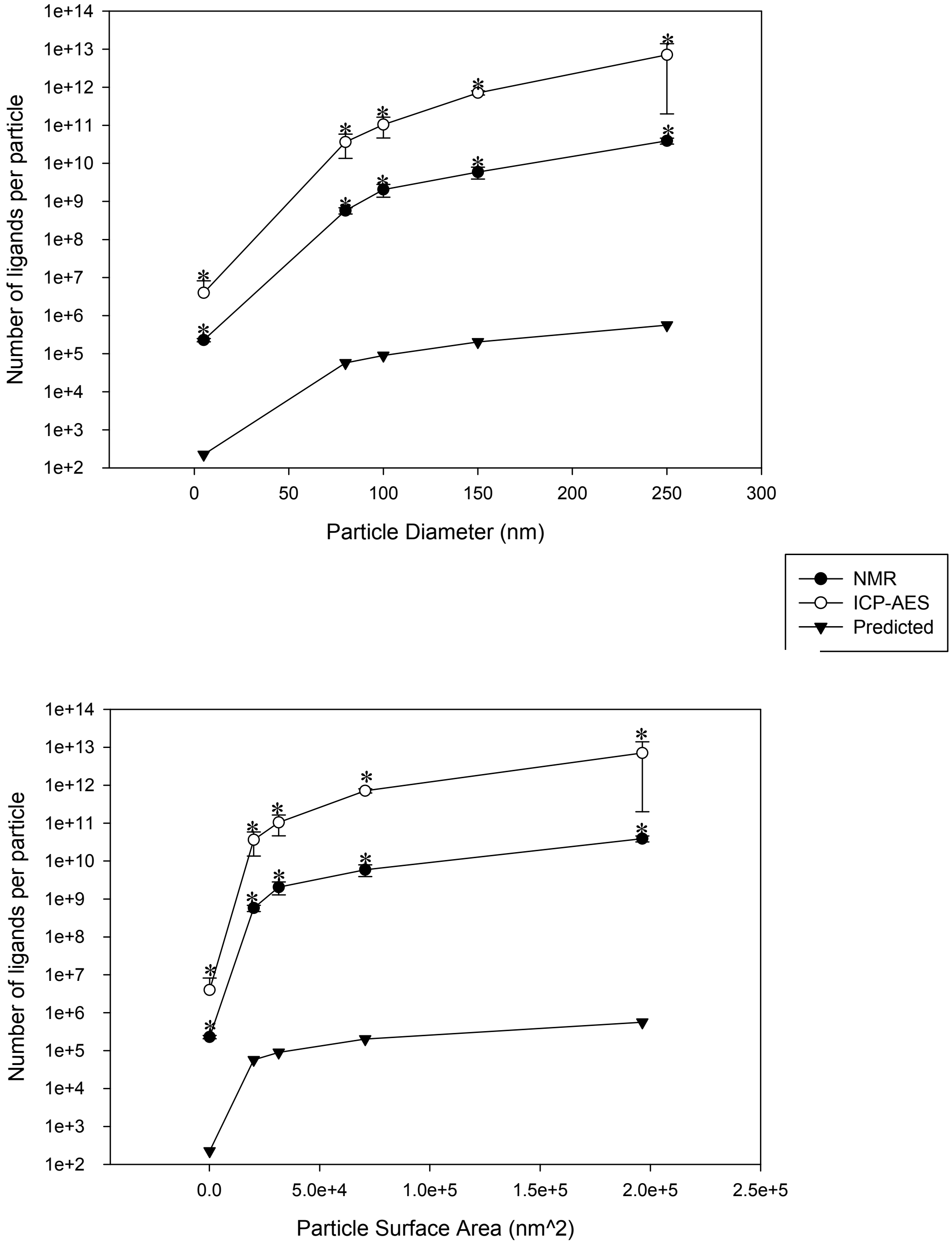

Figure 14. Conjugated ligand enumeration (ICP-AES). Top: number of ligands per particle as a function of particle diameter. Bottom: number of ligands per particle as a function of particle surface area. Data points represent the mean of three independent experiments with error bars as standard deviations. *Significant size increase for $p<0.05$ using Paired T-Test, comparing means within each curve.

Discussion

Studying the functionalization efficiency with respect to particle size was the overarching purpose of this work. In our initial assessment, we hypothesized that the molecular footprint of PEG on the surface of gold was constant, but unknown, especially as a function of substrate dimensions. Wuefling et al. estimated that the PEG-SH ligand footprint, the area occupied by the ligand on the surface of 2.8 nm gold particles, was 0.35 nm^2 [1]. Accordingly, we hypothesized that this ligand footprint held true across a range of particle sizes in a defect-free packing arrangement. Predicted trends calculated based on Wueling et al. and extended to larger particle diameters are shown in Figure 13.

In order to test this, the number of particles per particle surface area was calculated, thus elucidating the surface packing of PEG on gold over a range of nanoscale particle sizes. This is shown in Figure 16 as the density of PEG packing significantly increases as the particle size increases across the range of 5 nm to 100 nm. However, this trend of significant increase does not continue as steeply from 100 nm to 250 nm. It can be generally inferred that the packing density decreases as available particulate surface area decreases. Confirmation and assessment of this trend and its implications must first be carried out through comparison of the ligand enumeration with theoretical prediction.

Ligand enumeration using ICP-AES follows the same qualitative relationship with particle size and surface area as obtained by both theoretical prediction and NMR (Figure 14). The primary difference between all enumerative plots is the quantitative disparity between the prediction and each method. However, these disparities can be numerically related though a scaling factor. Results obtained from ICP-AES and NMR data and the predicted values can be normalized relative to the corresponding result for the 250 nm diameter particle in order to directly compare differences in ligand enumeration. The result of this data normalization is shown in Figure 15. Here, we speculate the differences in scaling between the enumerative methods and the predicted data represent both the inefficiency of the free thiol baseline strategy or the purification strategy used to remove free thiol and free disulfide bonded ligands from the reaction solution. Further, PEG-S-AuMPC samples in aerosol form tend to get lodged in the central channel of the ICP-AES causing cross-contamination and slight imperfections in data acquisition. These cross-contaminations are generally controlled by baseline protocols inherent in the acquisition procedure; but may still allow artifacts to be registered in the current sample. These artifacts usually register higher sample concentrations than really exist thus adding to the disparity between the predicted and acquired data above. Such disparities however have no bearing on trends formed though analysis of the data and further supports the effectiveness of both enumerative strategies at determining the amount of ligand in each sample.

An additional observation that can be noted from Figure 15 is that ligand coverage increases by over three orders of magnitude as particle diameters increase from 5 nm to 250 nm across both enumerative methods. Efficiency is maximized at 250 nm thus ligand packing efficiency is 50 to 100 times less for the smallest particles studied here. It can be speculated that such limitations at smaller sizes are governed both by certain ligand and particle characteristics that will be discussed shortly.

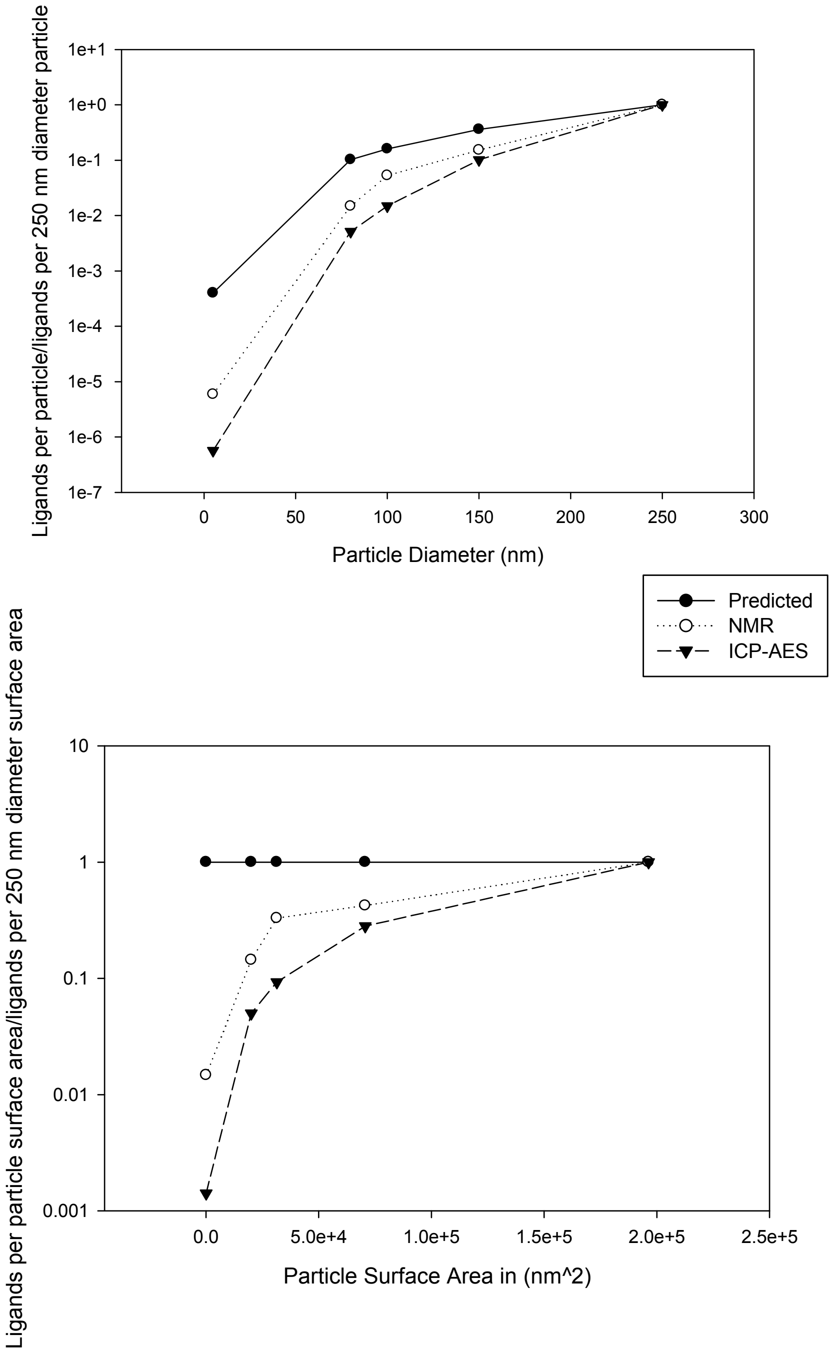

Figure 15. Normalized enumerative and ligand packing data. Both the ICP-AES and NMR data can normalized in order to directly compare differences in ligand enumeration from the predicted data by normalizing all data sets to their respective 250 nm particle.

PEG functionalization of AuMPCs measured by ICP-AES and NMR (Figure 14) follow the same qualitative trend as a function of particle surface area, but the enumerative data ranges from one to two orders of magnitude lower for the NMR data. This disparity can be explained due to the differences in the acquisitions of ligand concentrations. NMR, as shown in Figure 8, is a highly sensitive instrument relying on the magnetic resonance of nuclei to determine sample concentrations. The NMR technique can distinctly decipher liberated – previously conjugated - ligands from free ligands in solution due to differences in nuclear resonance; however, ICP-AES relies on an external baseline protocol to remove free ligands. Neither method however is completely efficient at resolving the difference between free and conjugated ligands – especially when their emission and resonance profiles are synonymous. These issues, however, do not prevent useful analysis of the ligand packing trends as a function of particle size, which is the primary objective of this work.

The ligand packing density significantly decreases as available particulate surface area decreases for particle sizes 5 nm to 100 nm. In addition, the packing density begins to become more constant for sizes ranging from 100 nm to 250 nm. It can be speculated that the packing density for these larger sizes is governed by characteristics of the particle and ligand. These speculative claims are supported by the characteristics of PEG and its conformational loading on gold particles.

Results from both analytical methods suggest that PEG surface packing density at the nanoscale decreases as available particle surface area decreases. A number of plausible physical and chemical interpretations are consistent with this trend. Steric hindrance of bound PEG molecules may impede the attachment of subsequent PEG association due to the length of the 5000 MW polymer [54]. For example, a single, surface-attached PEG molecule may be sufficiently long and flexible to block potential binding sites. An estimate of the potential for such bound-PEG inhibition of additional conjugation was carried out. PEG chain lengths were estimated using the average molecular weight of 5000 MW to calculate the number of monomers in each chain, n=112. The length of each monomer was estimated to be ~49.9 nm using linear bond lengths: C-C, 154 pm; C-O, 143 pm; C-S, 181 pm. In addition, the atom sizes were implemented using atomic diameters: C, 0.182 nm; O, 0.13 nm; S, 0.218 nm. Using these estimations and the commercially reported AuMPC diameters, a PEG length to particle diameter ratio was generated. Once can theoretically envision a functionalization circumstance where there are at least two idealized components represented: 1) the PEG molecules label gold straight (rather than coiled) and each polymer is projected normal to the AuMPC surface (rather than at a different orientation). Here, we would theoretically perceive that the surface area a single ligand occupies is invariable thus leading to a constant packing density across varying particle sizes. Departures from this ideal state will cause the bound PEG to occupy a proportionally greater surface area and reduce the capacity for additional PEG association with the AuMPC surface. Thus, it seems likely that steric hindrance in the experimental study would reduce the measured extent of PEG chain conjugation relative to the idealized, theoretical trend especially for smaller particles with less available surface area. Further, idealized PEG length is twenty-fold greater than the 5 nm diameter AuMPC, but only 40% of the 250 nm diameter particle thus increasing the probability that PEG will sterically hinder other polymer ligands especially at lower particle sizes.

Other factors may contribute to the observed departure from ideality. Studies have shown that PEG can assume a range of molecular conformations modulated by the local environment due to its malleability [55]. For example, PEG sparsely bound to surfaces has the opportunity to form self-associations that result in a ‘mushroom’ shape that occupies a larger cross-sectional area than the simple molecular diameter. This PEG characteristic supports the enumerative findings and is further substantiated by the post-conjugation size increase of larger particle sizes (Figure 7). DLS data confirms that particle diameters of 150 nm and 250 nm have significantly thicker PEG coats than the smaller particles. The coat thickness for these particle sizes is also coupled with a large increase in available surface area. Our previous speculation inferred that there exists a maximal packing density as particle size increases. Keeping in mind that the initial PEG mass was added to the functionalization reaction in excess, we can speculate that this maximal packing density is a function of the particle size, PEG length, and PEG conformational malleability. Between these two particle sizes, we can infer that there is a point where the available surface area is large enough to allow PEG of a certain length, to form blob-like ‘mushroom’ conformations instead of more erect ‘brush’ conformations. Although this change in PEG conformation will increase ligand footprint, any significant

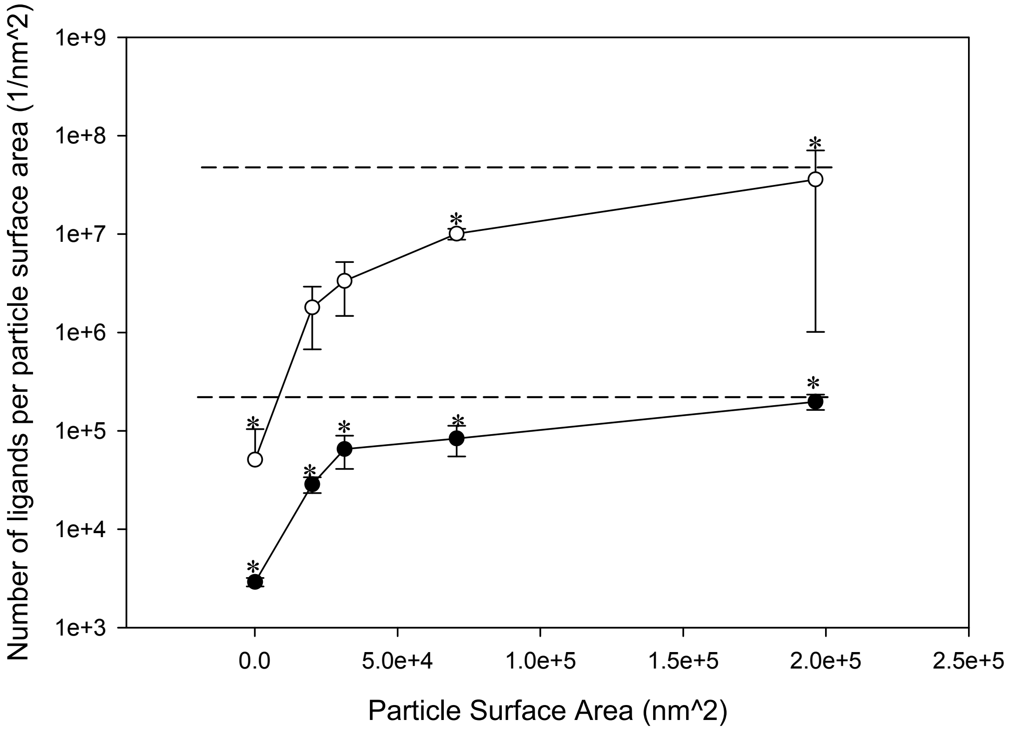

Figure 16. Surface packing of PEG on AuMPC as a function of particle surface area as quantified using ICP-AES (top) and NMR (bottom). Surface packing is defined as number of PEG ligands per particle surface area. (-) represents the predicted trend for each enumeration strategy if the ligand footprint remains constant over all particle sizes. Data points represent the mean of three independent experiments with error bars as standard deviations. *Significant size increase for $p<0.05$ using Paired T-Test for means within a single curve

increase in particle size will increase the available surface area such that the number of ligands per particle will continue to increase. From the experimental data, it can be concluded that this transition point for 5000 MW PEG occurs between 100 nm and 250 nm particle sizes – at a point where the erect length of the conjugated ligand approximates the particle diameter. Although such molecular conformations may be responsible, in whole or in part, for the observed trends in PEG-S-AuMPC functionalization, the scope of this study does not include such precise assessments. Nevertheless, the comparison of experimental results with theory suggest that PEG packing is more efficient on particles where its diameter approximates the erect length of the conjugated polymer - potentially implying that the potential for maximizing or enhancing bionanoparticulate effectiveness lies in the careful design and knowledge of the loading and packing profile of the protecting or targeting ligand that will be loaded on the desired particulate platform.

The ligand density of nanoparticles intended for use in living systems is a critical modulator of specific functions. Many biological functions depend on the activation multiple moieties to establish the desired effect. Because of this, knowledge of the ligand density is paramount in determining the effectiveness of the nanoparticle at stimulating the desired biological effect. Functionalization approaches that are successful *in vitro* on relatively large scale surfaces, or in proof-of-concept studies on microparticles may prove to be different – and possibly inadequate – as the achievable surface density decreases with particle size the nanoscale. In addition, accepted transport properties on the macroscale do not translate to studies carried out on the micro- or nanoscale because of unique nanoscale behavior and environment. Because of this, nanoscale based studies - like the above - characterizing functionalization, enumerating ligand density, and determining ligand conformation must be performed to obtain the knowledge necessary to effectively design, synthesize and implement efficient theranostic pharmaceuticals and bionanotechnology based drug delivery systems.

References

1. Wuelfing, W.P.G., Stephen M.; Miles, Deon T.; Murray, Royce W. , *Nanometer Gold Clusters Protected by Surface-Bound Monolayers of Thiolated Poly(ethylene glycol) Polymer Electrolyte.* Journal of the American Chemical Society, 1998. **120**(48): p. 12696-12697.
2. Daniel, M.-C.A., Didier *Gold Nanoparticles: Assembly, Supramolecular Chemistry, Quantum-Size-Related Properties, and Applications toward Biology, Catalysis, and Nanotechnology* Chemical Reviews (Washington, DC, United States), 2004. **104**(1): p. 293-346.
3. White, C.W.Z., D. S.; Budai, J. D.; Zuhr, R. A.; Magruder, R. H., III; Osborne, D. H. , *Colloidal Au nanoclusters formed in fused silica by MeV ion implantation and annealing* Materials Research Society Symposium Proceedings, 1994 **316**(Materials Synthesis and Processing Using Ion Beams): p. 499-506.
4. Faraday, M., *Experimental relations of gold (and other metals) to light.* Philos. Trans. R. Soc. London., 1857. **147**: p. 145.
5. Weiser, H.B., Inorganic Colloid Chemistry, 1933. **1**: p. 21-57.
6. Hayat, M.A., *Colloidal Gold: Principles, Methods, and Applications*. Vol. 1. 1989, San Diego, Calif: Academic Press, Inc. 536.
7. Handley, D.A., *The Development and Application of Colloidal GTold as a Microscopic Probe*, in *Colloidal Gold: Principles, Methods, and Applications*, M.A. Hayat, Editor. 1989, Academic Press, Inc.: San Diego, Calif. p. 1-8.
8. Handley, D.A., *Methods for Synthesis of Collodial Gold*, in *Colloidal Gold: Priniciples, Methods, and Applications*, M.A. Hayat, Editor. 1989, Academic Press, Inc.: San Diego, Calif. p. 13-31.
9. Brust, M.W., Merryl; Bethell, Donald; Schiffrin, David J.; Whyman, Robin *Synthesis of thiol-derivatized gold nanoparticles in a two-phase liquid-liquid system* Journal of the Chemical Society, Chemical Communications, 1994(7): p. 801-802.
10. Turkevitch, J., Discuss. Faraday Soc., 1951. **11**: p. 55-59.
11. Yonezawa, T.K., T., *Practical Preparation of Anionic Mercapto Ligand-Stabilized Gold Nanoparticles and Their Immobilization.* Colloids Surf. A: Physicochem. Eng. Asp., 1999. **149**: p. Colloids Surf. A: Physicochem. Eng. Asp.
12. Brust, M.F., J.; Bethell, D.; Schiffrin, D. J.; Kiely, C. J., *Synthesis and Reactions of Functionalised Gold Nanoparticles.* J. Chem. Soc., Chem. Commun., 1995: p. 1655-1656.
13. Templeton, A.C.W., W. Peter; Murray, Royce W. , *Monolayer-Protected Cluster Molecules* Accounts of Chemical Research, 2000. **33**(1): p. 27-36.
14. Hostetler, M.J.G., Stephen J.; Stokes, Jennifer J.; Murray, Royce W. , *Monolayers in three dimensions: synthesis and electrochemistry of ω-functionalized*

alkanethiolate-stabilized gold cluster compounds. Journal of the American Chemical Society, 1996. **118**(17): p. 4212-4213.

15. Chen, S.M., Royce W., *Arenethiolate Monolayer-Protected Gold Clusters* Langmuir, 1999. **15**(3): p. 682-689.
16. Antonii, F., *Panacea Aurea-Auro Potabile*, in *Bibliopolio Frobeniano*. 1618: Hamburg.
17. Lv M, Z.E., Su Y, Li Q, Li W, Zhao Y, Huang Q, *Trypsin-Gold Nanoparticle Conjugates: Binding, Enzymatic Activity, and Stability.* Preparative Biochemistry and Biotechnology, 2009. **39**(4): p. 429-438.
18. Roa W, Z.X., Guo L, Shaw A, Hu X, Xiong Y, Gulavita S, Patel S, Sun X, Chen J, Moore R, Xing JZ., *Gold nanoparticle sensitize radiotherapy of prostate cancer cells by regulation of the cell cycle.* . Nanotechnology 2009. **2**(37).
19. Prabaharan M, G.J., Pilla S, Steeber DA, Gong S., *Gold nanoparticles with a monolayer of doxorubicin-conjugated amphiphilic block copolymer for tumor-targeted drug delivery.* Biomaterials, 2009. **30**(30): p. 6065-75.
20. Jain RK, G.L., *Extravascular transport in normal and tumor tissues.* Crit Rev Oncol Hematol., 1986. **5**(2): p. 115-70.
21. Pegaz B, D.E., Ballini JP, Konan-Kouakou YN, van den Bergh H, *Effect of nanoparticle size on the extravasation and the photothrombic activity of meso(p-tetracarboxyphenyl)porphyrin.* J Photochem Photobiol B., 2006. **85**(3): p. 216-22.
22. Ishida O, M.K., Sasaki K, Iwatsuru M., *Size-dependent extravasation and interstitial localization of polyethyleneglycol liposomes in solid tumor-bearing mice.* Int J Pharm., 1999. **190**(1): p. 49-56.
23. Unezaki S, M.K., Hosoda J, et al., *Direct measurement of extravasation of polyethyleneglycol-coated liposomes into solid tumor tissue by in vivo fluorescence microscopy.* Int J Pharm 1996. **144**: p. 11-7.
24. Kong G, B.R., Dewhirst MW., *Hyperthermia enables tumor-specific nanoparticle delivery: effect of particle size.* Cancer Res., 2000 **60**(16): p. 4440-5.
25. Olivier JC, H.R., Lee HJ, Calon F, Pardridge WM., *Synthesis of pegylated immunonanoparticles.* Pharm Res., 2002 **19**(8): p. 1137-43.
26. Marsh D, B.R., Sportelli L., *Lipid membranes with grafted polymers: physicochemical aspects.* Biochim Biophys Acta, 2003 **1615**(1-2): p. 33-59.
27. Klemperer, P., *The reticulo-endothelial system.* Hawaii Med J., 1948. **8**(2): p. 96.
28. Marshall AH, W.R., *Reactions of the reticular tissues to antigens.* Br J Exp Pathol., 1950 **31**(2): p. 157-74.
29. Crawford, J., Cancer treat. Rev., 2002. **A**: p. 7-11.
30. al., D.O.N.e., Cancer Lett., 2004. **209**: p. 171-176.
31. al., L.H.e., Proc. Natl. Acad. Sci. U.S.A., 2004. **100**: p. 13549-13554.
32. Loo C, L.A., Halas N, West J, Drezek R., *Immunotargeted nanoshells for integrated cancer imaging and therapy.* Nano Lett., 2005. **5**(4): p. 709-711.
33. Loo C, L.A., Hirsch L, Lee MH, Barton J, Halas N, West J, Drezek R., *Nanoshell-enabled photonics-based imaging and therapy of cancer.* Technol Cancer Res Treat., 2004 **3**(1): p. 33-40.
34. Gooden, J., *Nuclear resonance and magnetic field changes of 1 in 106.* Nature, 1950. **165**(4208): p. 1014-5.

35. Sheppard, N., *Appendix-Notes on the nuclear-magnetic-resonance spectrum of omega-fluorodecanoic acid and of a fluoro-octadecenoic acid of unknown structure.* Biochem J. , 1960. **77**(1): p. 22-3.
36. JH Ridd, R.W., *Nuclear magnetic resonance spectrum of beta-pyrazol-1-ylalanine.* Biochem J., 1960. **77**: p. 546-7.
37. F. Bloch, W.H.a.M.P., *Nuclear induction.* Phys. Rev., 1946. **69**: p. 127.
38. Swift TJ, F.O.J., *A proton spin-echo study of the state of water in frog nerves.* Biophys J., 1969 **9**(1): p. 54-9.
39. Claridge, T.D.W., *High Resolution NMR Techniques in Organic Chemistry*. Tetrahedron Organic Chemistry Series, ed. J.E.B. J.-E. Backvall, R.M. Williams. Vol. 27. 2009, Amsterdam: Elsevier.
40. Ailette Aguila, R.W.M., *Monolayer-Protected Clusters with Fluorescent Dansyl Ligands.* Langmuir, 2000. **16**(14): p. 5949–5954.
41. Hurst SJ, L.-J.A., Mirkin CA., *Maximizing DNA loading on a range of gold nanoparticle sizes.* Anal Chem., 2006. **78**(24): p. 8313-8.
42. S Takae, Y.A., H Otsuka, T Nakamura, Y Nagasaki, K Kataoka, *Ligand Density Effect on Biorecognition by PEGylated Gold Nanoparticles: Regulated Interaction of RCA120 Lectin with Lactose Installed to the Distal End of Tethered PEG Strands on Gold Surface.* Biomacromolecules, 2005. **6**: p. 818-824.
43. Verma A, U.O., Hu Y, Hu Y, Han HS, Watson N, Chen S, Irvine DJ, Stellacci F., *Surface-structure-regulated cell-membrane penetration by monolayer-protected nanoparticles.* Nat Mater., 2008. **7**(7): p. 588-95.
44. Templeton AC, H.M., Kraft CT, and Murray RC, *Reactivity of Monolayer-Protected Gold Cluster Molecules: Steric Effects.* J. Am. Chem. Soc., 1998. **120**(8): p. 1906-1911.
45. Levin, C., Bishnoi, SW, Grady, NK, Halas, NJ., *Determining the Conformation of Thiolated Poly(ethylene glycol) on Au Nanoshells by Surface-Enhanced Raman Scattering Spectroscopic Assay.* Analytical Chemistry, 2006. **78**(10): p. 3277-3281.
46. Eck W, C.G., Sigdel A, Ritter G, Old LJ, Tang L, Brennan MF, Allen PJ, Mason MD, *PEGylated gold nanoparticles conjugated to monoclonal F19 antibodies as targeted labeling agents for human pancreatic carcinoma tissue.* ACS Nano, 2008. **2**(11): p. 2263-72.
47. Robin, J.T., Christian *Stimulated emission of aluminum and titanium resonance lines at very low concentration in a HF [high frequency] argon plasma.* Sciences Physiques, 1975. **281**(16): p. 345-7.
48. Lichte, F.K., SR, *Induction coupled plasma emission from a different angle.* ICP. Inf. Newsl., 1976. **2**: p. 192.
49. Lichte, F.E.K., S. R., *A simplified torch design for inductively coupled plasma optical emission spectrometry.* ICP Information Newsletter, 1976. **1**(9): p. 200-2.
50. H Karami, O.R.-O., *Synthesis of Iron Nanoclusters by Pulsed Current Method.* . Journal of Cluster Science 2009. **20**(3): p. 587-600.
51. K. Zhu, J.H., and R. Richards., *Aerobic oxidation of cyclohexane by gold nanoparticles immobilized upon mesoporous silica.* Catalysis Letters, 2005. **100**(3-4): p. 195-199.

52. Fischer, H.F.-B., S; Pang, KS; Chan, WCW, *Quantitative detection of engineered nanoparticles in tissues and organs: an investigation of efficacy and linear dynamic ranges using ICP-AES.* NanoBiotechnology 2007. **3**(1): p. 46-54.
53. Hill, S., *Inductively Coupled Plasma Spectrometry and its Applications*. Analytical Chemistry, ed. A.J.H.a.J.M. Chalmers. 2007, Oxford: Blackwell Publishing Ltd.
54. Harris JM, M.N., Modi M., *Pegylation: a novel process for modifying pharmacokinetics.* Clinical Pharmacokinetics, 2001. **40**(7): p. 539-51.
55. Frisman I, S.D., Bianco-Peled H., *Nanostructuring of PEG-fibrinogen polyneric scaffolds.* Acta Biomaterialia, 2009. **Article in Press**.

CHAPTER IV

CONCLUSIONS AND FUTURE WORK

Conclusions

Bionanotechnology is a field quickly gaining popularity among researchers seeking to specifically target cancer and pathogens for diagnostics and treatment. Most targeting agents require surface protection and passivation to improve vascular circulation time, delivery probability and biocompatibility. The protective and targeting efficiency of such nanotechnology is characterized by the number of protective and targeting ligands on the particle. In order to characterize the therapeutic capacity of such ligand-coated particles, the number of ligands bound must be quantified. To accomplish this, previous studies used molecularly-tethered or fluorescently-tagged ligands which affect surface packing. Here, a “label-free” method of conjugate quantification was described thus circumventing the disadvantageous surface packing disparity introduced by previous methods.

Conjugated PEG-S ligands were quantified using ^{1}H nuclear magnetic resonance (NMR) spectroscopy and inductively coupled plasma mass spectroscopy (ICP-AES). Both the NMR and ICP-AES enumeration of conjugated ligands aligned with assumed predicted considerations following the implementation of normalization. The ligand packing density significantly decreases as available particulate surface area decreases for particle sizes 5 nm to 100 nm. Steric hindrance and the inherent conformational malleability of PEG is presumed to decrease total ligand binding from the predicted considerations and cause this decreasing trend for lower particle sizes. In addition, the packing density begins to become more constant for sizes ranging from 100 nm to 250 nm. It can be speculated that the packing density for these larger sizes are governed by some characteristic of the particle or ligand for sizes. From the experimental data, it can be concluded that this transition point for 5000 MW PEG occurs between 100 nm and 250 nm particle sizes – at a point where the erect length of the conjugated ligand approximates the particle diameter. The comparison of experimental results with theory suggest that PEG packing is more efficient on particles where its diameter approximates the erect length of the conjugated polymer - potentially implying that the potential for maximizing or enhancing bionanoparticulate effectiveness lies in the careful design and knowledge of the loading and packing profile of the protecting or targeting ligand that will be loaded on the desired particulate platform.

This work on this enumerative technique, along with future expansion, will provide investigators with the ability to quantify the number of ligands on the surface of their nanoscale constructs. Such knowledge will enable investigators insight into the efficacy of their nanotechnology as it is related to, and possibly governed by, the surface functionalization efficiency.

Future Work

The ultimate goal of this work was to establish a “label-free” strategy to determine the functionalization efficiency of gold nanoparticles over a range of nanoparticle sizes. The future of this work is to further elucidate the factors that govern functionalization and ligand surface packing. In addition, the present work has generated new questions regarding the molecular principles that control the surface functionalizion of long ligands to an assortment of particles.

Reconciliation of the enumerative data from the NMR and ICP-AES studies should be attempted experimentally without a correction factor. DLS results can be supported by data acquired from transmission electron microscopy. A PEG stain could be used to quantitatively monitor the size increase of AuMPCs following conjugation using TEM. This approach will be helpful in determining PEG conformations following conjugation.

Further studies could investigate other factors that govern functionalization and ligand surface packing. Instead of varying particle size, the initial PEG concentration used to initiate conjugation processes could be varied across a single particles size. Furthermore, these experiments could be extended across particles sizes. Also, PEG conformation could be monitored across a range of particles sizes to support the speculation in this study. Once this is determined, surface protection as a function of PEG conformation could also be investigated. These further studies will provide definitive insight as to how PEG conformation on the particle surface affects both packing and surface passivation. Even further, researchers could use these new studies to generate conformation -

functionalization profiles for individual ligands. Such studies would further provide investigators invaluable insight into how to best conjugate their nanoscale materials for biological and medical applications.

APPENDIX A

NMR SPECTRA OF NMR INTEGRAL RATIO PROOF OF CONCEPT

Table of Spectra

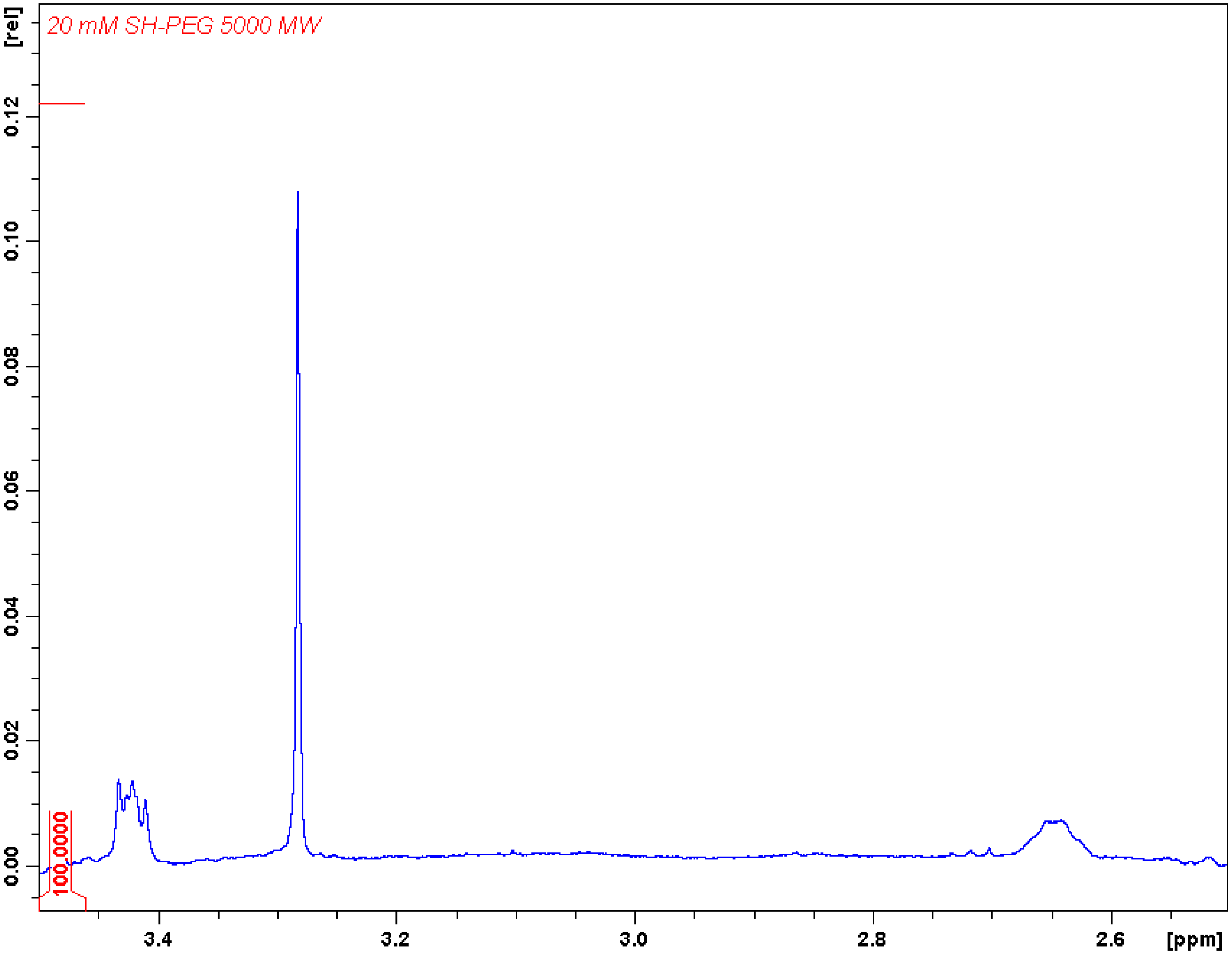

Spectrum A - 1. NMR Spectrum of 20mM solution of 5000 MW SH-PEG used for the serial dilution and the stock standard for subsequent spectra

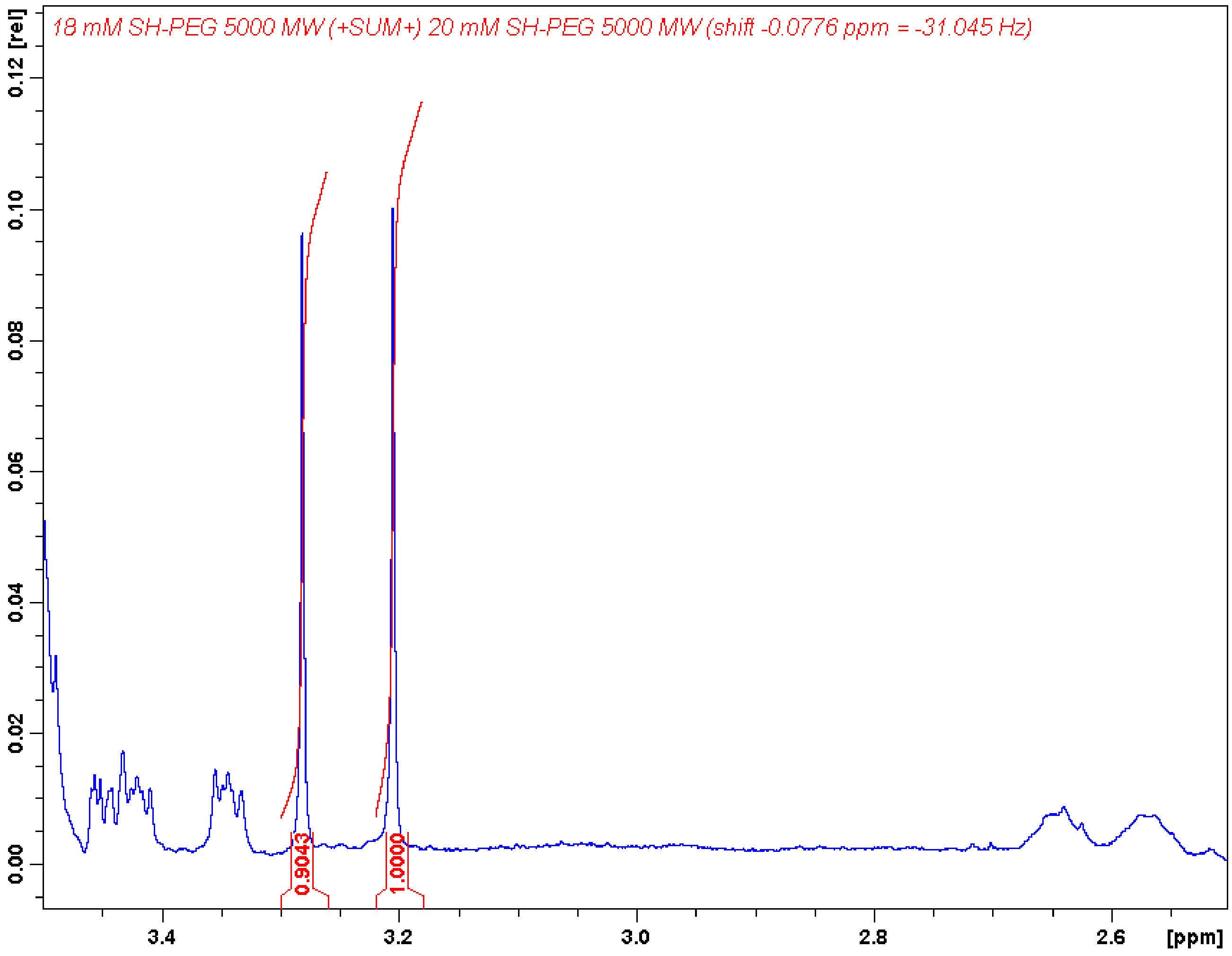

Spectrum A - 2. Summed NMR Spectrum of 18mM and 20 mM SH-PEG for determination of the integral ratio

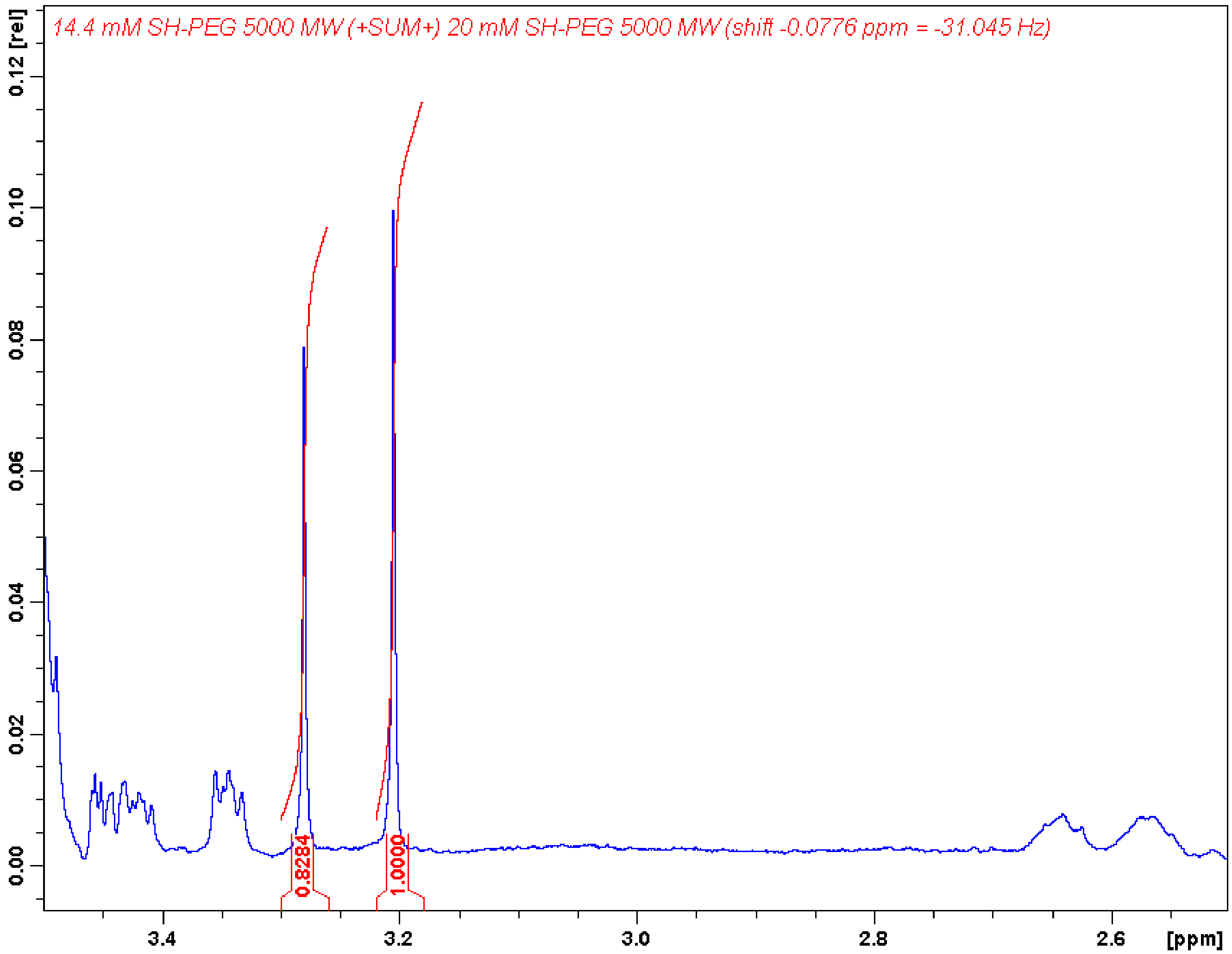

Spectrum A - 3. Summed NMR Spectrum of 14.4 mM and 20 mM SH-PEG for determination of the integral ratio

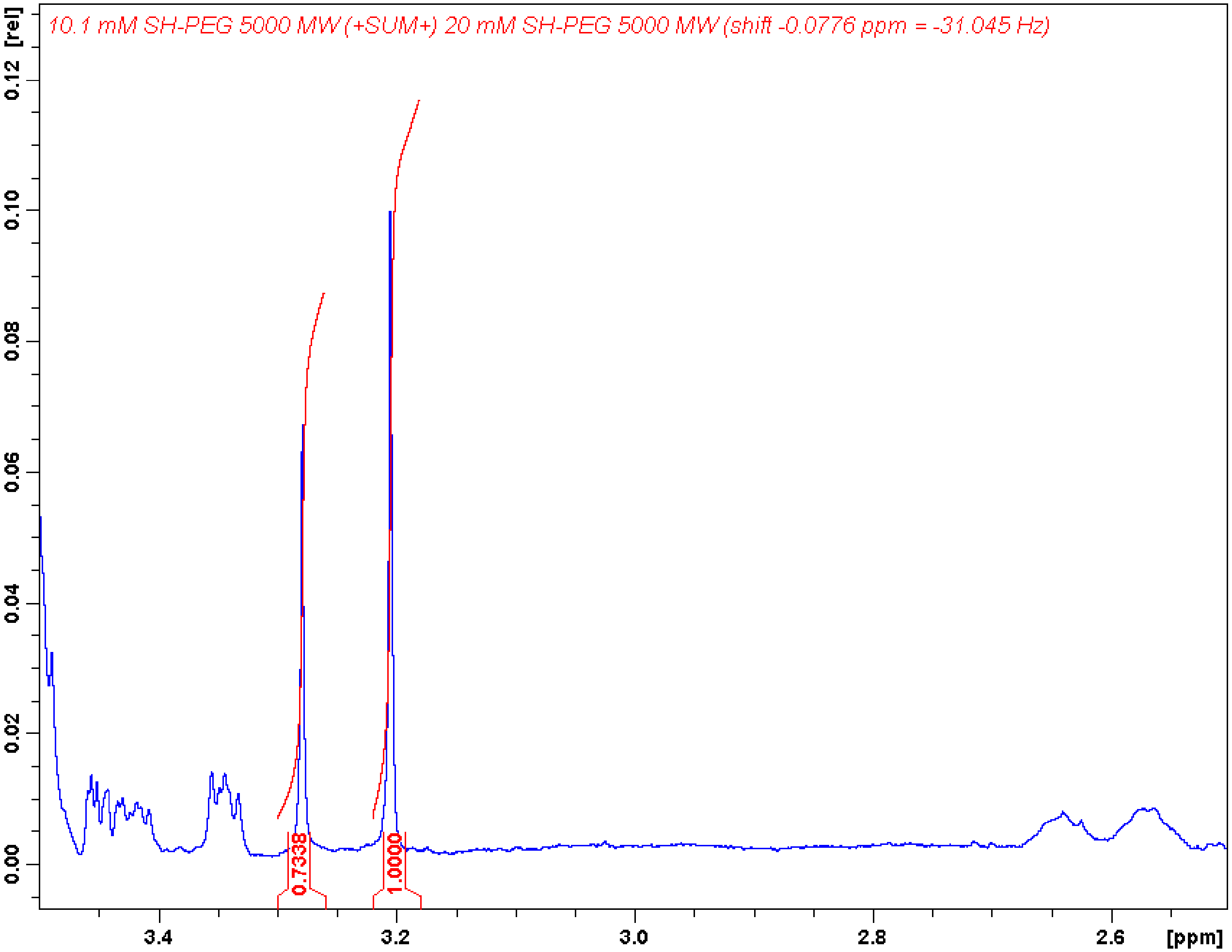

Spectrum A - 4. Summed NMR Spectrum of 10.1 mM and 20 mM SH-PEG for determination of the integral ratio

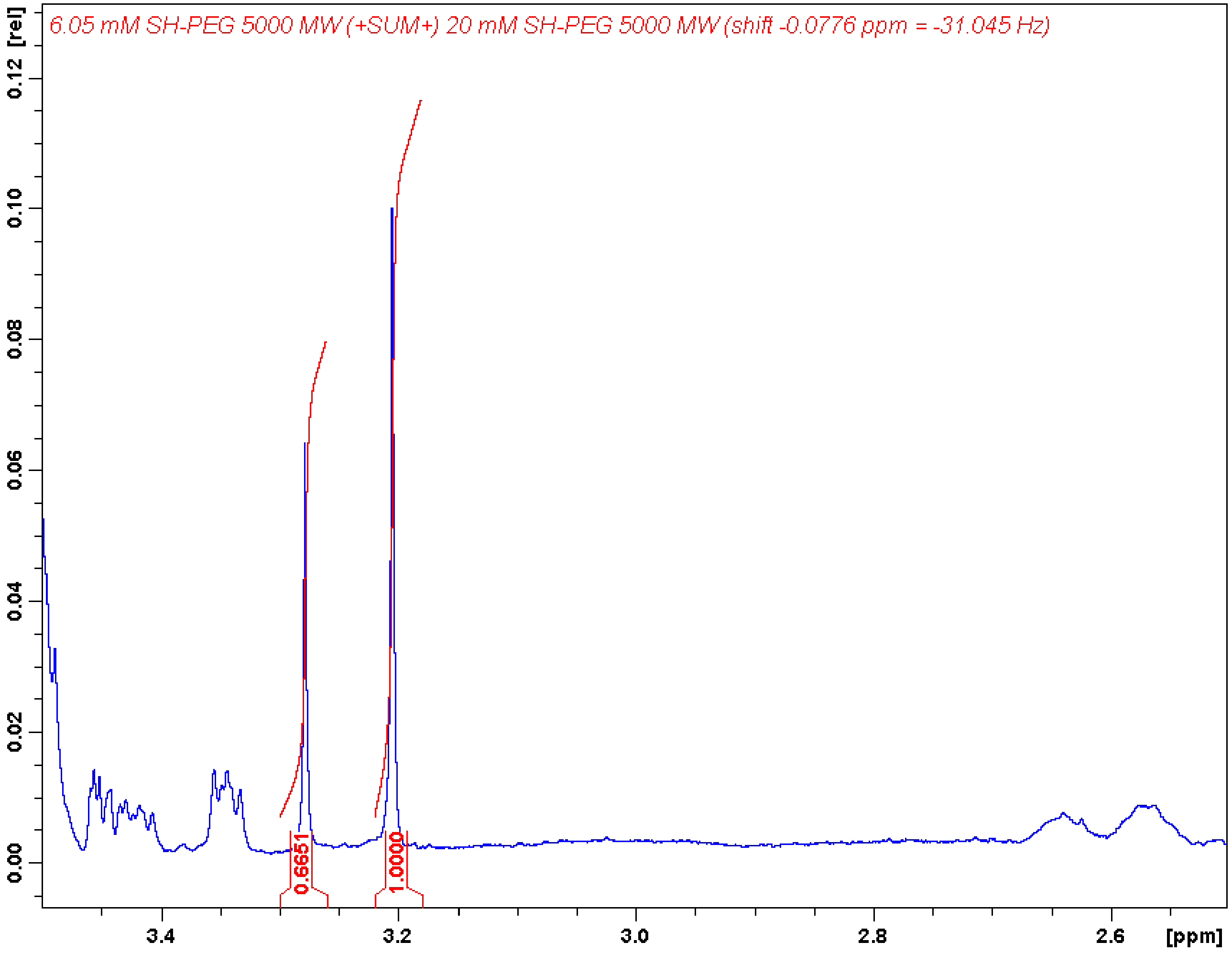

Spectrum A - 5. Summed NMR Spectrum of 6.05 mM and 20 mM SH-PEG for determination of the integral ratio

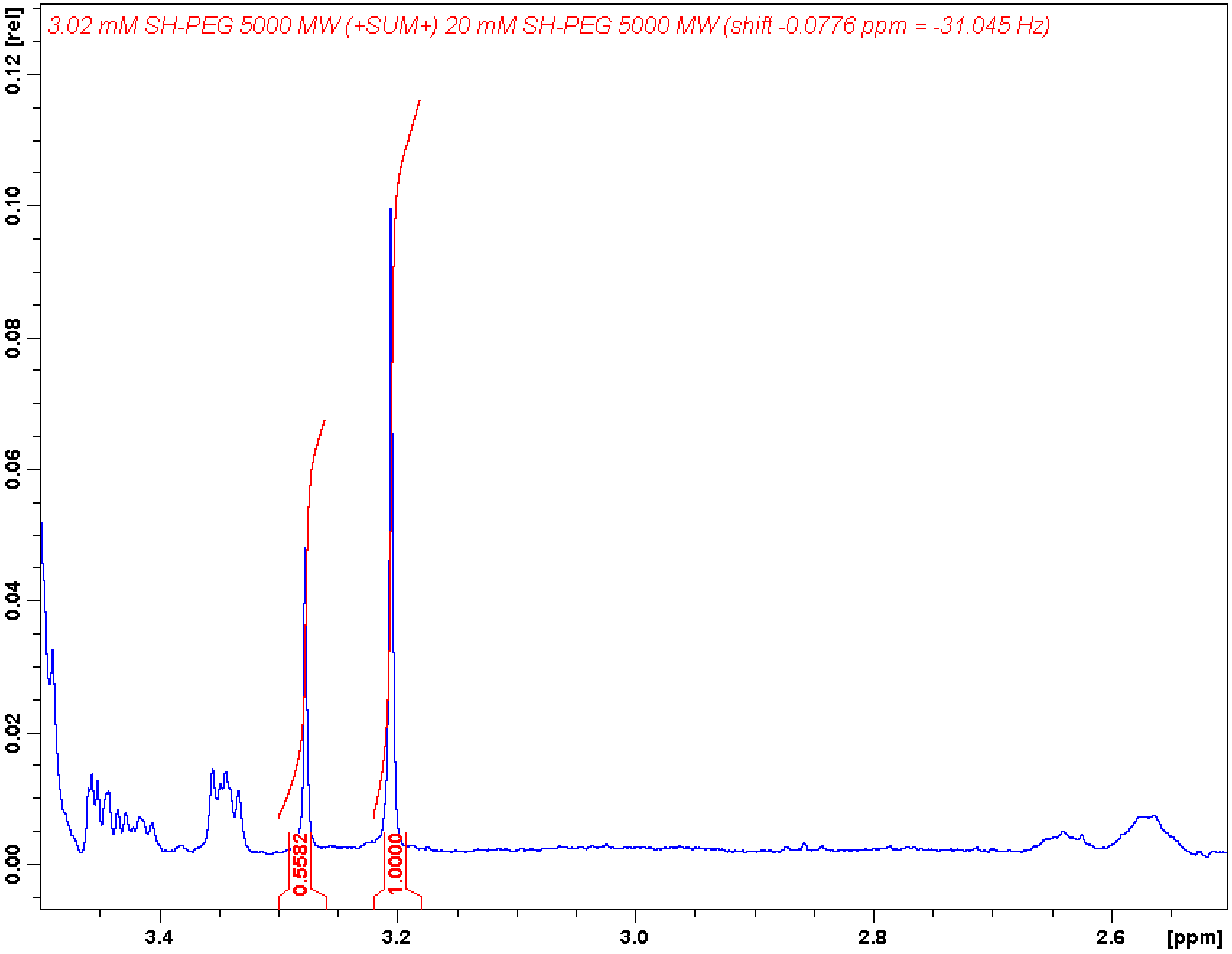

Spectrum A - 6. Summed NMR Spectrum of 3.02 mM and 20 mM SH-PEG for determination of the integral ratio

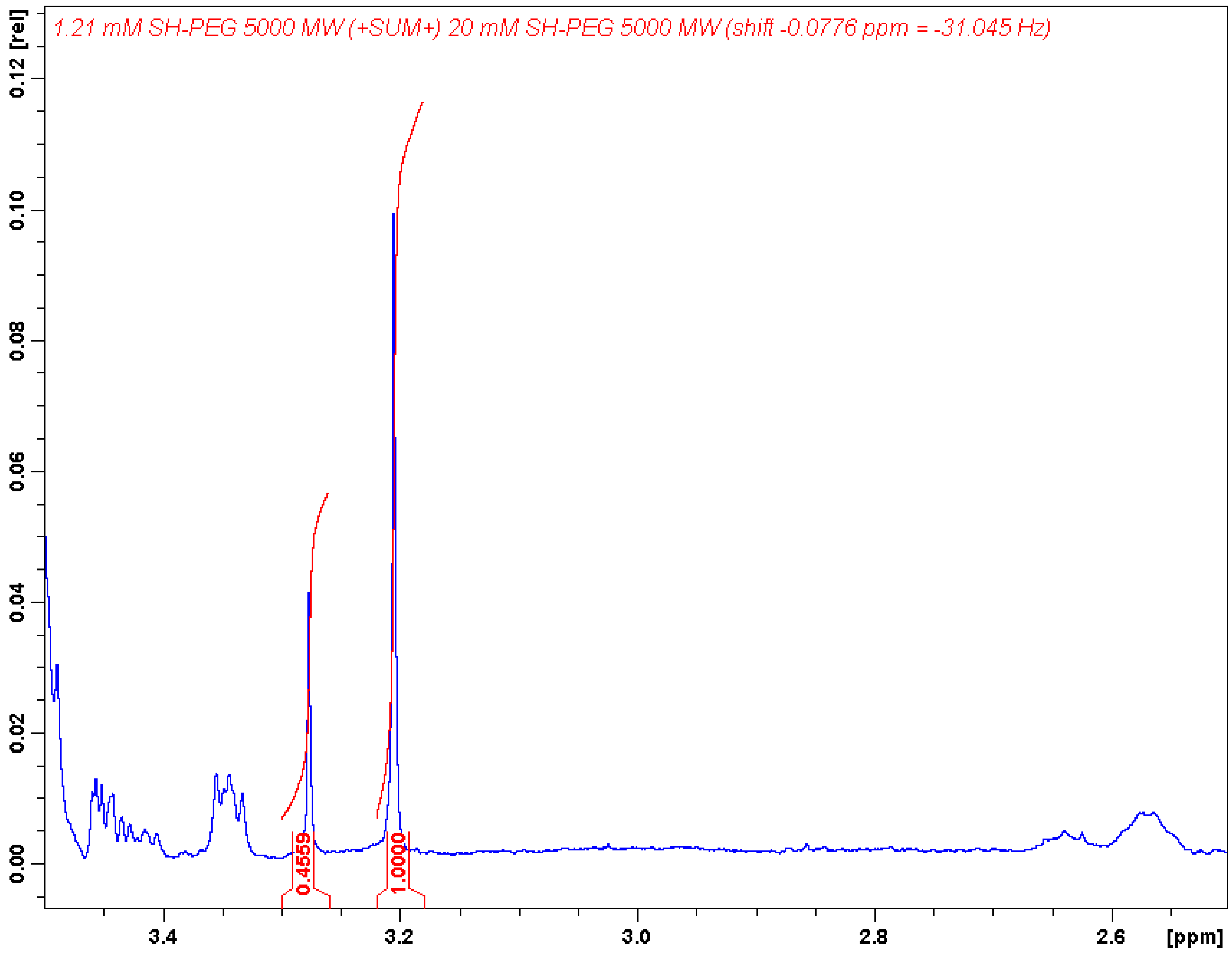

Spectrum A - 7. Summed NMR Spectrum of 1.21 mM and 20 mM SH-PEG for determination of the integral ratio

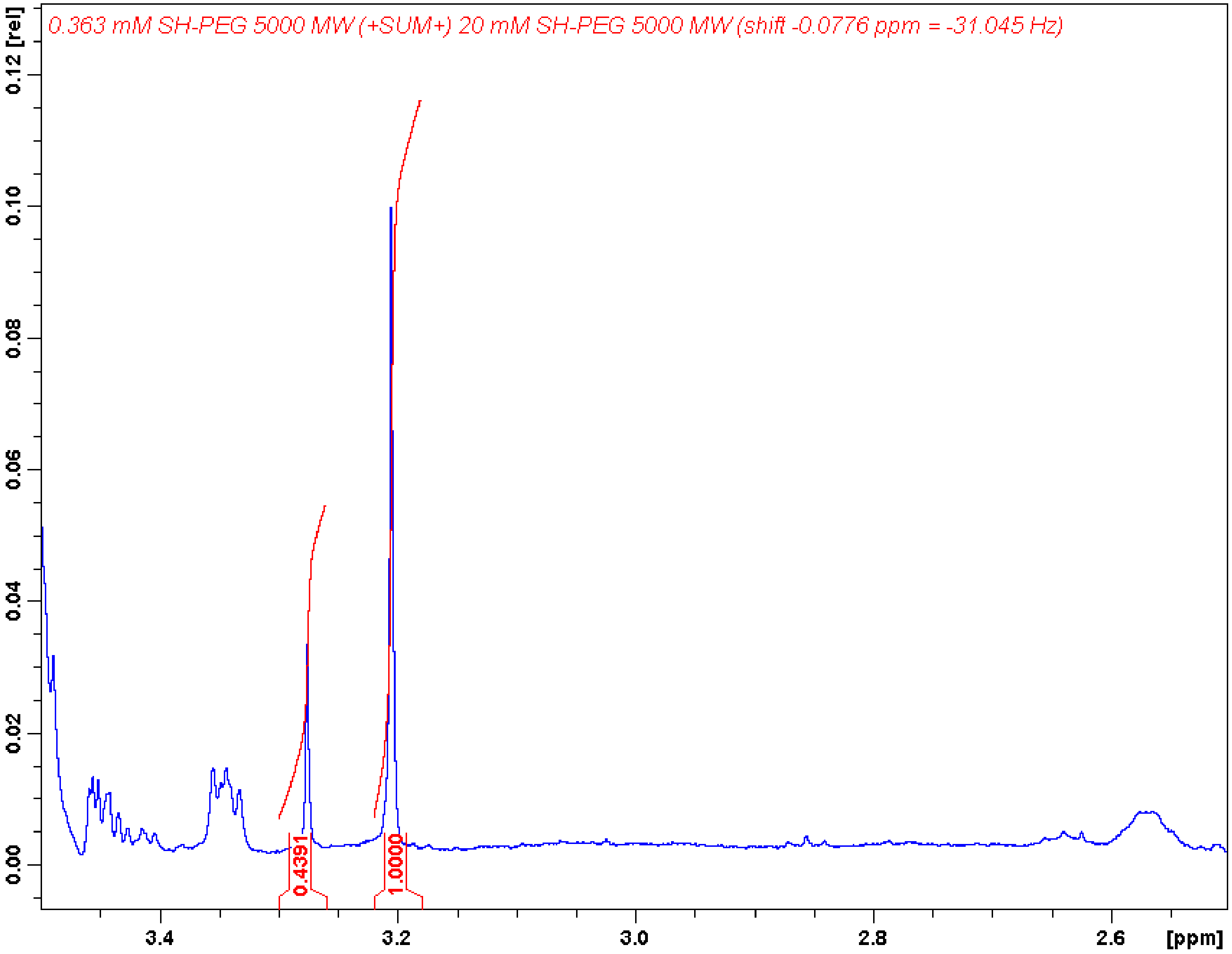

Spectrum A - 8. Summed NMR Spectrum of 0.363 mM and 20 mM SH-PEG for determination of the integral ratio

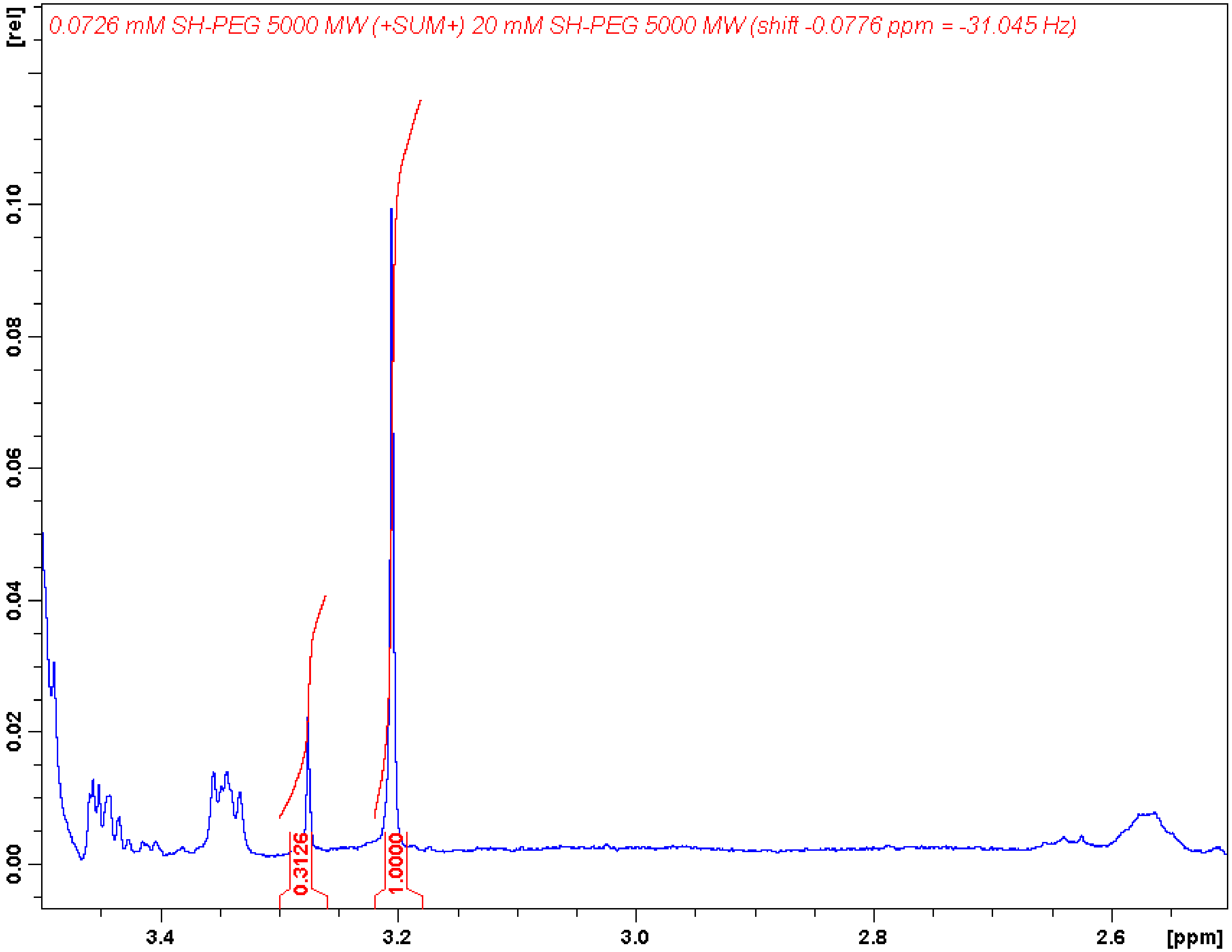

Spectrum A - 9. Summed NMR Spectrum of 0.0726 mM and 20 mM SH-PEG for determination of the integral ratio

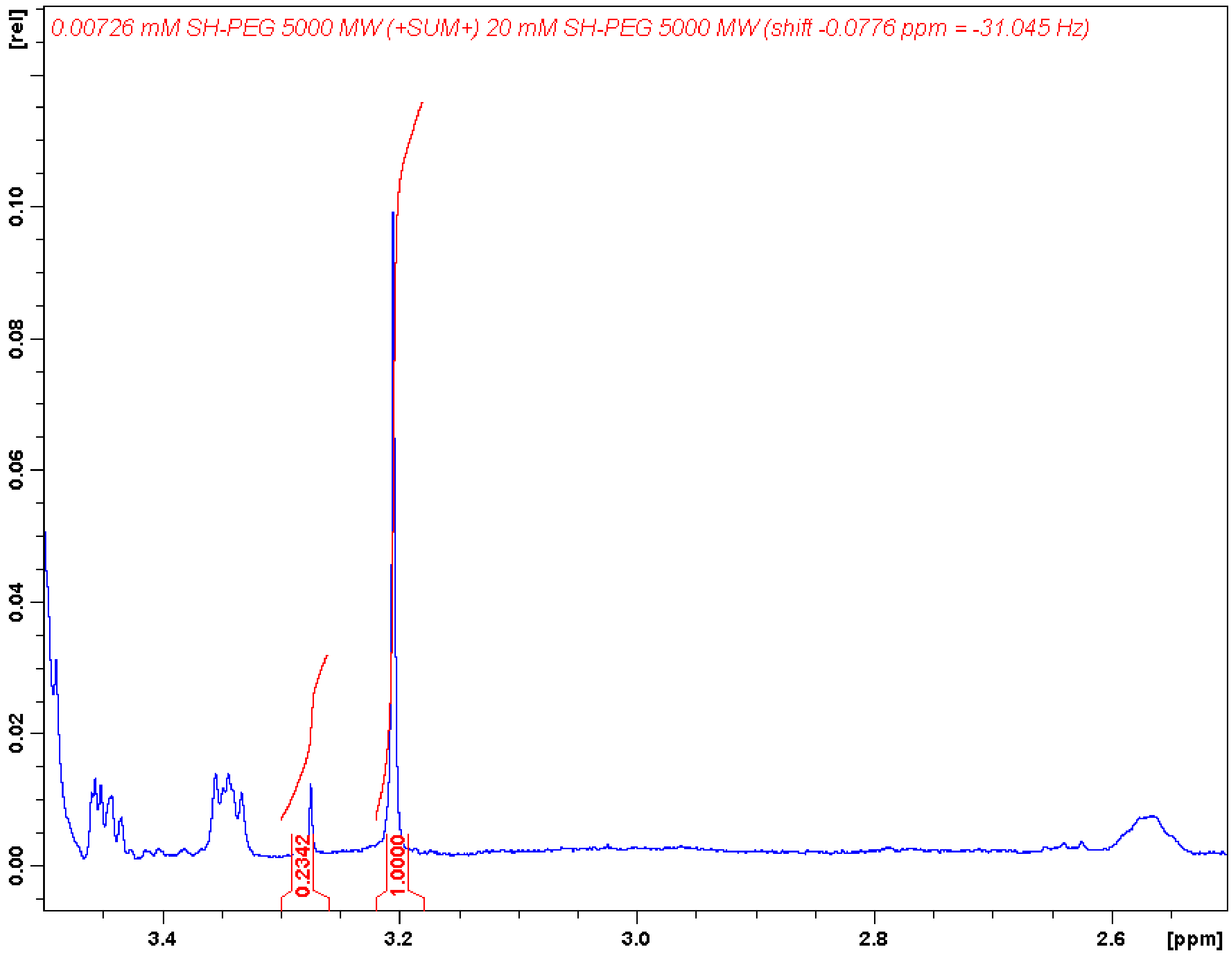

Spectrum A - 10. Summed NMR Spectrum of 0.00726 mM and 20 mM SH-PEG for determination of the integral ratio

APPENDIX B

NON PRE-SATURATED NMR SPECTRA OF DECOMPOSED PEGYLATED MONOLAYER PROTECTED CLUSTERS

Table of Spectra

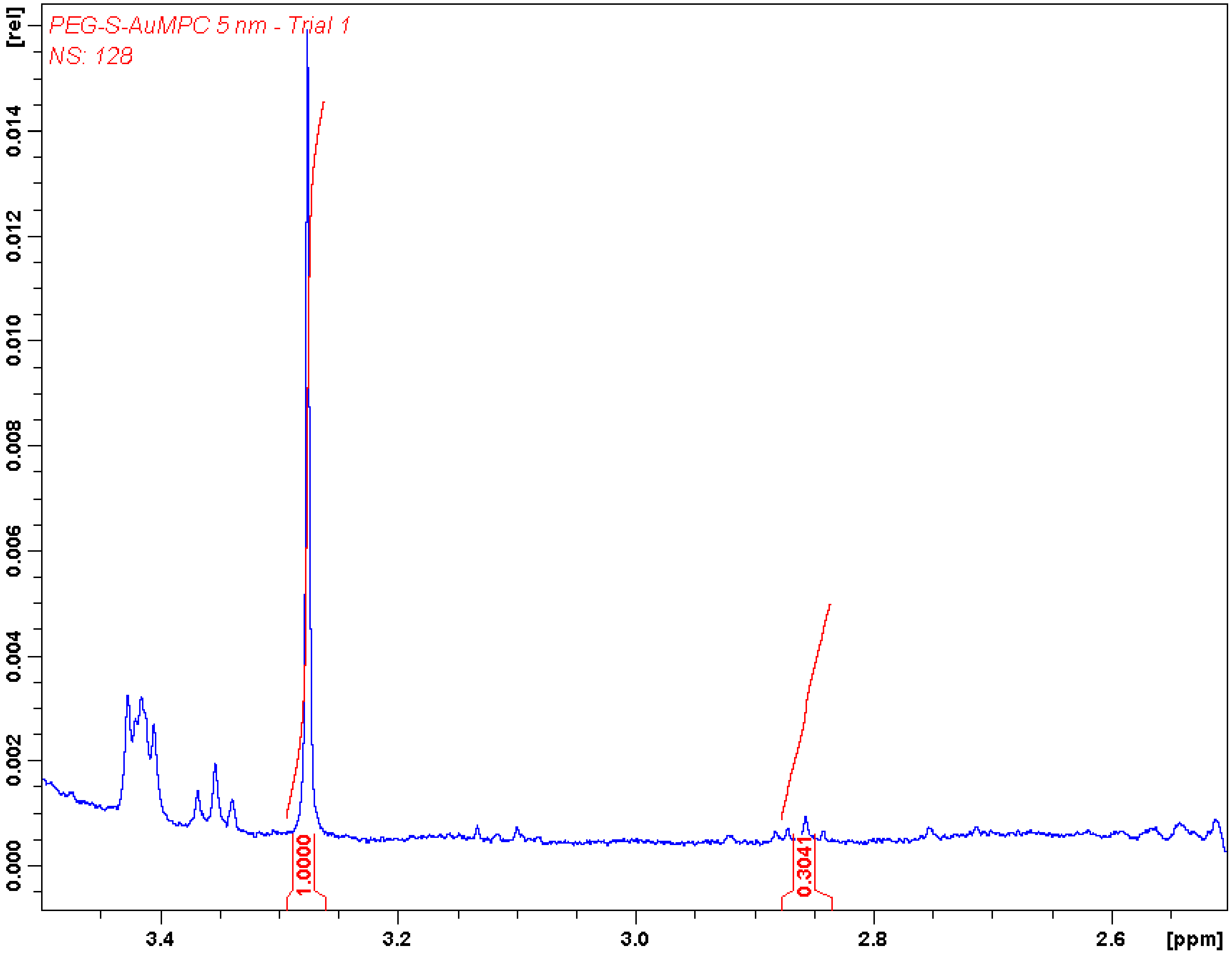

Spectrum B - 1. Trial 1 of 5 nm PEG-S-AuMPC spectrum showing quantitiatve integral ratio between total PEG and liberated (previously conjugated) PEG ligands

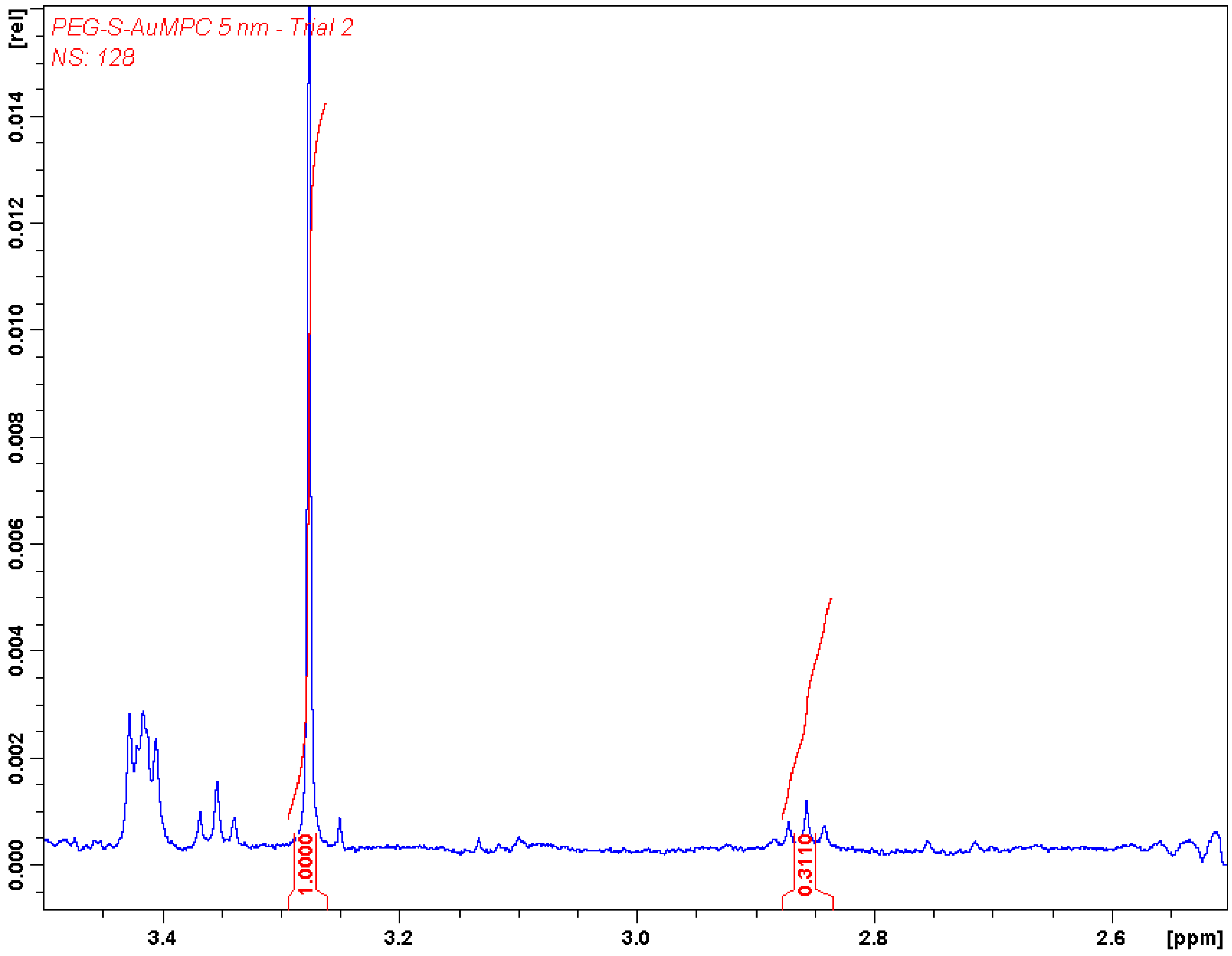

Spectrum B - 2. Trial 2 of 5 nm PEG-S-AuMPC spectrum showing quantitiatve integral ratio between total PEG and liberated (previously conjugated) PEG ligands

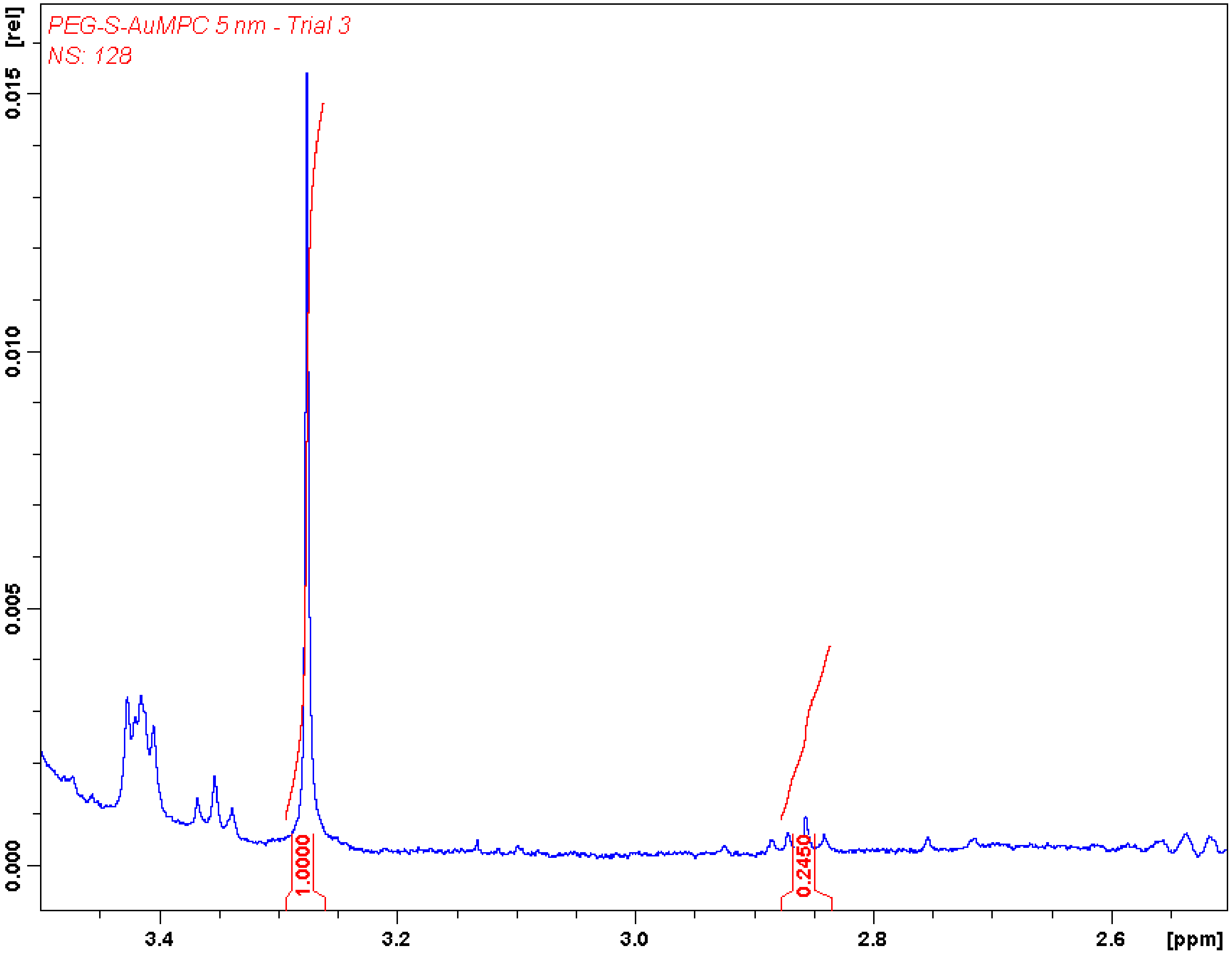

Spectrum B - 3. **Trial 3 of 5 nm PEG-S-AuMPC spectrum showing quantitiatve integral ratio between total PEG and liberated (previously conjugated) PEG ligands.**

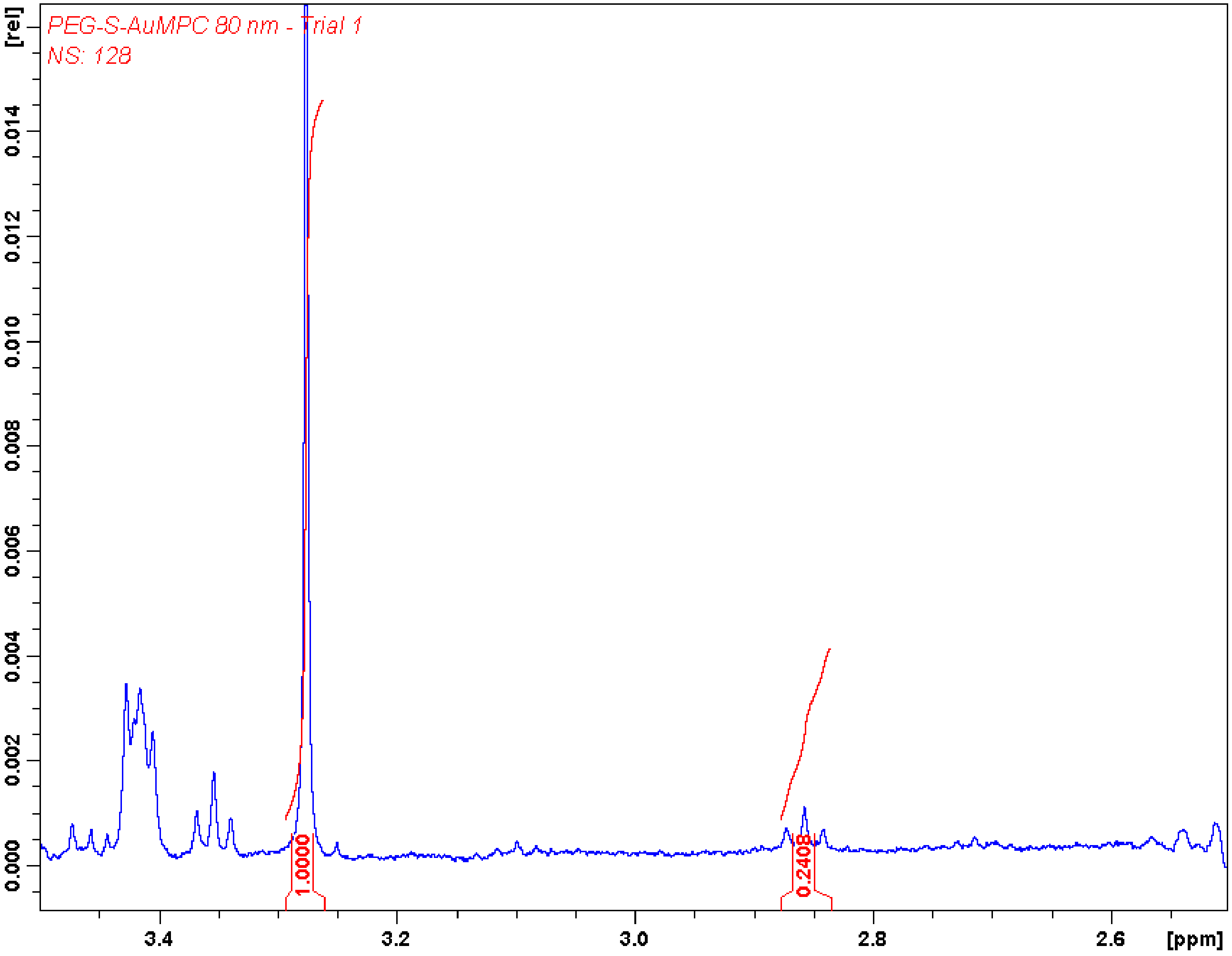

Spectrum B - 4. Trial 1 of 80 nm PEG-S-AuMPC spectrum showing quantitiatve integral ratio between total PEG and liberated (previously conjugated) PEG ligands

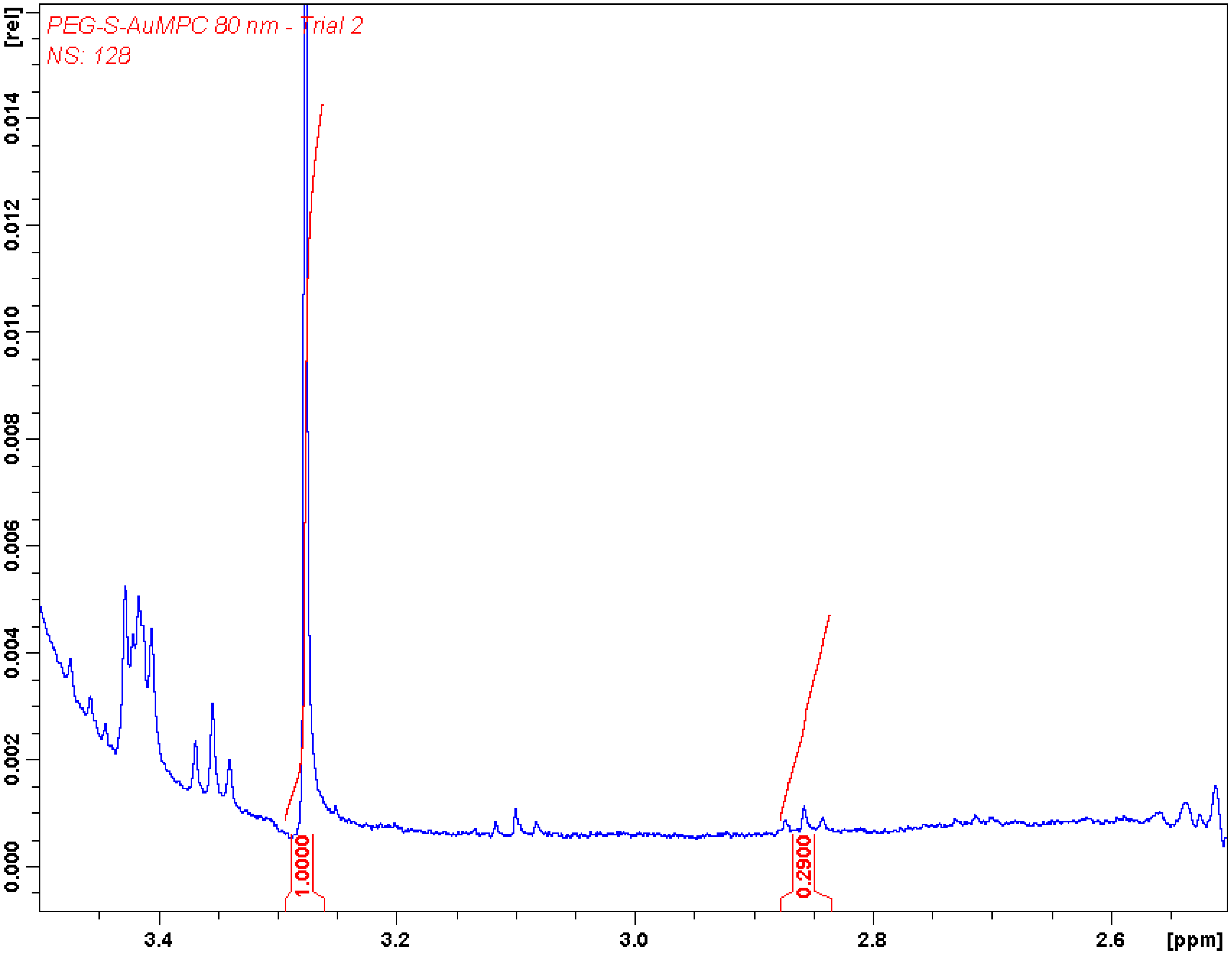

Spectrum B - 5. Trial 2 of 80 nm PEG-S-AuMPC spectrum showing quantitiatve integral ratio between total PEG and liberated (previously conjugated) PEG ligands

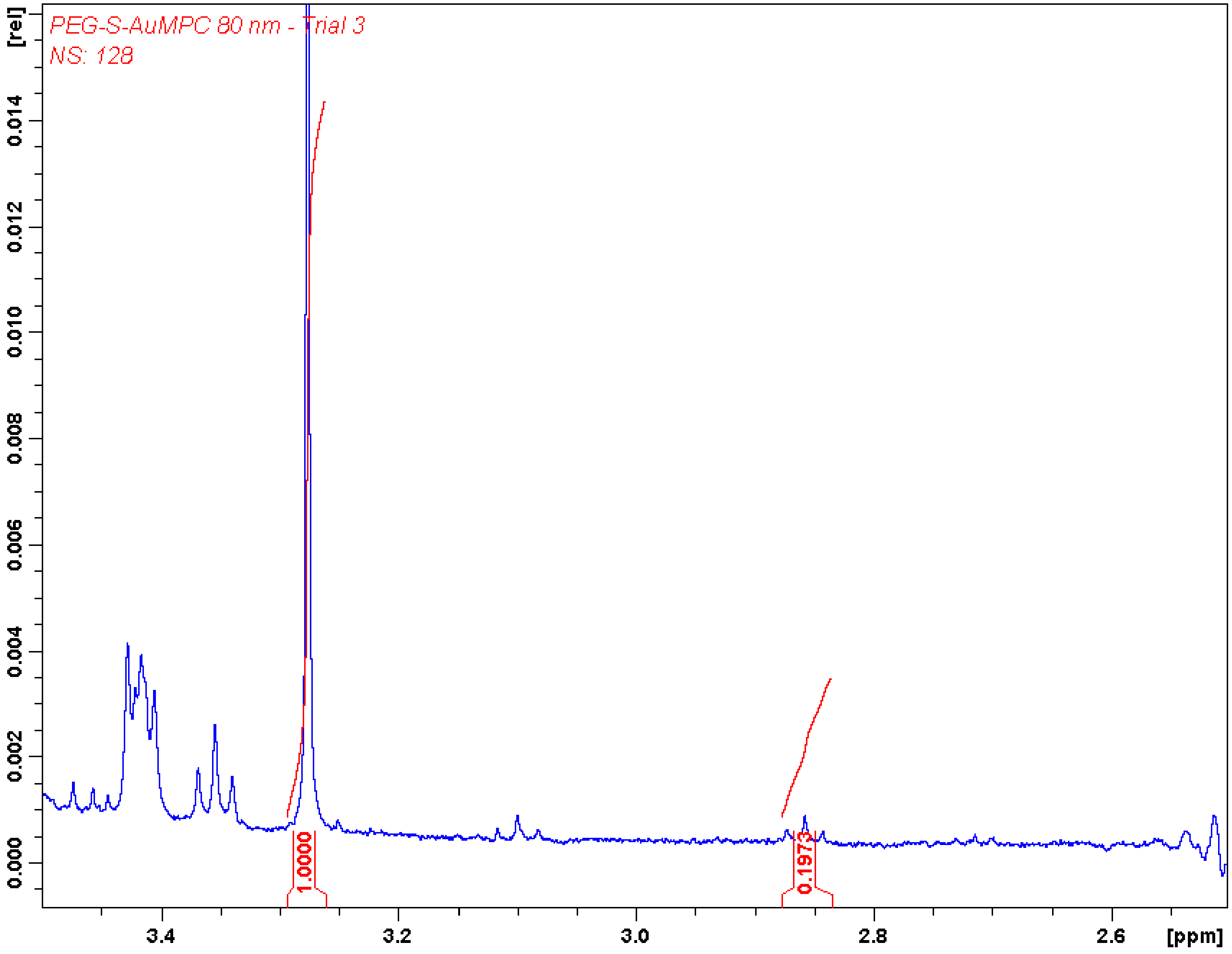

Spectrum B - 6. Trial 3 of 80 nm PEG-S-AuMPC spectrum showing quantitiatve integral ratio between total PEG and liberated (previously conjugated) PEG ligands

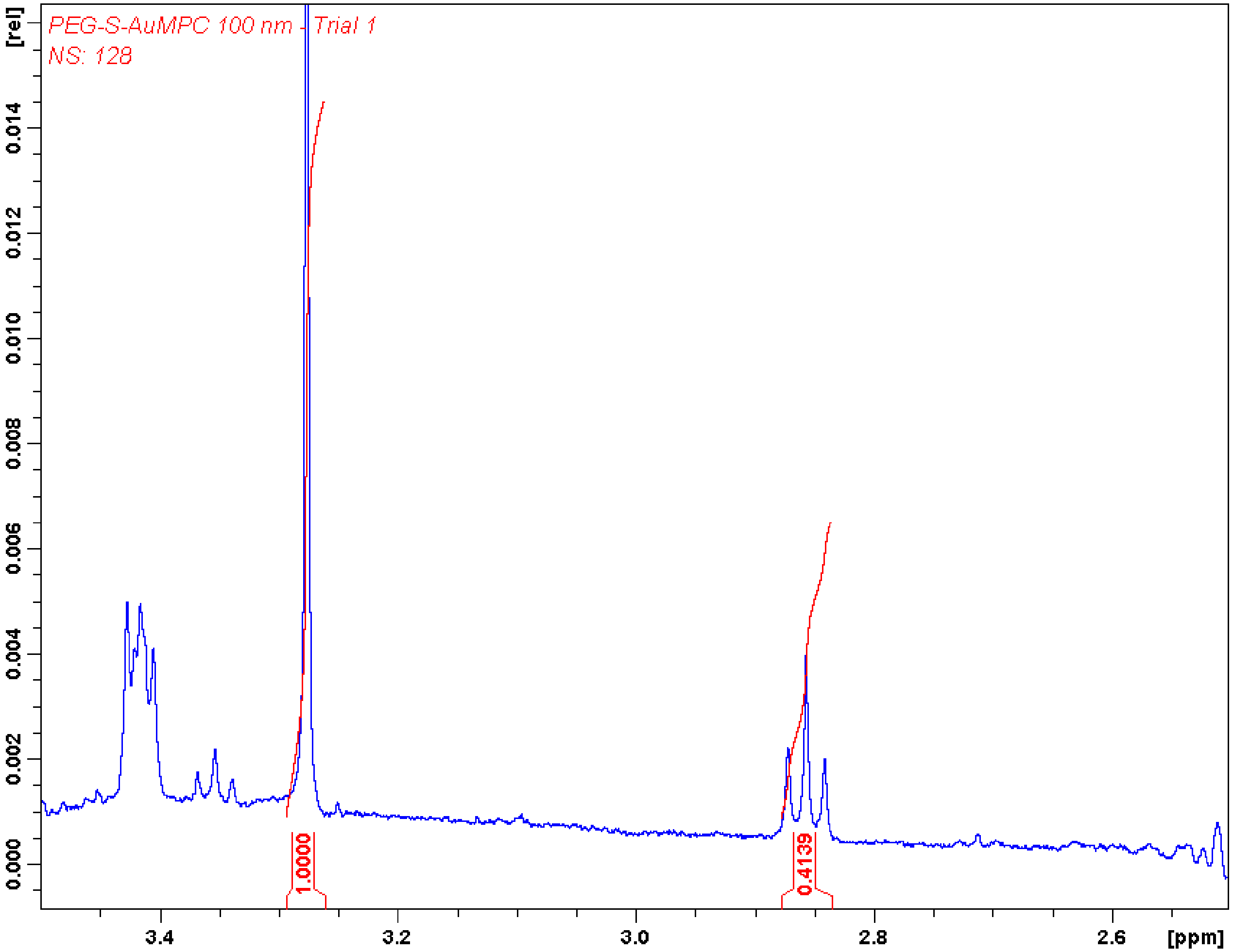

Spectrum B - 7. Trial 1 of 100 nm PEG-S-AuMPC spectrum showing quantitiatve integral ratio between total PEG and liberated (previously conjugated) PEG ligands

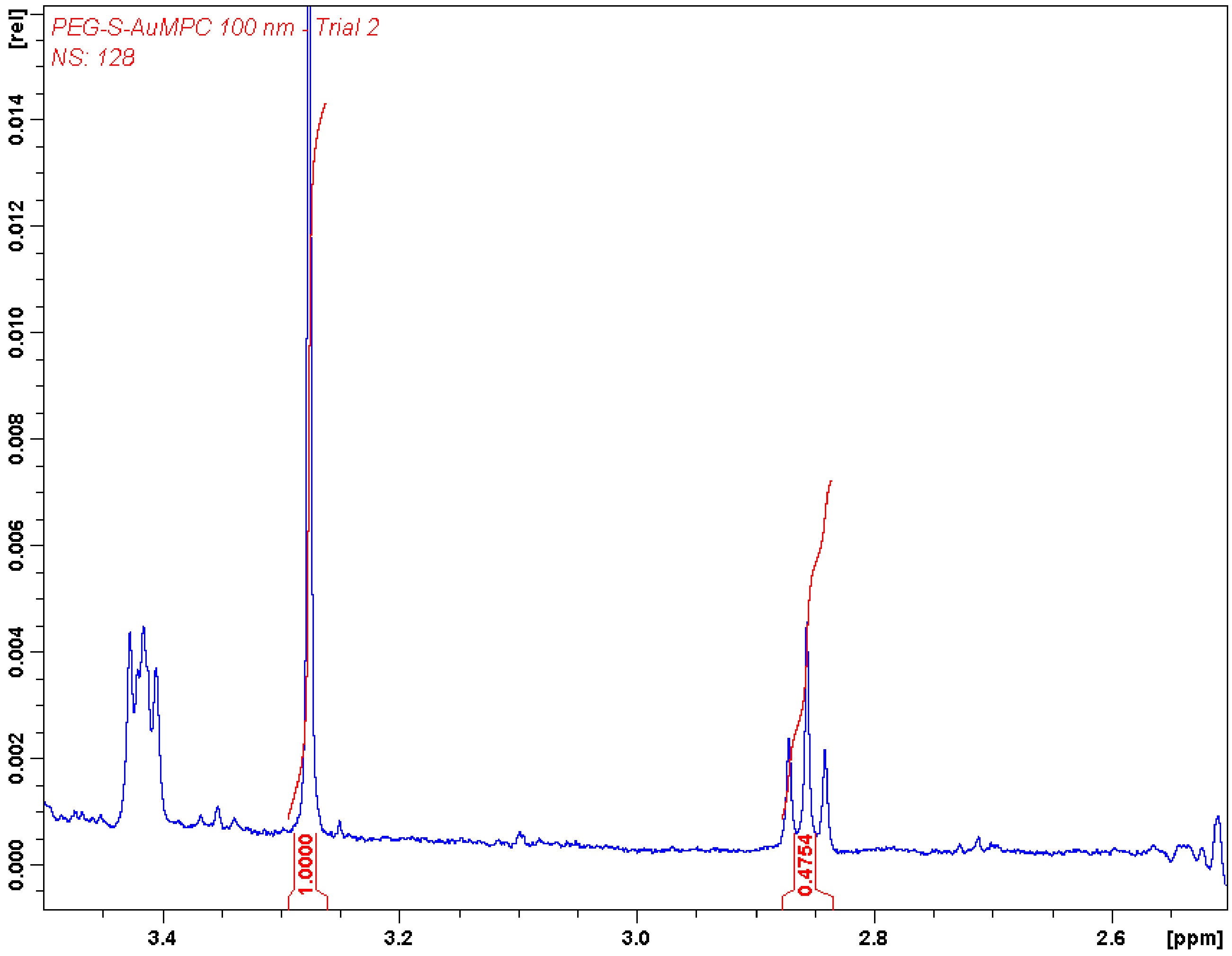

Spectrum B - 8. **Trial 2 of 100 nm PEG-S-AuMPC spectrum showing quantitiatve integral ratio between total PEG and liberated (previously conjugated) PEG ligands**

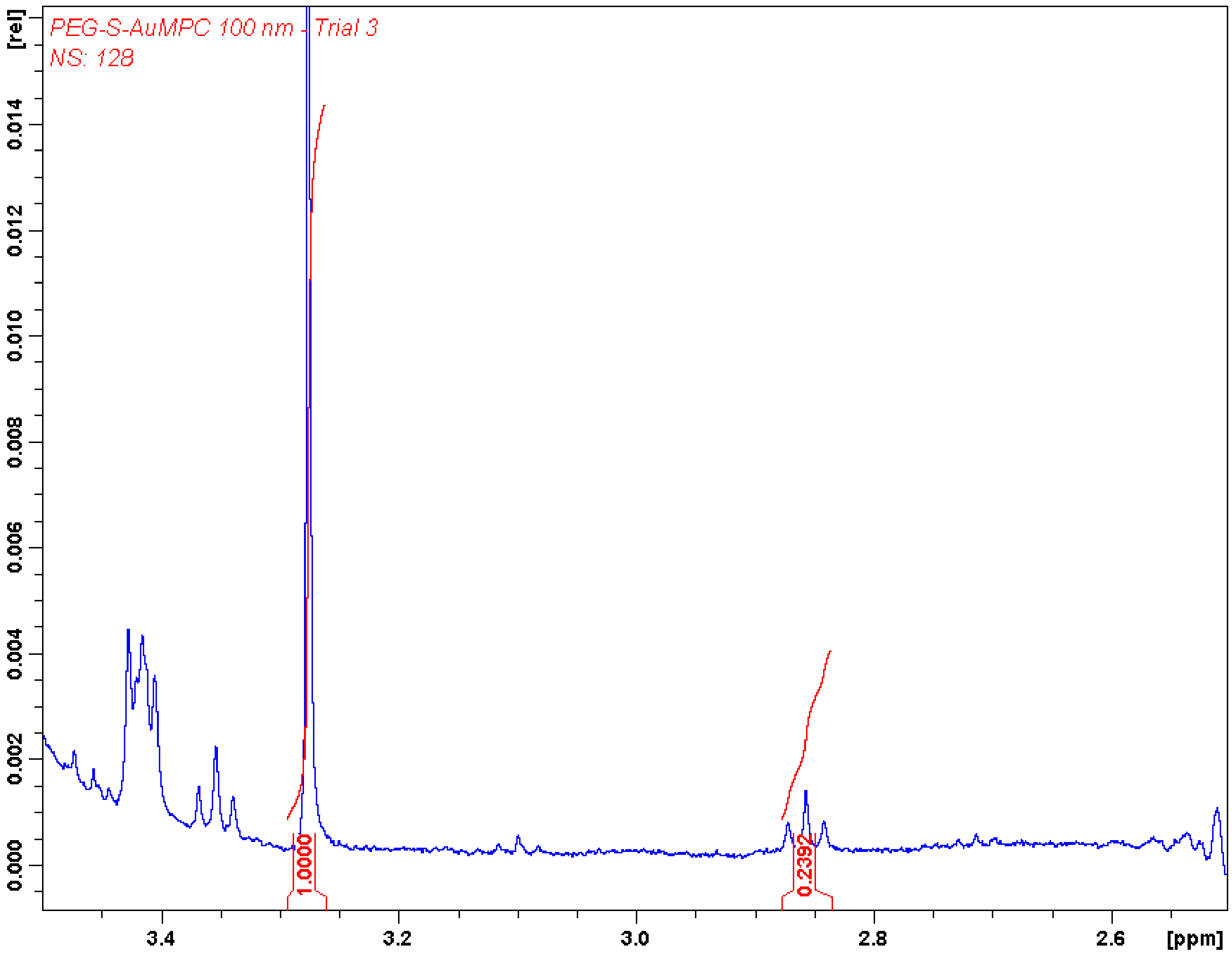

Spectrum B - 9. Trial 3 of 100 nm PEG-S-AuMPC spectrum showing quantitiatve integral ratio between total PEG and liberated (previously conjugated) PEG ligands

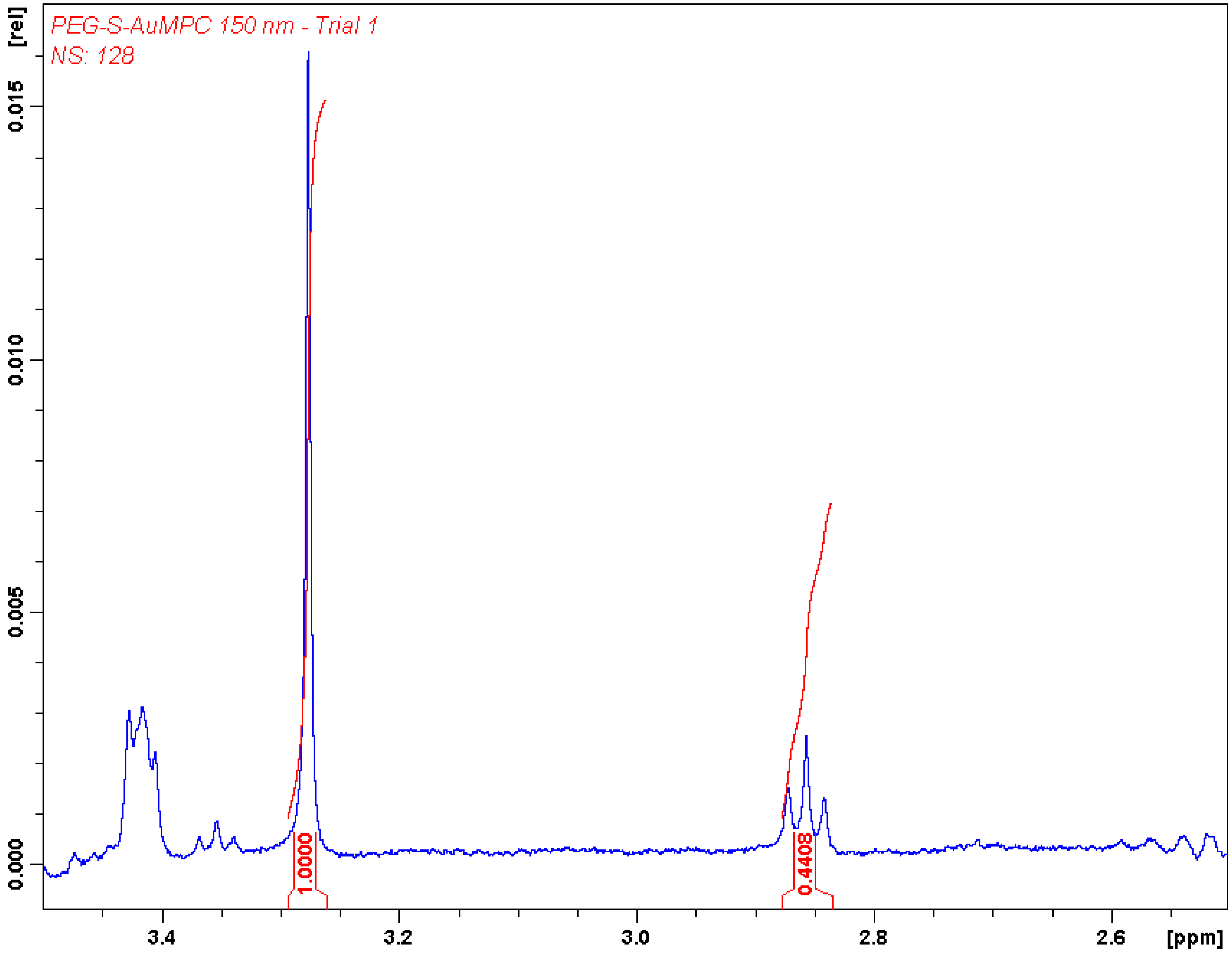

Spectrum B - 10. **Trial 1 of 150 nm PEG-S-AuMPC spectrum showing quantitiatve integral ratio between total PEG and liberated (previously conjugated) PEG ligands**

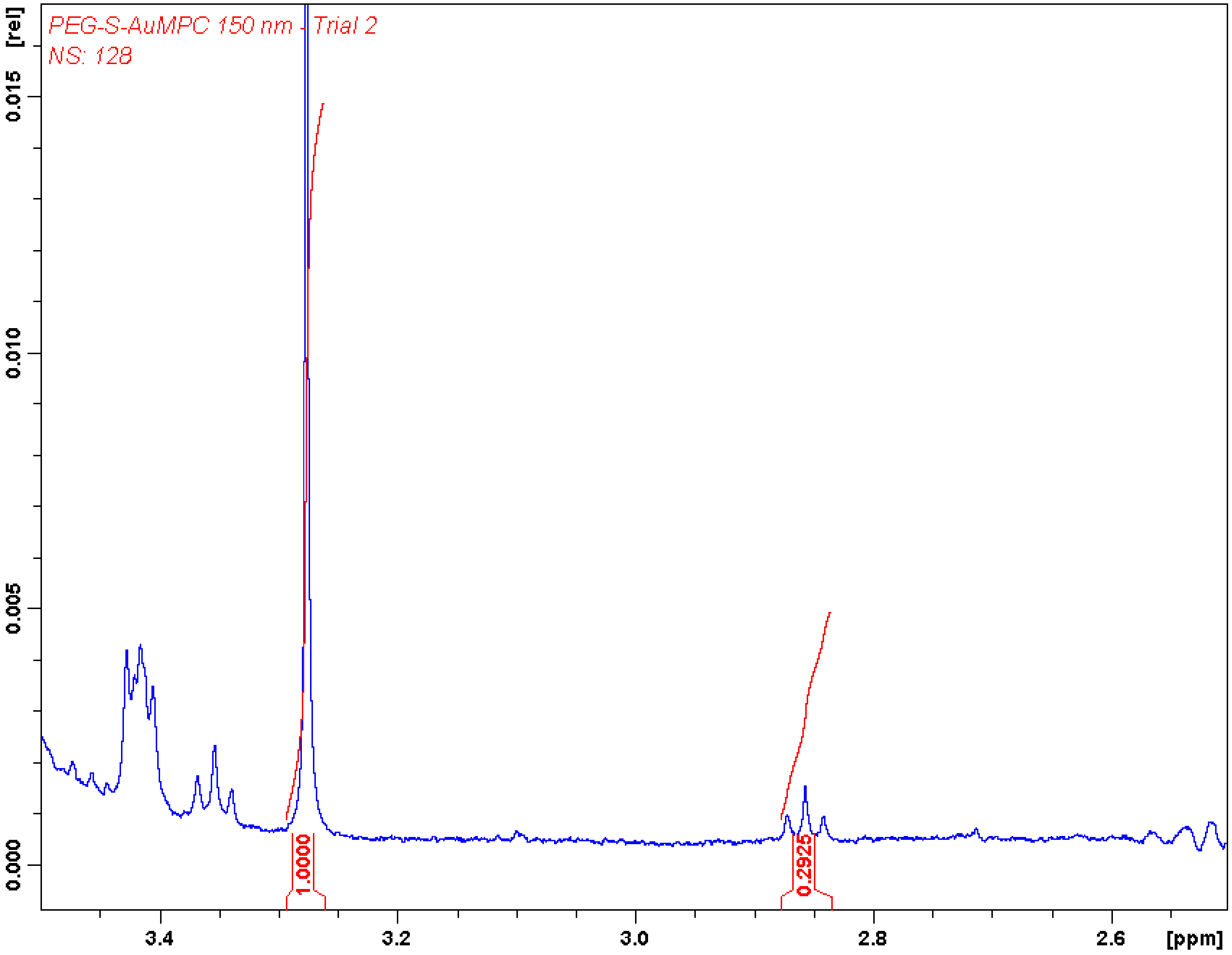

Spectrum B - 11. **Trial 2 of 150 nm PEG-S-AuMPC spectrum showing quantitiatve integral ratio between total PEG and liberated (previously conjugated) PEG ligands**

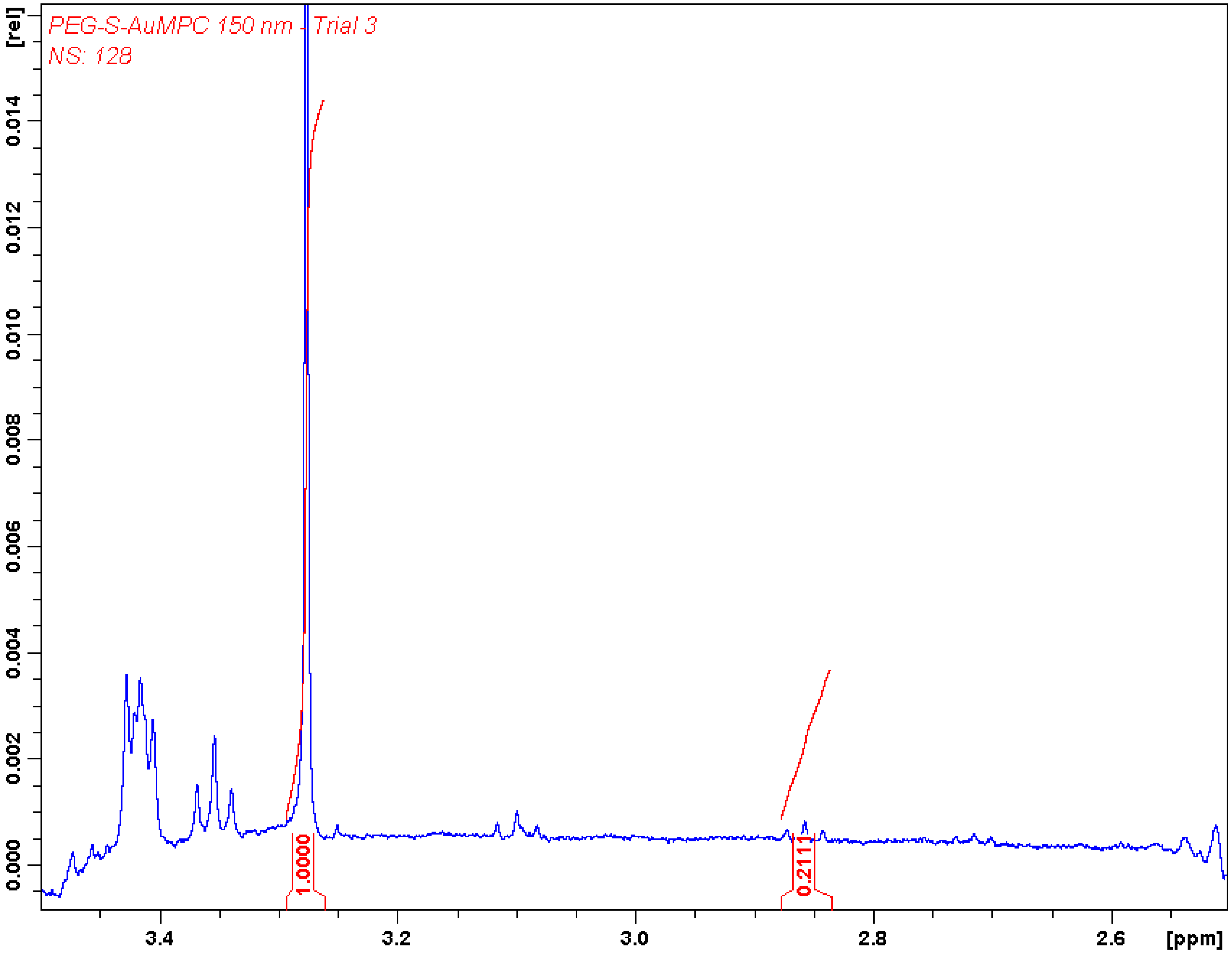

Spectrum B - 12. Trial 3 of 150 nm PEG-S-AuMPC spectrum showing quantitiatve integral ratio between total PEG and liberated (previously conjugated) PEG ligands

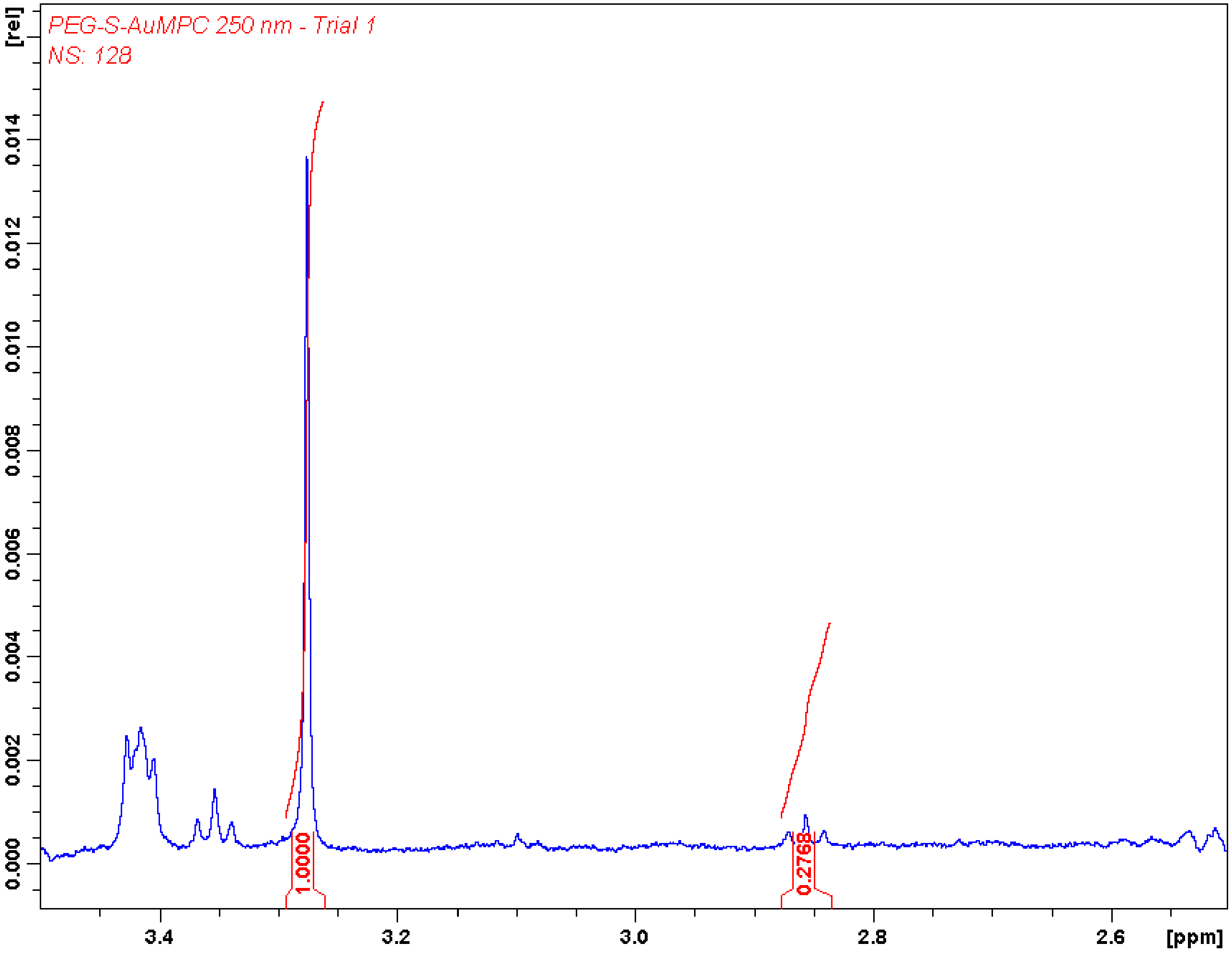

Spectrum B - 13. **Trial 1 of 250 nm PEG-S-AuMPC spectrum showing quantitiatve integral ratio between total PEG and liberated (previously conjugated) PEG ligands**

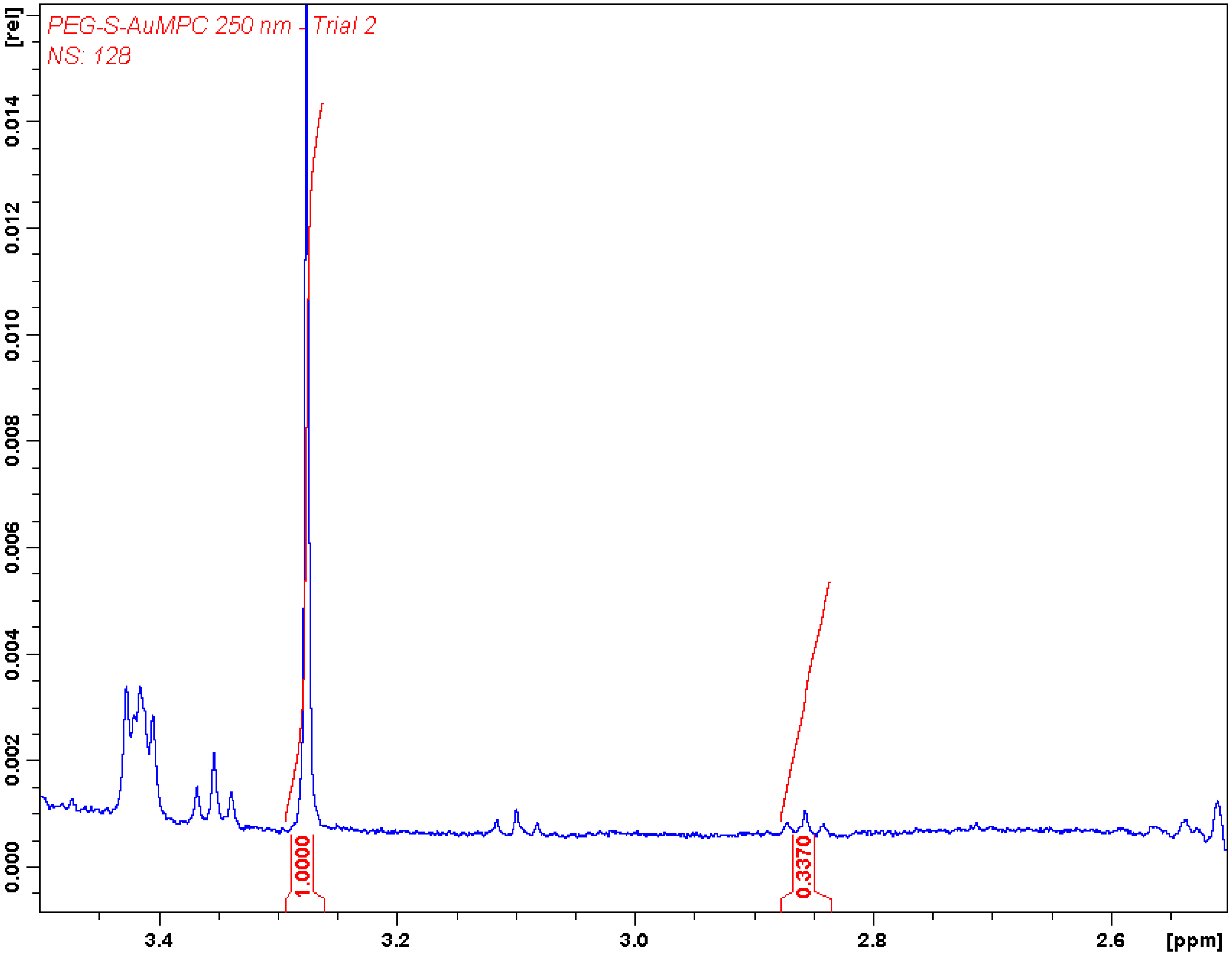

Spectrum B - 14. Trial 2 of 250 nm PEG-S-AuMPC spectrum showing quantitiatve integral ratio between total PEG and liberated (previously conjugated) PEG ligands

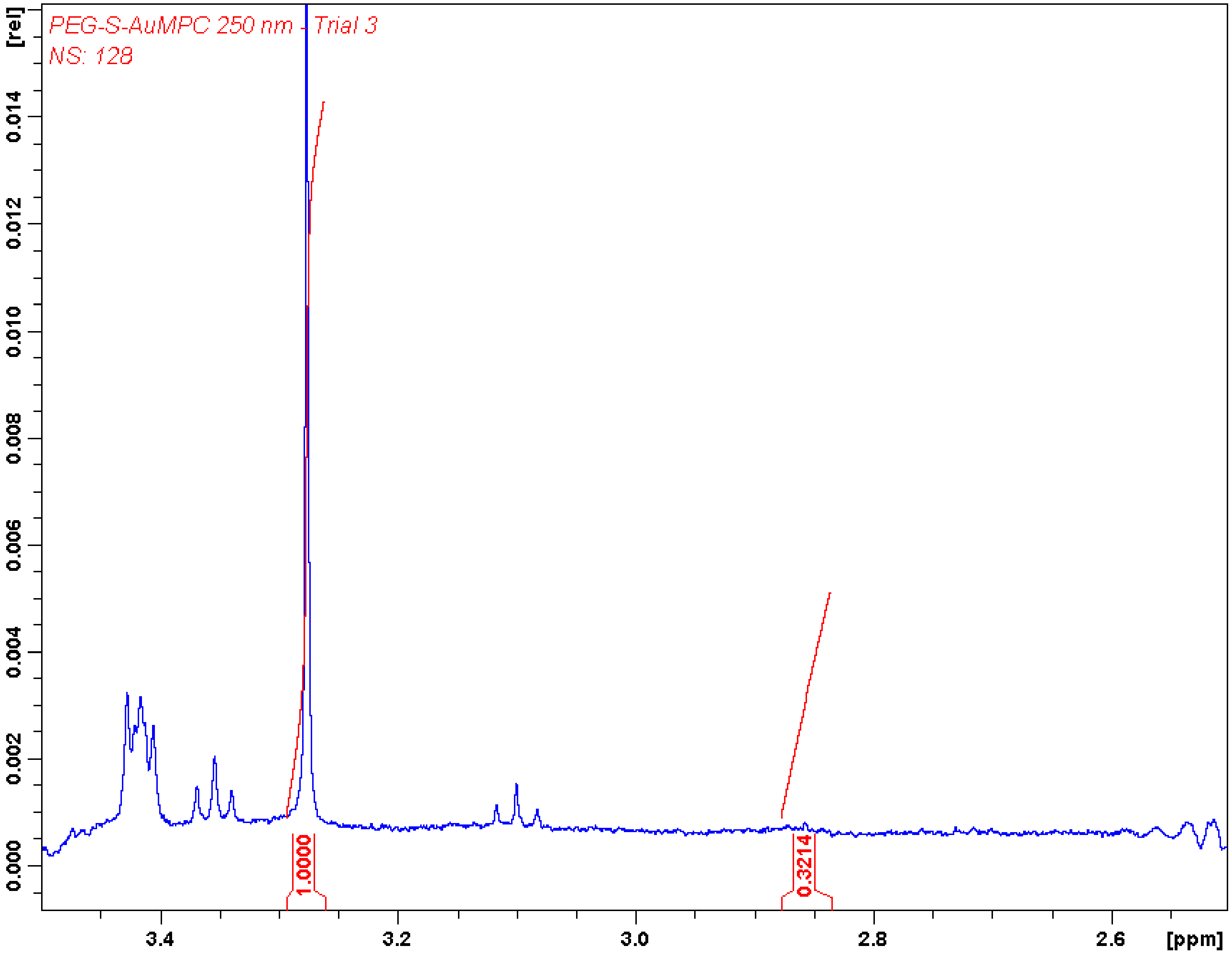

Spectrum B - 15. Trial 3 of 250 nm PEG-S-AuMPC spectrum showing quantitiatve integral ratio between total PEG and liberated (previously conjugated) PEG ligands

APPENDIX C

PRE-SATURATED NMR SPECTRA OF DECOMPOSED PEGYLATED MONOLAYER PROTECTED CLUSTERS

Table of Spectra

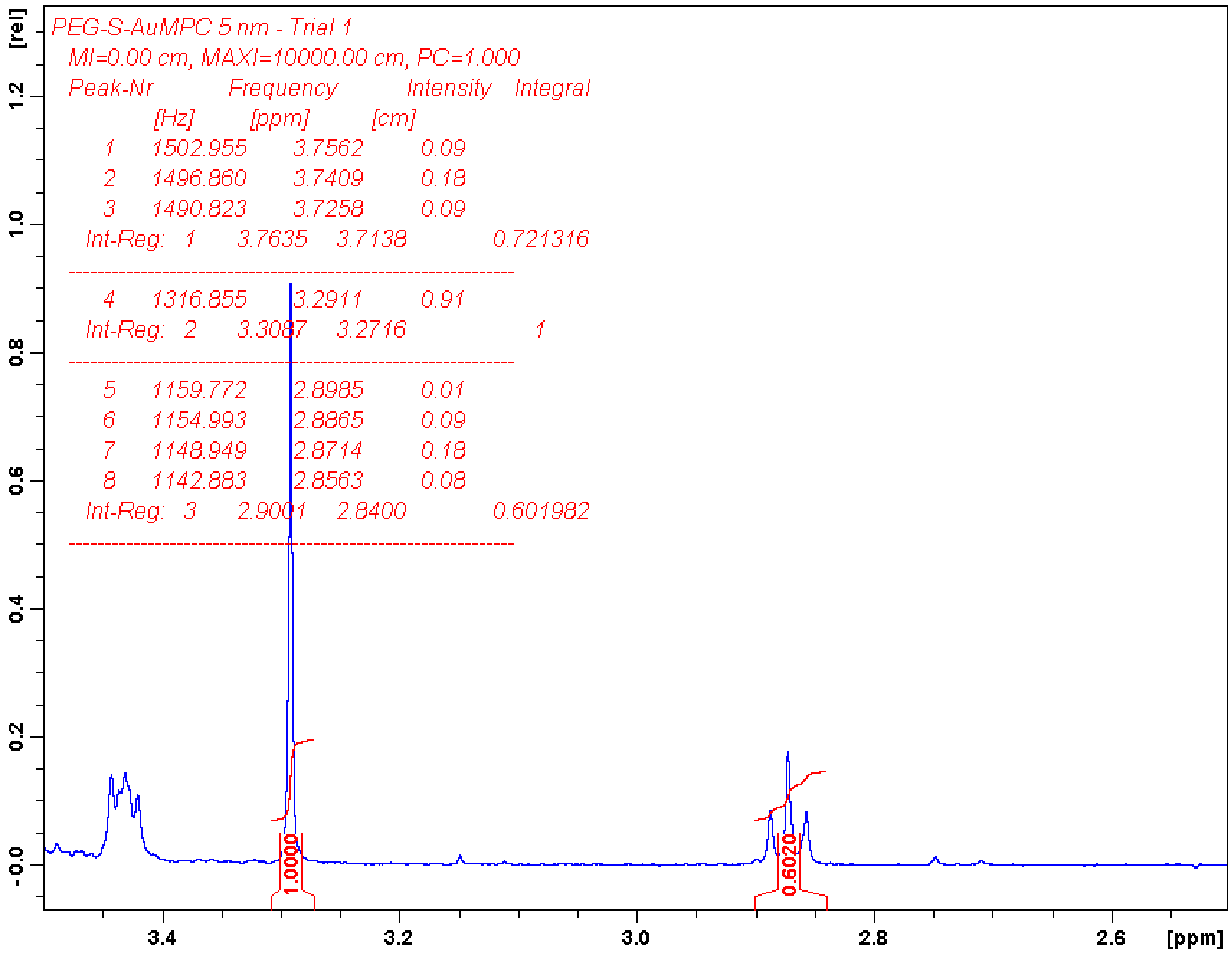

```
PEG-S-AuMPC 5 nm - Trial 1
  MI=0.00 cm, MAXI=10000.00 cm, PC=1.000
  Peak-Nr          Frequency          Intensity   Integral
              [Hz]        [ppm]         [cm]
     1     1502.955      3.7562        0.09
     2     1496.860      3.7409        0.18
     3     1490.823      3.7258        0.09
   Int-Reg:  1      3.7635    3.7138             0.721316
  -------------------------------------------------------------
     4     1316.855      3.2911        0.91
   Int-Reg:  2      3.3087    3.2716                    1
  -------------------------------------------------------------
     5     1159.772      2.8985        0.01
     6     1154.993      2.8865        0.09
     7     1148.949      2.8714        0.18
     8     1142.883      2.8563        0.08
   Int-Reg:  3      2.9001    2.8400             0.601982
  -------------------------------------------------------------
```

Spectrum C - 1. Trial 1 of 5 nm PEG-S-AuMPC spectrum showing qualitative integral ratio between total PEG and liberated (previously conjugated) PEG ligands

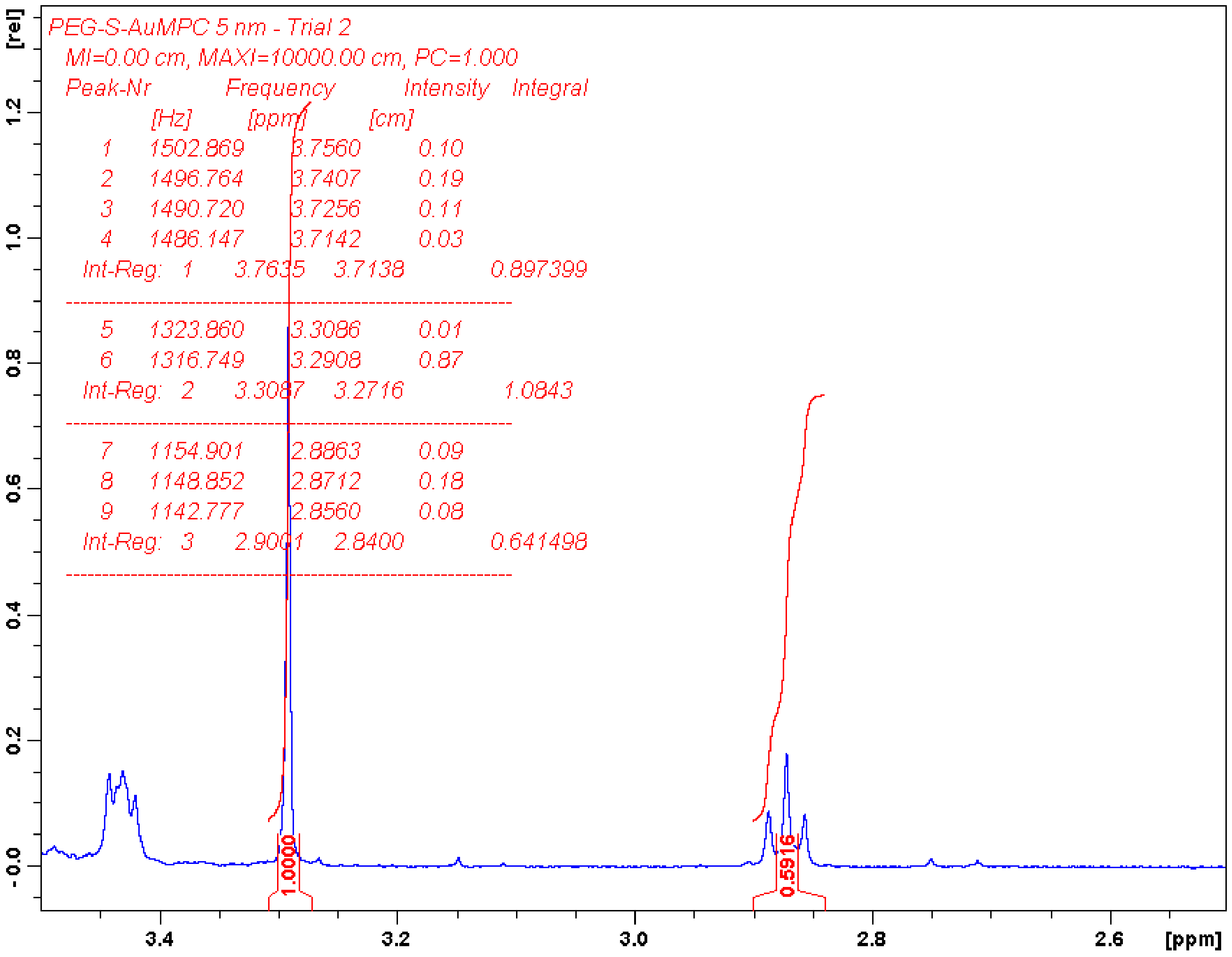

Spectrum C - 2. Trial 2 of 5 nm PEG-S-AuMPC spectrum showing qualitative integral ratio between total PEG and liberated (previously conjugated) PEG ligands

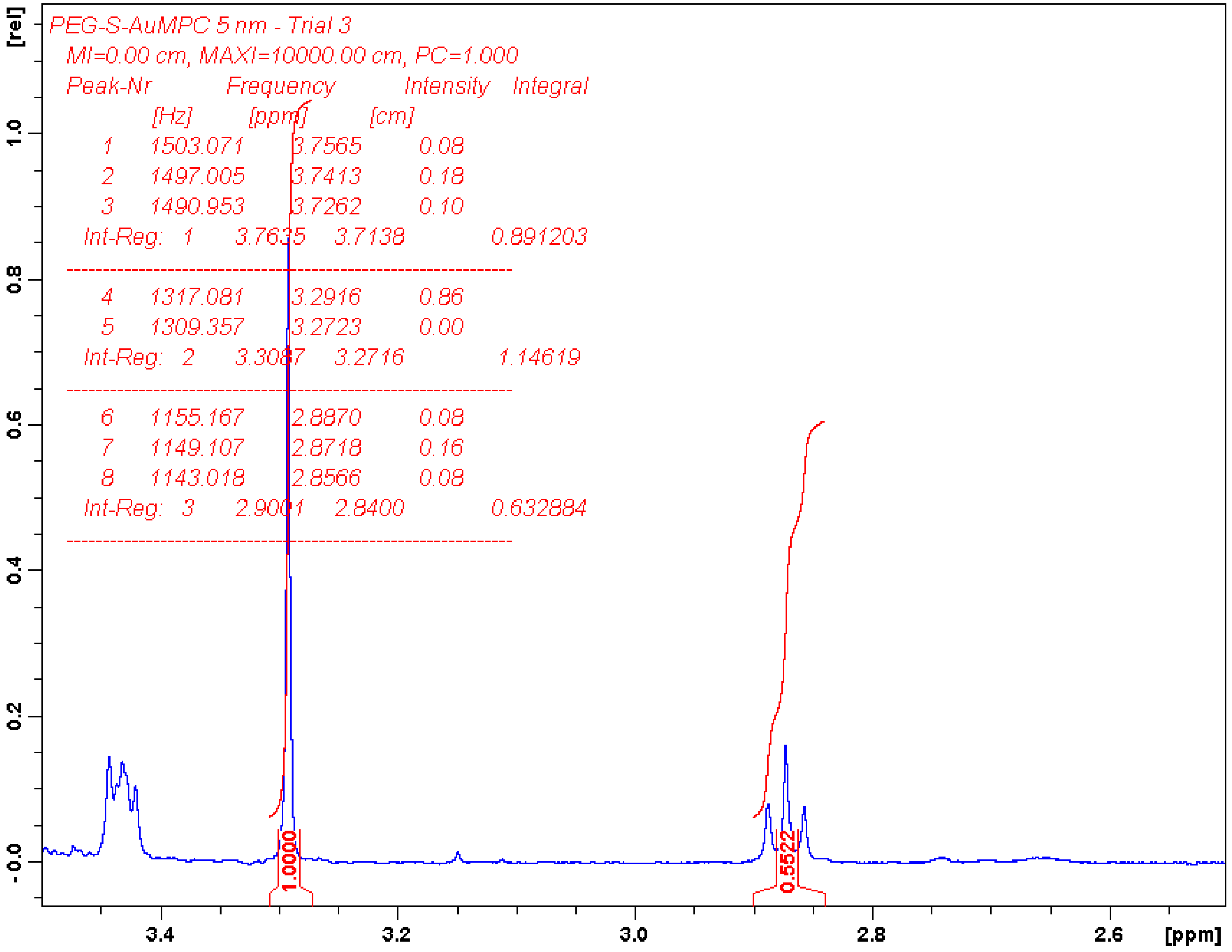

```
PEG-S-AuMPC 5 nm - Trial 3
  MI=0.00 cm, MAXI=10000.00 cm, PC=1.000
  Peak-Nr        Frequency        Intensity   Integral
           [Hz]        [ppm]        [cm]
     1    1503.071      3.7565        0.08
     2    1497.005      3.7413        0.18
     3    1490.953      3.7262        0.10
    Int-Reg:  1     3.7635    3.7138            0.891203
  ---------------------------------------------------------------
     4    1317.081      3.2916        0.86
     5    1309.357      3.2723        0.00
    Int-Reg:  2     3.3087    3.2716             1.14619
  ---------------------------------------------------------------
     6    1155.167      2.8870        0.08
     7    1149.107      2.8718        0.16
     8    1143.018      2.8566        0.08
    Int-Reg:  3     2.9001    2.8400            0.632884
  ---------------------------------------------------------------
```

Spectrum C - 3. Trial 3 of 5 nm PEG-S-AuMPC spectrum showing qualitative integral ratio between total PEG and liberated (previously conjugated) PEG ligands

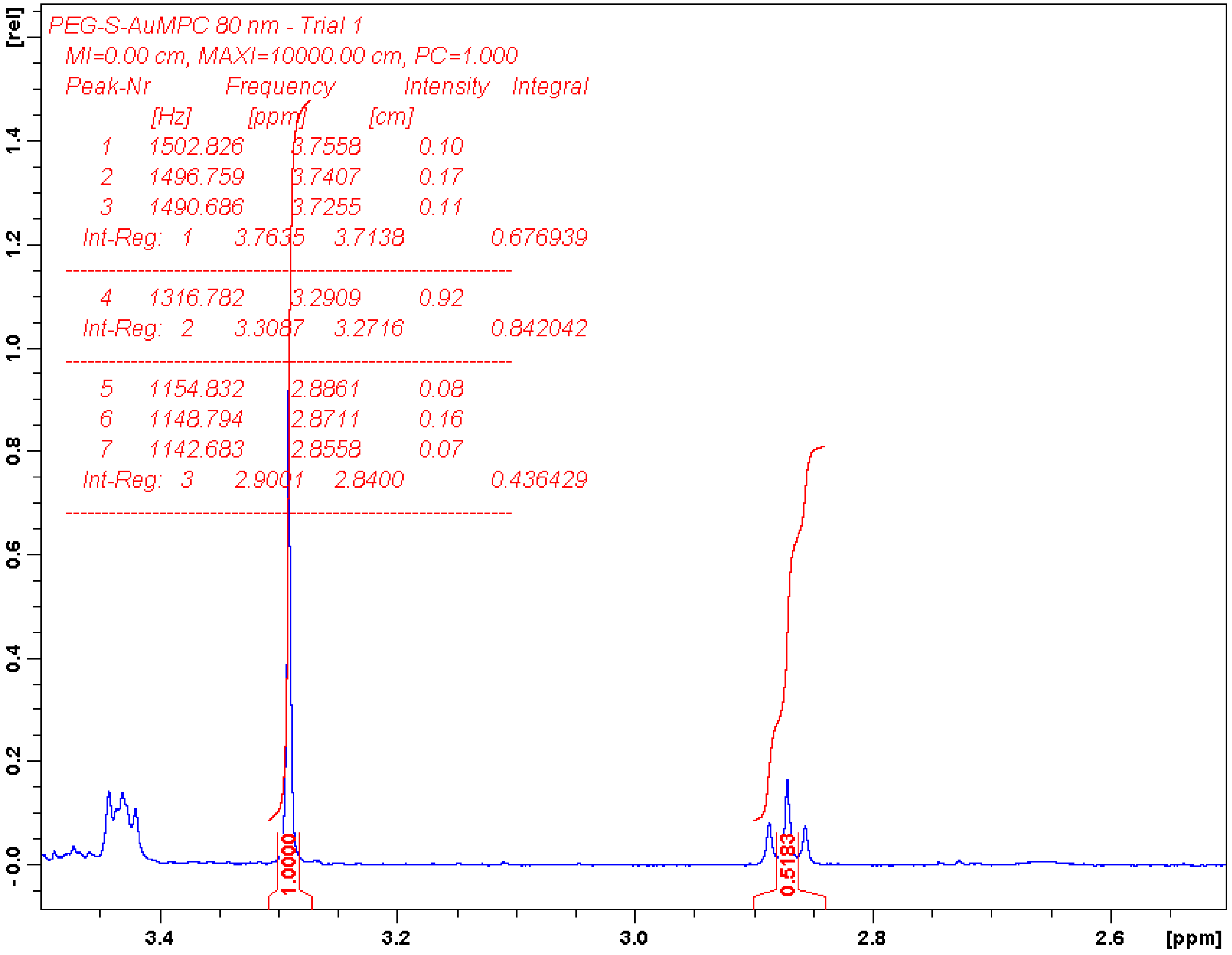

```
PEG-S-AuMPC 80 nm - Trial 1
  MI=0.00 cm, MAXI=10000.00 cm, PC=1.000
  Peak-Nr        Frequency        Intensity   Integral
            [Hz]       [ppm]         [cm]
     1     1502.826    3.7558        0.10
     2     1496.759    3.7407        0.17
     3     1490.686    3.7255        0.11
   Int-Reg:  1     3.7635    3.7138            0.676939
  ------------------------------------------------------------
     4     1316.782    3.2909        0.92
   Int-Reg:  2     3.3087    3.2716            0.842042
  ------------------------------------------------------------
     5     1154.832    2.8861        0.08
     6     1148.794    2.8711        0.16
     7     1142.683    2.8558        0.07
   Int-Reg:  3     2.9001    2.8400            0.436429
  ------------------------------------------------------------
```

Spectrum C - 4. Trial 1 of 80 nm PEG-S-AuMPC spectrum showing qualitative integral ratio between total PEG and liberated (previously conjugated) PEG ligands

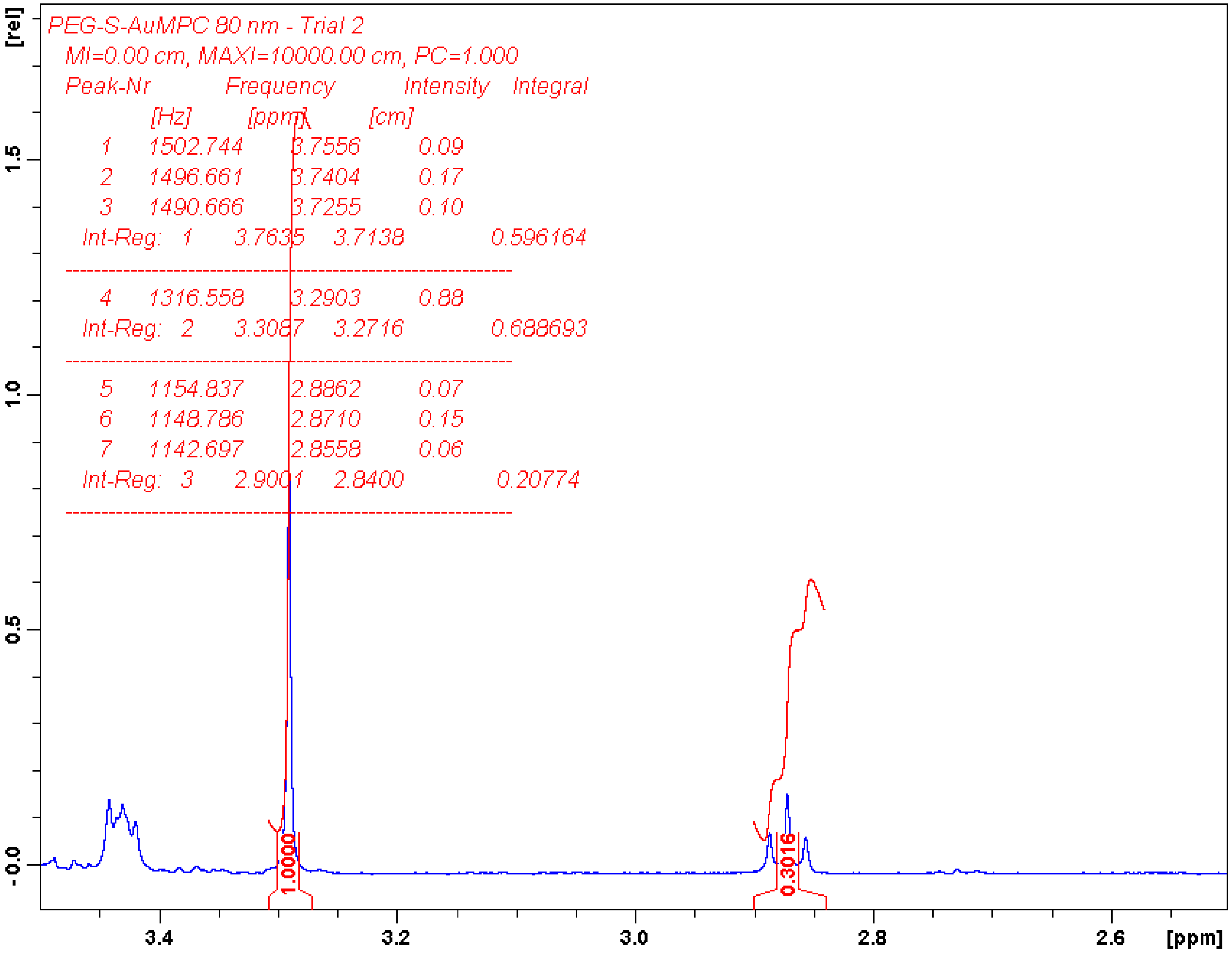

```
PEG-S-AuMPC 80 nm - Trial 2
  MI=0.00 cm, MAXI=10000.00 cm, PC=1.000
  Peak-Nr        Frequency         Intensity   Integral
             [Hz]       [ppm]        [cm]
     1     1502.744     3.7556       0.09
     2     1496.661     3.7404       0.17
     3     1490.666     3.7255       0.10
   Int-Reg:  1      3.7635    3.7138            0.596164
  -------------------------------------------------------------
     4     1316.558     3.2903       0.88
   Int-Reg:  2      3.3087    3.2716            0.688693
  -------------------------------------------------------------
     5     1154.837     2.8862       0.07
     6     1148.786     2.8710       0.15
     7     1142.697     2.8558       0.06
   Int-Reg:  3      2.9001    2.8400            0.20774
  -------------------------------------------------------------
```

Spectrum C - 5. Trial 2 of 80 nm PEG-S-AuMPC spectrum showing qualitative integral ratio between total PEG and liberated (previously conjugated) PEG ligands

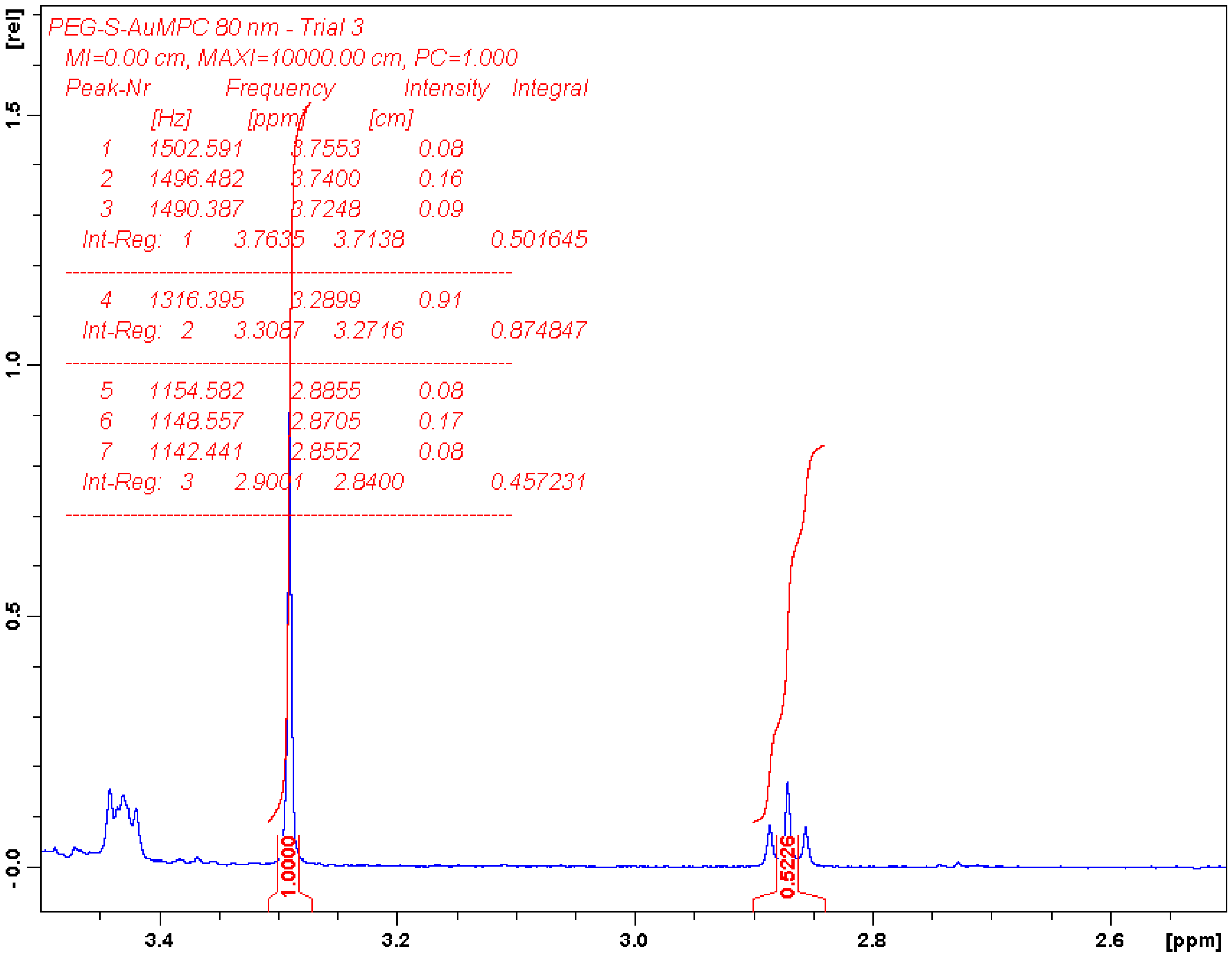
```
PEG-S-AuMPC 80 nm - Trial 3
  MI=0.00 cm, MAXI=10000.00 cm, PC=1.000
  Peak-Nr        Frequency        Intensity   Integral
            [Hz]        [ppm]         [cm]
      1     1502.591    3.7553        0.08
      2     1496.482    3.7400        0.16
      3     1490.387    3.7248        0.09
    Int-Reg:  1     3.7635    3.7138              0.501645
  ------------------------------------------------------------
      4     1316.395    3.2899        0.91
    Int-Reg:  2     3.3087    3.2716              0.874847
  ------------------------------------------------------------
      5     1154.582    2.8855        0.08
      6     1148.557    2.8705        0.17
      7     1142.441    2.8552        0.08
    Int-Reg:  3     2.9001    2.8400              0.457231
  ------------------------------------------------------------
```

Spectrum C - 6. Trial 3 of 80 nm PEG-S-AuMPC spectrum showing qualitative integral ratio between total PEG and liberated (previously conjugated) PEG ligands

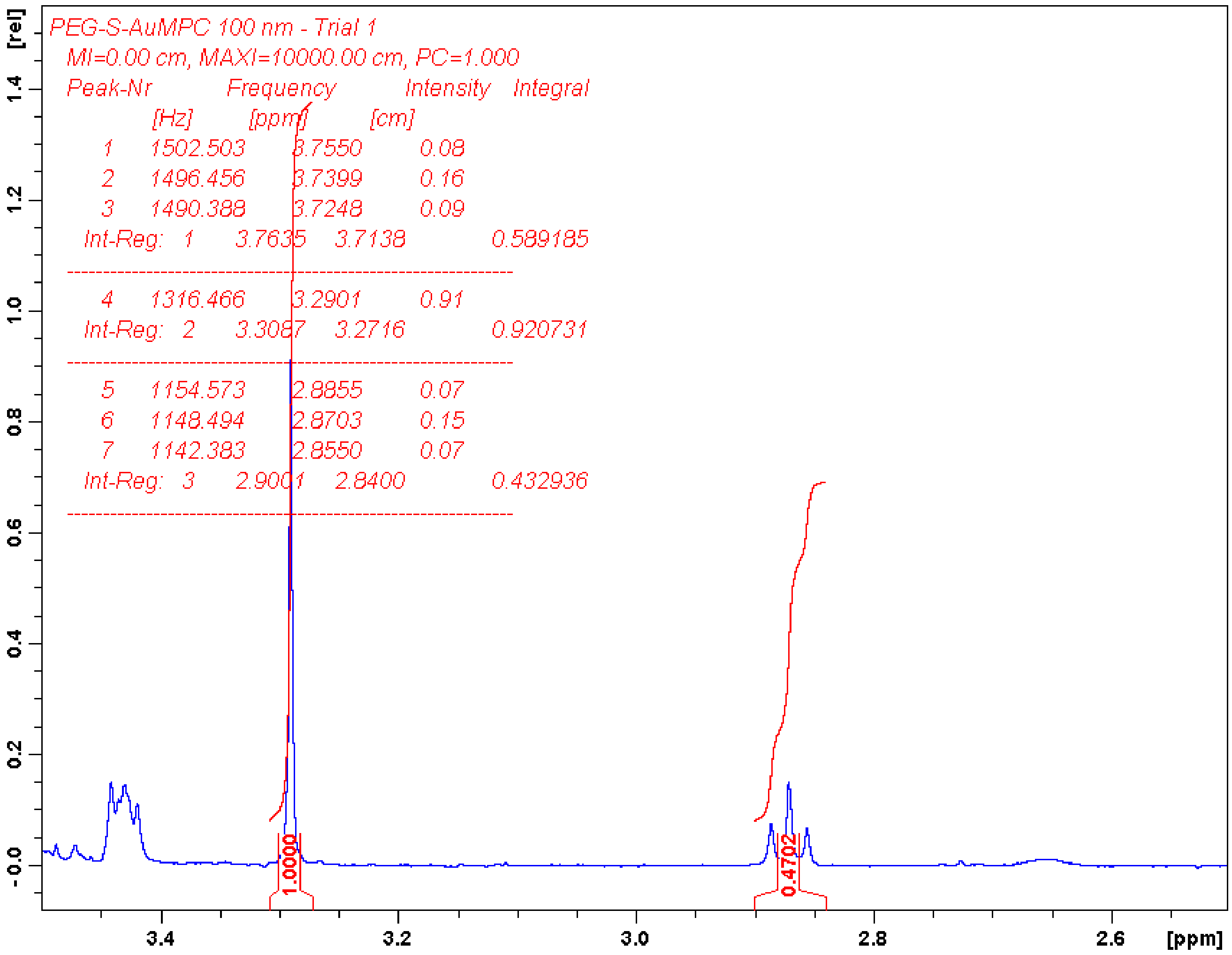

```
PEG-S-AuMPC 100 nm - Trial 1
  MI=0.00 cm, MAXI=10000.00 cm, PC=1.000
  Peak-Nr         Frequency          Intensity   Integral
             [Hz]        [ppm]          [cm]
     1     1502.503      3.7550        0.08
     2     1496.456      3.7399        0.16
     3     1490.388      3.7248        0.09
    Int-Reg:  1      3.7635    3.7138          0.589185
  ------------------------------------------------------------
     4     1316.466      3.2901        0.91
    Int-Reg:  2      3.3087    3.2716          0.920731
  ------------------------------------------------------------
     5     1154.573      2.8855        0.07
     6     1148.494      2.8703        0.15
     7     1142.383      2.8550        0.07
    Int-Reg:  3      2.9001    2.8400          0.432936
  ------------------------------------------------------------
```

Spectrum C - 7. Trial 1 of 100 nm PEG-S-AuMPC spectrum showing qualitative integral ratio between total PEG and liberated (previously conjugated) PEG ligands

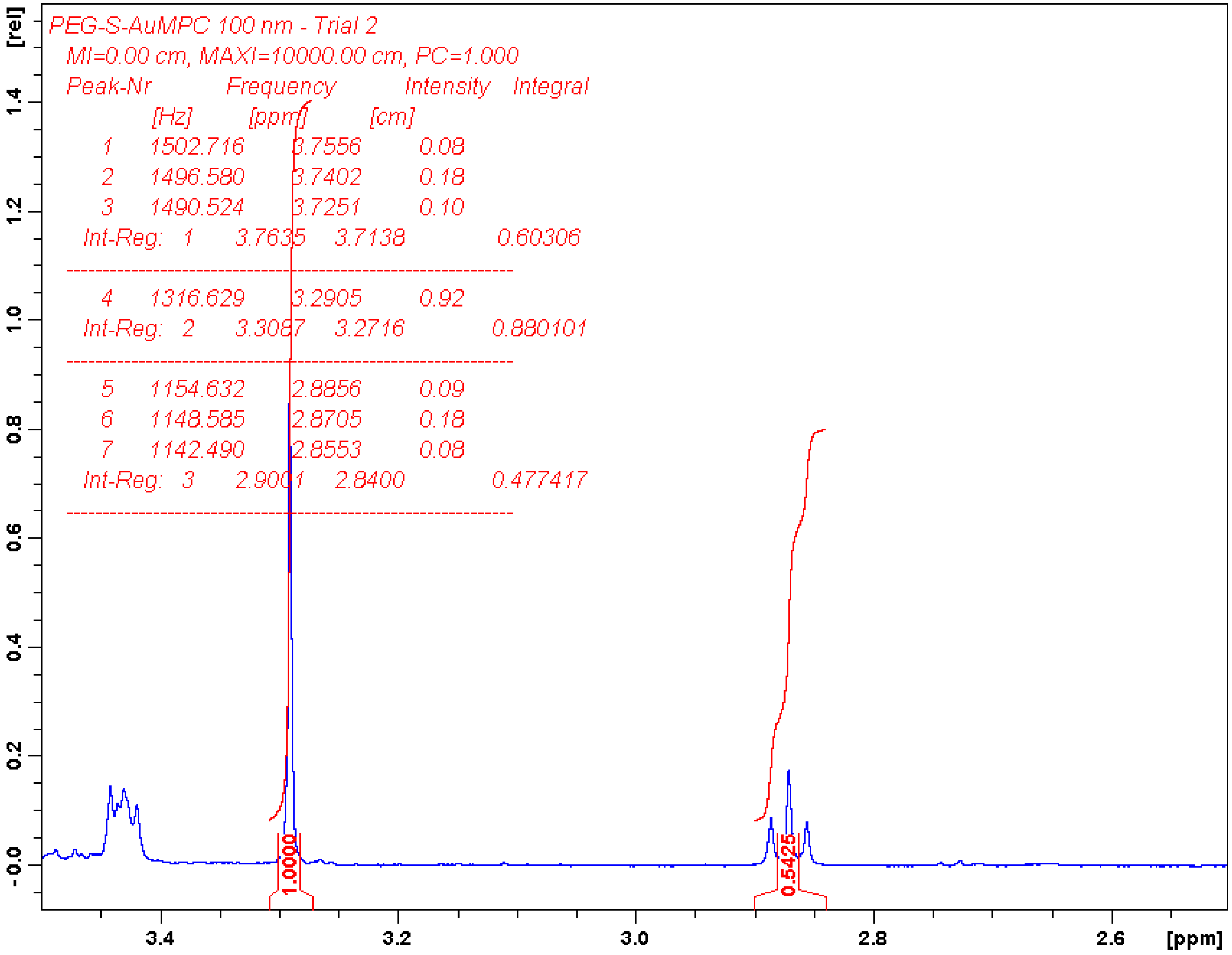

```
PEG-S-AuMPC 100 nm - Trial 2
  MI=0.00 cm, MAXI=10000.00 cm, PC=1.000
  Peak-Nr       Frequency        Intensity   Integral
             [Hz]      [ppm]       [cm]
      1    1502.716    3.7556      0.08
      2    1496.580    3.7402      0.18
      3    1490.524    3.7251      0.10
   Int-Reg:  1    3.7635   3.7138           0.60306
  ------------------------------------------------------------
      4    1316.629    3.2905      0.92
   Int-Reg:  2    3.3087   3.2716           0.880101
  ------------------------------------------------------------
      5    1154.632    2.8856      0.09
      6    1148.585    2.8705      0.18
      7    1142.490    2.8553      0.08
   Int-Reg:  3    2.9001   2.8400           0.477417
  ------------------------------------------------------------
```

Spectrum C - 8. Trial 2 of 100 nm PEG-S-AuMPC spectrum showing qualitative integral ratio between total PEG and liberated (previously conjugated) PEG ligands

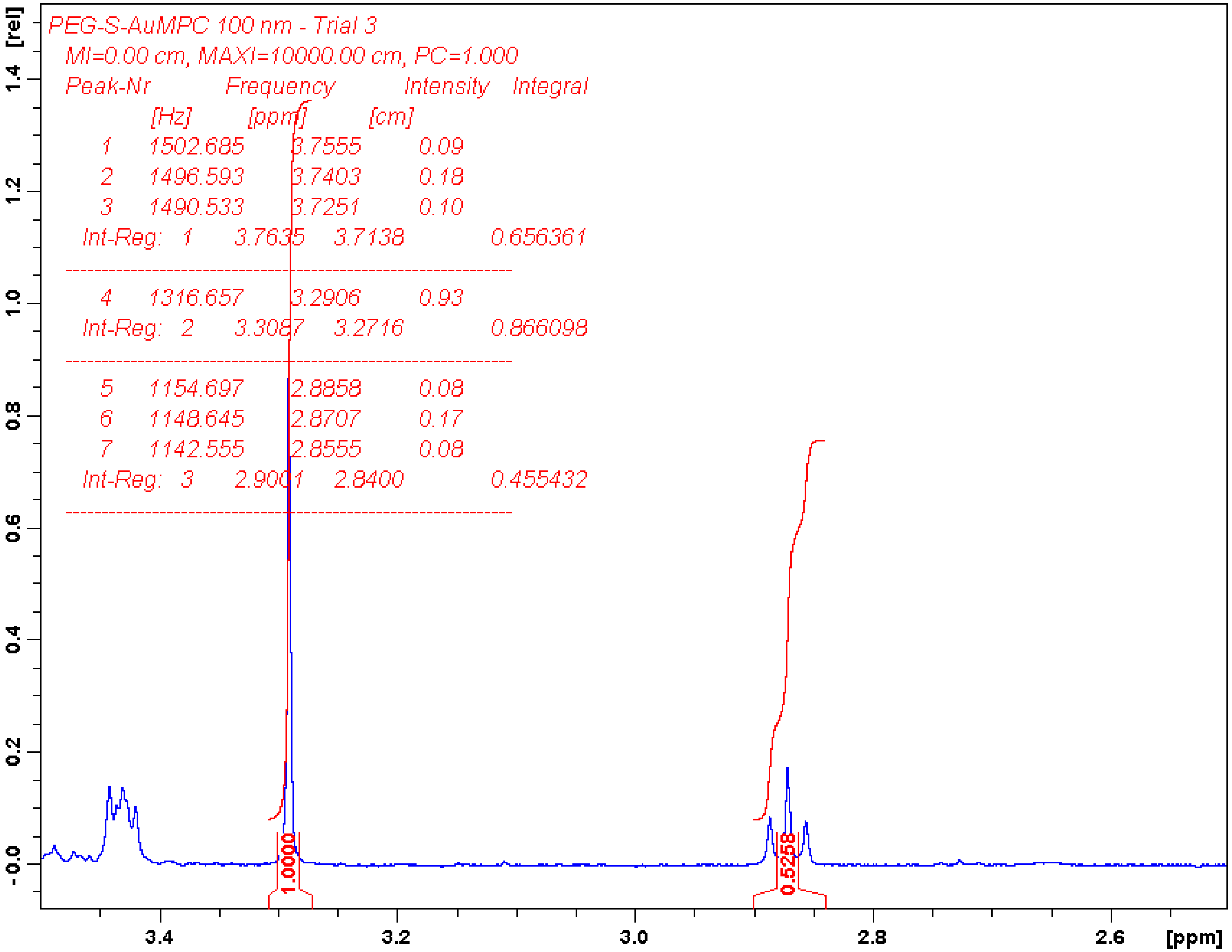

```
PEG-S-AuMPC 100 nm - Trial 3
  MI=0.00 cm, MAXI=10000.00 cm, PC=1.000
  Peak-Nr          Frequency          Intensity   Integral
            [Hz]        [ppm]         [cm]
       1      1502.685       3.7555        0.09
       2      1496.593       3.7403        0.18
       3      1490.533       3.7251        0.10
    Int-Reg:   1      3.7635     3.7138            0.656361
  ------------------------------------------------------------
       4      1316.657       3.2906        0.93
    Int-Reg:   2      3.3087     3.2716            0.866098
  ------------------------------------------------------------
       5      1154.697       2.8858        0.08
       6      1148.645       2.8707        0.17
       7      1142.555       2.8555        0.08
    Int-Reg:   3      2.9001     2.8400            0.455432
  ------------------------------------------------------------
```

Spectrum C - 9. Trial 3 of 100 nm PEG-S-AuMPC spectrum showing qualitative integral ratio between total PEG and liberated (previously conjugated) PEG ligands

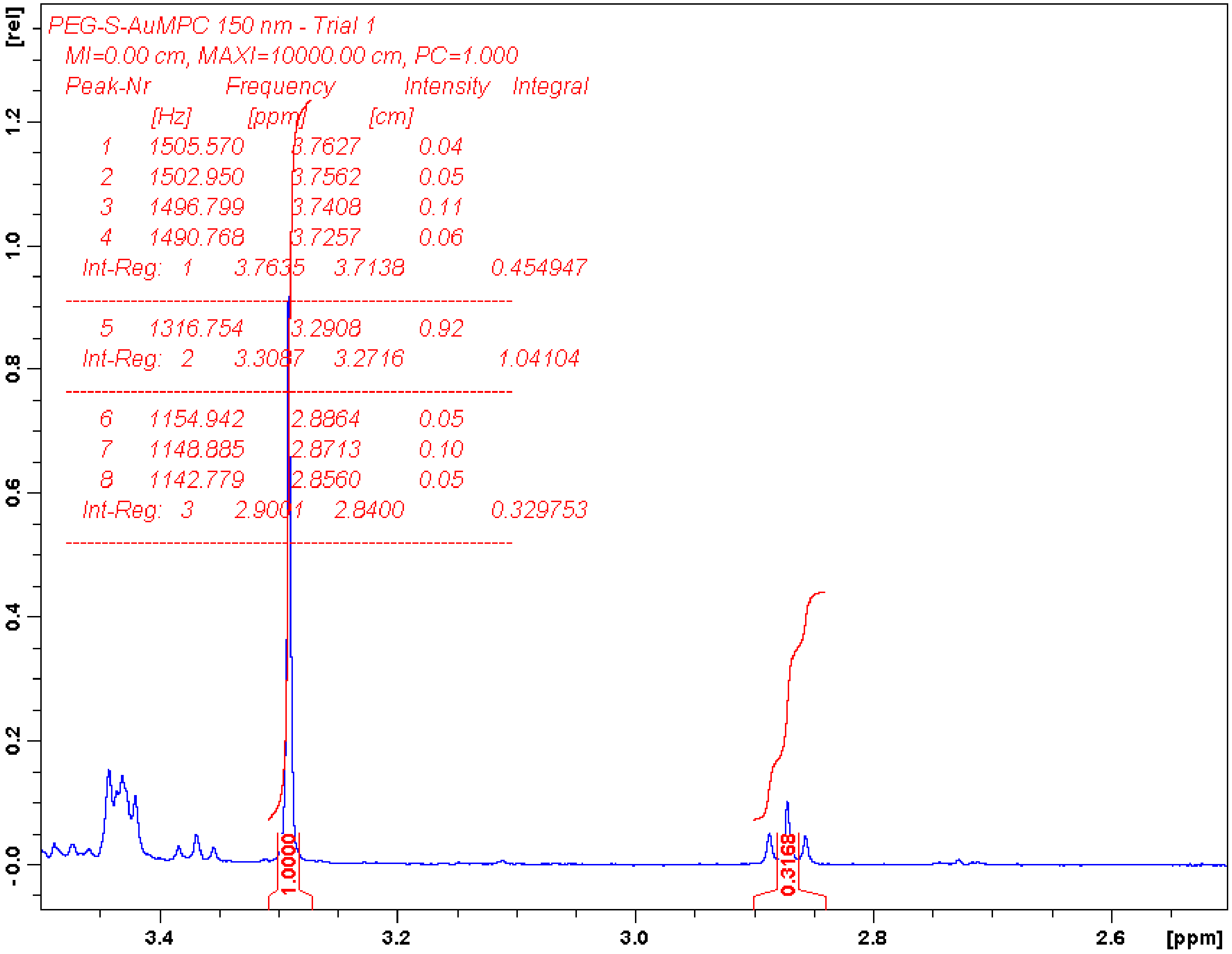

```
PEG-S-AuMPC 150 nm - Trial 1
  MI=0.00 cm, MAXI=10000.00 cm, PC=1.000
  Peak-Nr          Frequency          Intensity   Integral
             [Hz]        [ppm]          [cm]
     1     1505.570        3.7627        0.04
     2     1502.950        3.7562        0.05
     3     1496.799        3.7408        0.11
     4     1490.768        3.7257        0.06
   Int-Reg:  1       3.7635     3.7138             0.454947
  -------------------------------------------------------------
     5     1316.754        3.2908        0.92
   Int-Reg:  2       3.3087     3.2716              1.04104
  -------------------------------------------------------------
     6     1154.942        2.8864        0.05
     7     1148.885        2.8713        0.10
     8     1142.779        2.8560        0.05
   Int-Reg:  3       2.9001     2.8400             0.329753
  -------------------------------------------------------------
```

Spectrum C - 10. Trial 1 of 150 nm PEG-S-AuMPC spectrum showing qualitative integral ratio between total PEG and liberated (previously conjugated) PEG ligands

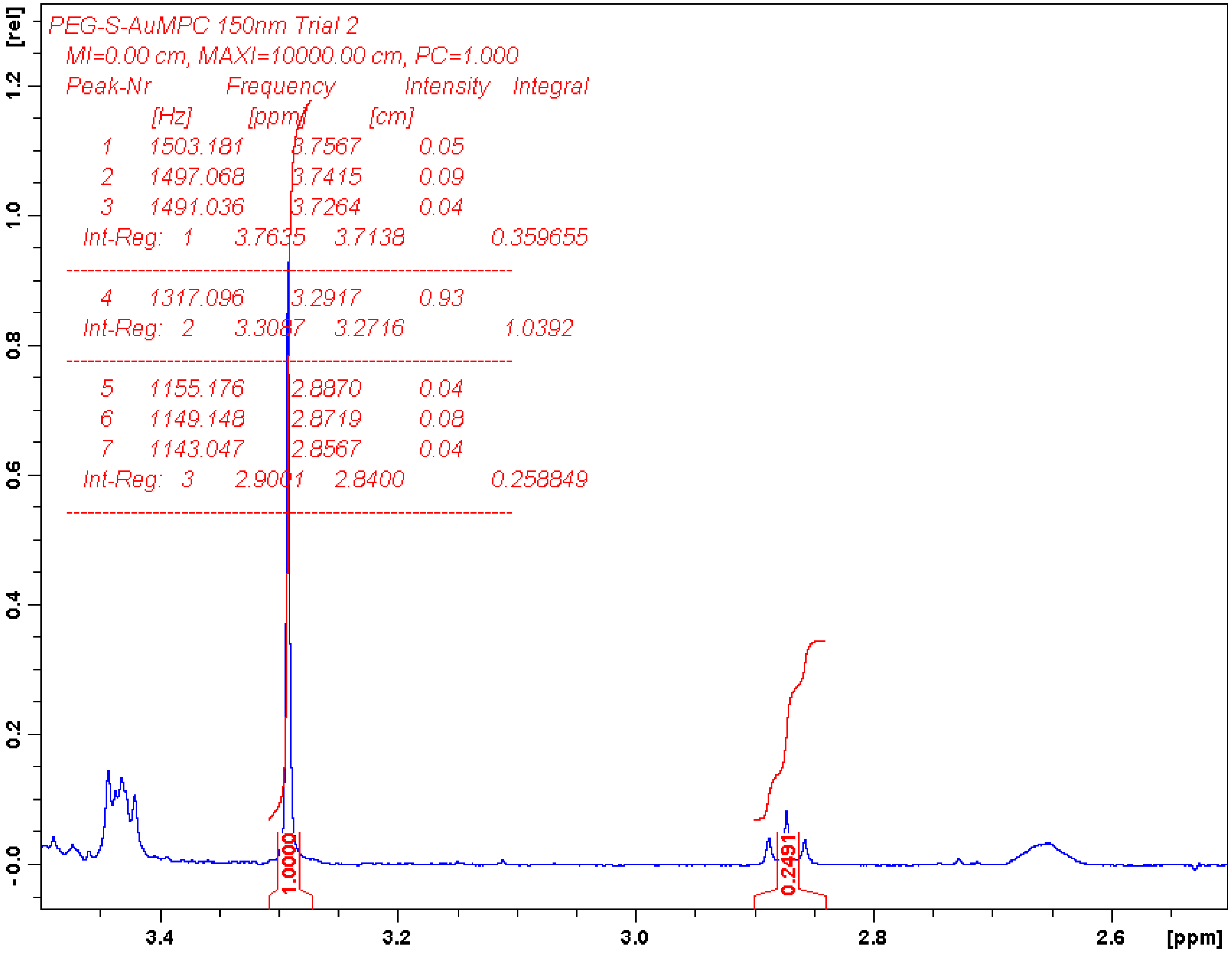

Spectrum C - 11. Trial 2 of 150 nm PEG-S-AuMPC spectrum showing qualitative integral ratio between total PEG and liberated (previously conjugated) PEG ligands

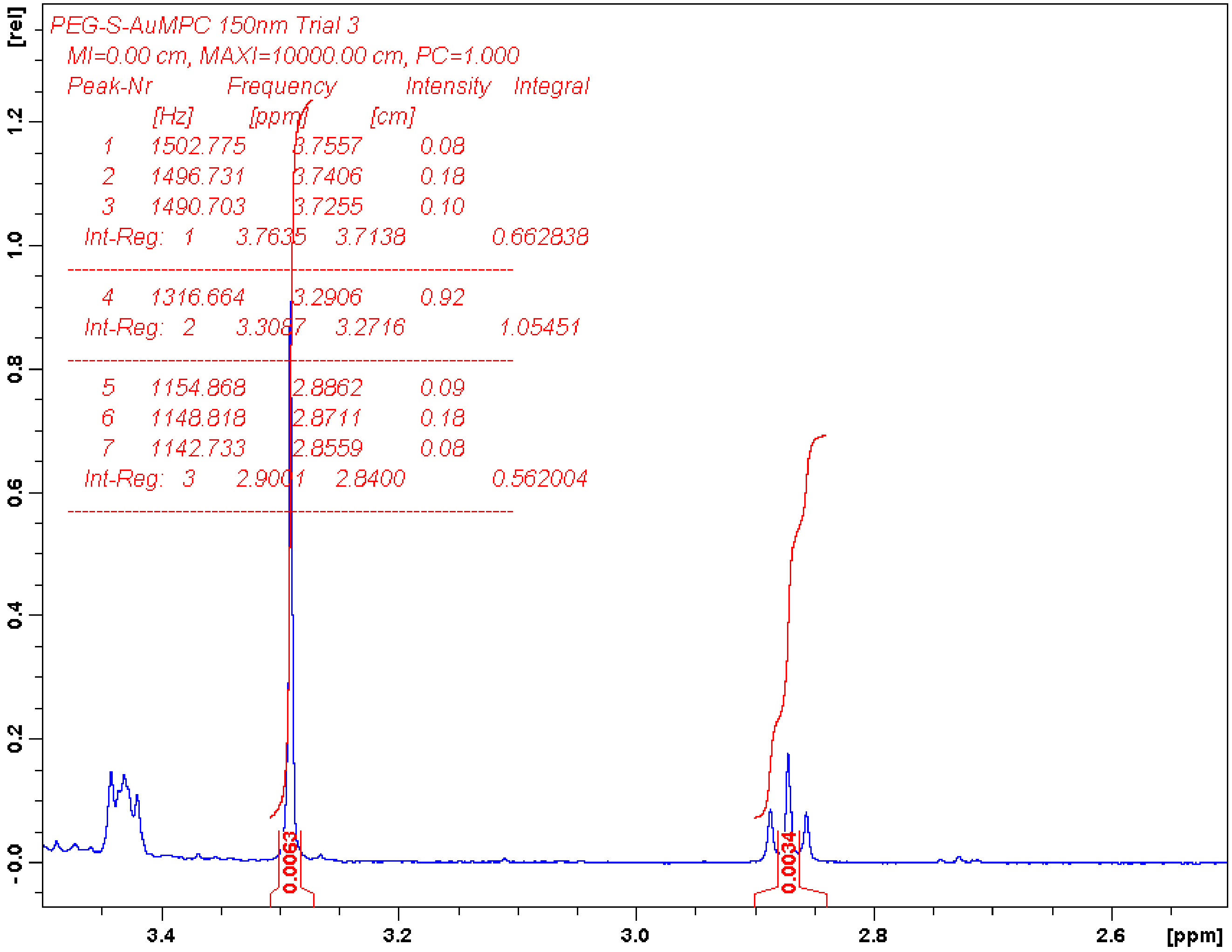

```
PEG-S-AuMPC 150nm Trial 3
  MI=0.00 cm, MAXI=10000.00 cm, PC=1.000
  Peak-Nr          Frequency          Intensity   Integral
            [Hz]         [ppm]          [cm]
      1     1502.775      3.7557         0.08
      2     1496.731      3.7406         0.18
      3     1490.703      3.7255         0.10
   Int-Reg:   1      3.7635     3.7138             0.662838
  --------------------------------------------------------------
      4     1316.664      3.2906         0.92
   Int-Reg:   2      3.3087     3.2716              1.05451
  --------------------------------------------------------------
      5     1154.868      2.8862         0.09
      6     1148.818      2.8711         0.18
      7     1142.733      2.8559         0.08
   Int-Reg:   3      2.9001     2.8400             0.562004
  --------------------------------------------------------------
```

Spectrum C - 12. Trial 3 of 150 nm PEG-S-AuMPC spectrum showing qualitative integral ratio between total PEG and liberated (previously conjugated) PEG ligands

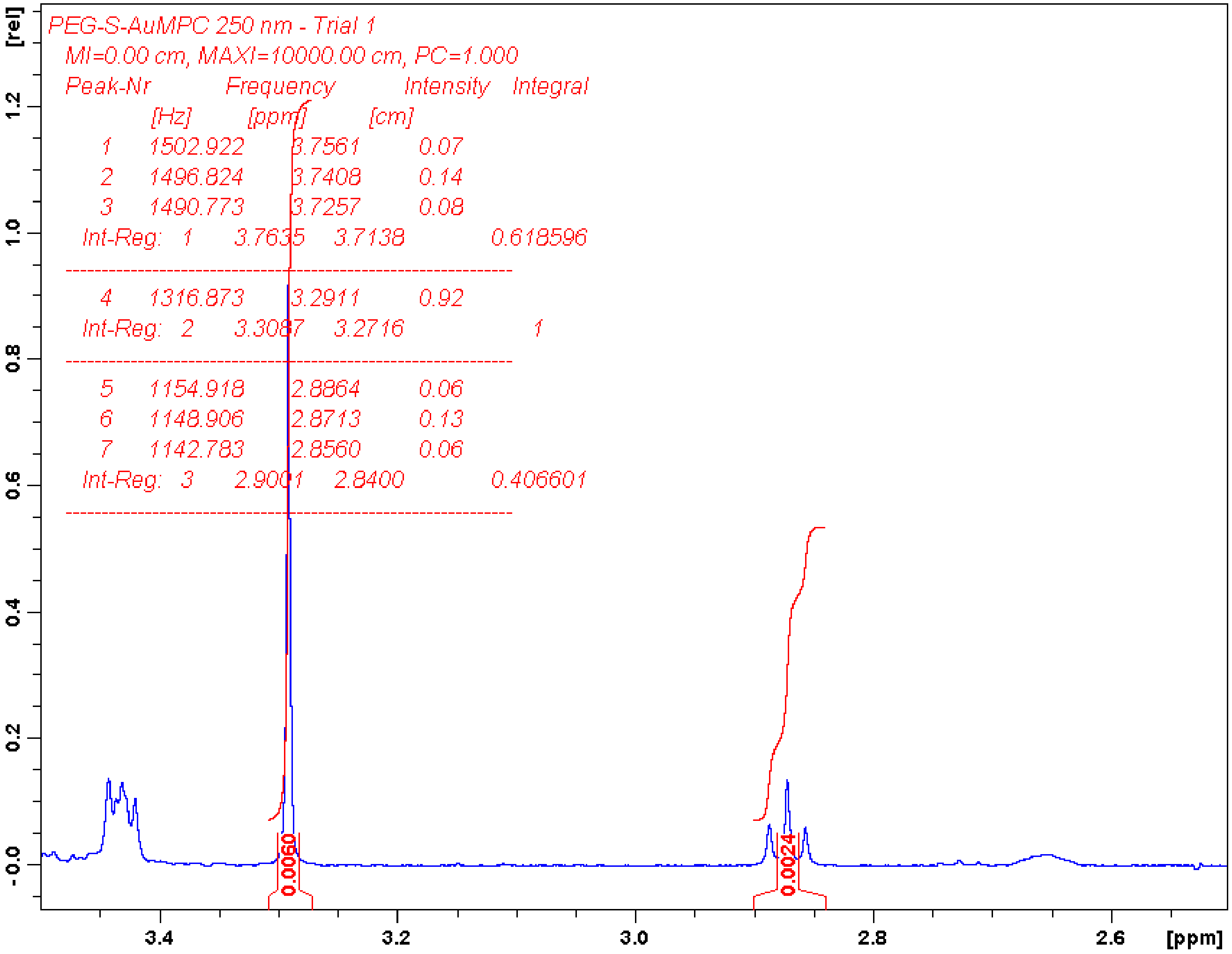

Spectrum C - 13. Trial 1 of 250 nm PEG-S-AuMPC spectrum showing qualitative integral ratio between total PEG and liberated (previously conjugated) PEG ligands

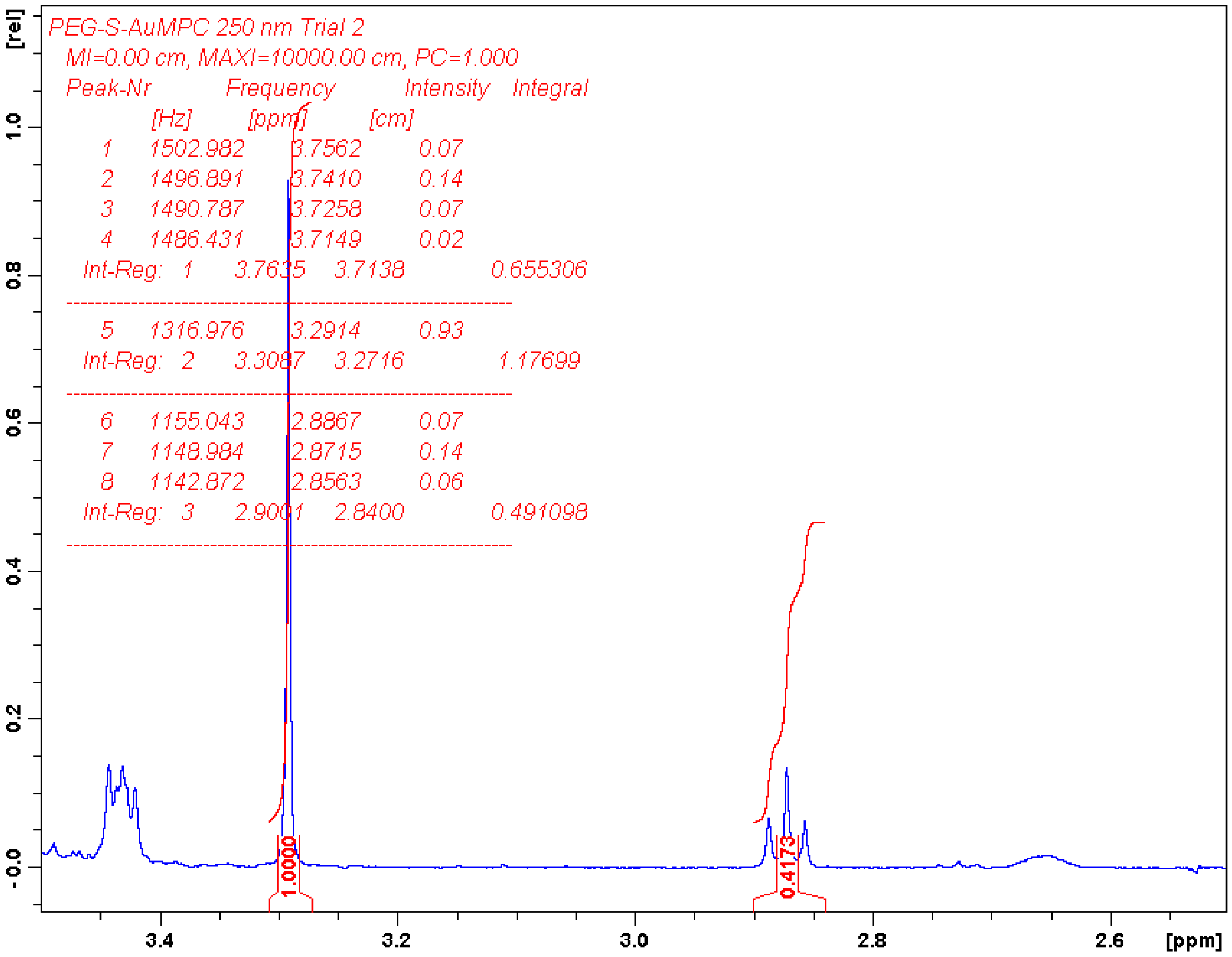

```
PEG-S-AuMPC 250 nm Trial 2
  MI=0.00 cm, MAXI=10000.00 cm, PC=1.000
  Peak-Nr          Frequency           Intensity   Integral
              [Hz]         [ppm]          [cm]
      1     1502.982      3.7562        0.07
      2     1496.891      3.7410        0.14
      3     1490.787      3.7258        0.07
      4     1486.431      3.7149        0.02
    Int-Reg:  1       3.7635     3.7138            0.655306
  -------------------------------------------------------------------------
      5     1316.976      3.2914        0.93
    Int-Reg:  2       3.3087     3.2716             1.17699
  -------------------------------------------------------------------------
      6     1155.043      2.8867        0.07
      7     1148.984      2.8715        0.14
      8     1142.872      2.8563        0.06
    Int-Reg:  3       2.9001     2.8400            0.491098
  -------------------------------------------------------------------------
```

Spectrum C - 14. Trial 2 of 250 nm PEG-S-AuMPC spectrum showing qualitative integral ratio between total PEG and liberated (previously conjugated) PEG ligands

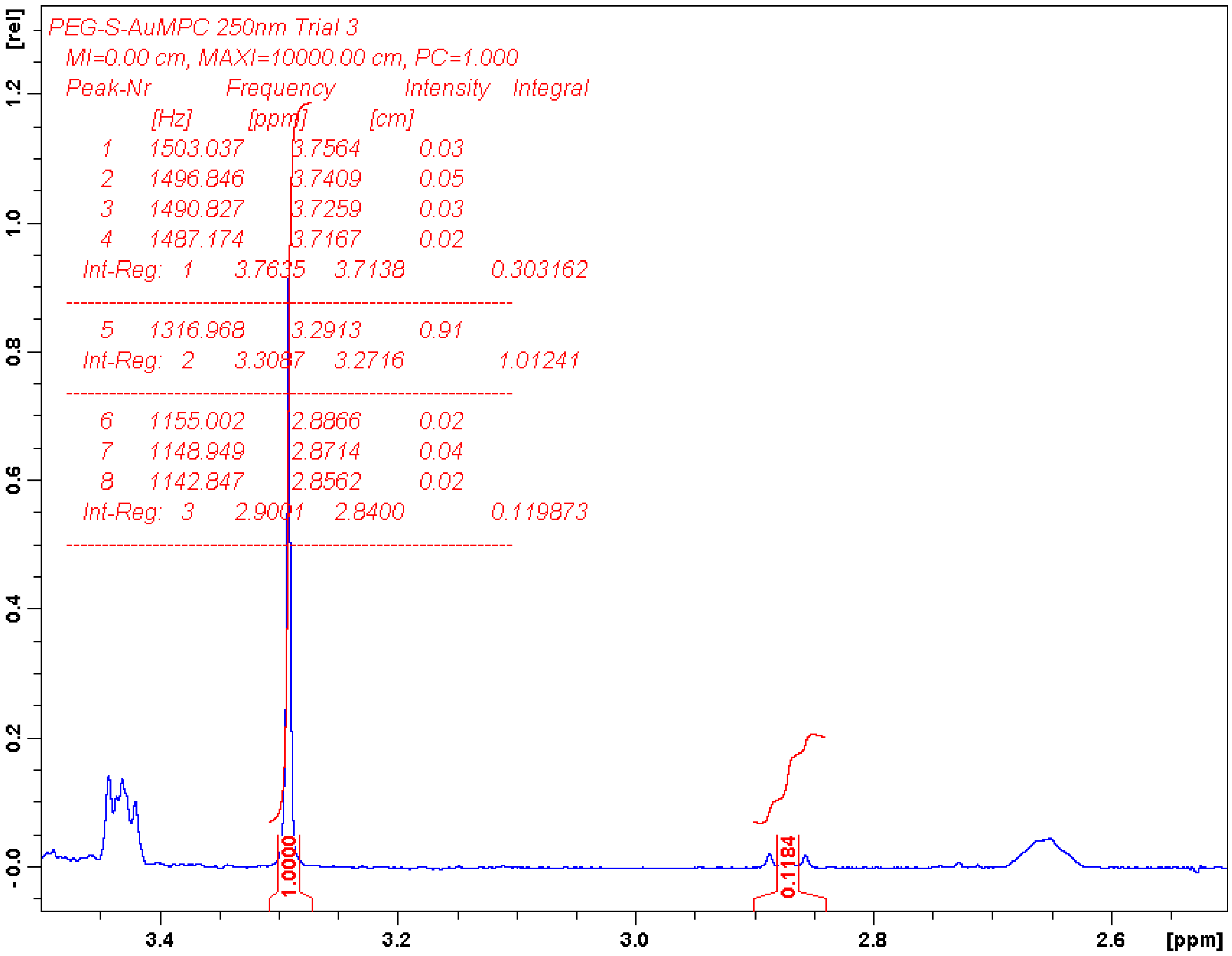

Spectrum C - 15. Trial 3 of 250 nm PEG-S-AuMPC spectrum showing qualitative integral ratio between total PEG and liberated (previously conjugated) PEG ligands